Capillary-based gripping
for laparoscopic bowel surgery

R.J. van den Berg

Technische Universiteit Delft

Delft University of Technology

Challenge the future

CAPILLARY-BASED GRIPPING

FOR LAPAROSCOPIC BOWEL SURGERY

by

R.J. van den Berg

in partial fulfillment of the requirements for the degree of

Master of Science
in Mechanical Engineering

at the Delft University of Technology,
to be defended publicly on Thursday May 3, 2018 at 14:00 AM.

Supervisors:	Dr. D. Dodou	
	Ir. P. van Assenbergh	
Thesis committee:	Dr. ir. D.H. Plettenburg,	TU Delft
	Dr. D. Dodou,	TU Delft
	Ir. P. van Assenbergh,	TU Delft

Delft University of Technology

Preface

The idea for this thesis came up after finishing my 4-month internship in the Crosby research group at the Polymer Science & Engineering at UMass Amherst in 2015-2016, where I had a good time and enjoyed doing research as part of a team. Al Crosby directed me to the work of the Insect Biomechanics Workgroup of Walter Federle at Cambridge who are working on adhesion of biological systems. After reading a few articles about ants and treefrogs, I became fascinated by the interplay of microstructures and liquids to generate adhesion.

At the time, the BioMechanical Engineering department of the faculty 3mE started a collaboration with Wageningen University on the adhesion of treefrogs, and a graduation assignment posted on the intranet in this area of research was just what I was looking for: "Design, fabrication and evaluation of an adhesion-based medical gripping instrument". Supervised by Dimitra Dodou and Peter van Assenbergh, I started the literature review with the goal to publish it, but this effort was stopped due to time constraints. Instead, some work of the literature review was presented on a poster at the 2016 Gordon conference from 24-29th of July at Mount Holyoke College in Massachusetts by Peter. After finishing writing the review in the summer and presenting a colloquium, a couple of brainstorm sessions were done together with Paul Breedveld about applications for laparoscopic surgical instruments. However, clear design rules for gripping with adhesion and the achievable forces were not available. Therefore, the research aim shifted from designing an instrument to an experimental study into generating adhesion with capillary forces.

I formulated the research questions, did force simulations and delivered the mould design to Henny van der Ster, the precision technician from the DEMO workshop. The samples were fabricated and inspected at the faculty of TNW and I did the force measurements in the MISIT lab with the support of lab technician Arjan van Dijke and Jos van Driel from the MeetShop. Although the results of this work do not prove that capillary-based gripping is effective, I pursued my own research topic despite the setbacks encountered and gained experience and confidence in my ability to conduct a research project.

For those who say that writing a thesis is an individualistic process, I argue that without supervision, scientific discussions, enthusiastic colleagues, family and friends, the motivation and purpose to deliver quality science is at risk. Therefore, I would like to thank Peter for the discussions and reviewing my work and Dimitra for her passion of experimental research and a sharp eye on scientific writing. Furthermore, I want to thank the Solvay Studiefonds for the scholarship they provided me with during my studies. Finally, I thank everyone else for their input and inspiration, het soggen and the music!

R.J. van den Berg
Delft, April 2018

CONTENTS

Abstract

Lifting an object by capillary forces is mostly done with a single liquid bridge which connects the target object to a probe. In this work the potential of capillary forces for soft-tissue manipulation is investigated; not only a single liquid bridge is used, but multiple bridges as well since capillary forces can be enhanced by contact splitting. Specifically, laparoscopic bowel surgery was chosen, because with current instruments it remains difficult to atraumatically grip soft delicate tissues.

Three 30 by 30 mm grippers were cast from PDMS (1:10 weight ratio curing agent to base) with pillars of diameter 2, 1 and 0.5 mm, named D2, D1 and D05 respectively. The ratio of pillar area to total gripper area is 0.6. The pillar structures and a flat reference sample were wetted with demi water and placed on the substrate (glass and 15 wt.% gelatin as tissue phantom). A preload is applied to attach the gripper to the connector and the both are retracted at 0.1 mm/s to measure the adhesion. From the camera footage of the measurements on glass was confirmed for D1 and D2 that capillary forces were measured. The best performing pillar structure was D1 with adhesion values between 1.3 – 3.4 kPa, but it did not outmatch the flat samples' adhesion: 2.2 – 3.1 kPa. On gelatin, the evidence for measuring capillary forces was not conclusive. The mean adhesion of all geometries on gelatin was 0.8 kPa and there was no clear effect of the different pillar diameters on the measured adhesion values.

From these results it is concluded that capillary forces should not be used as the main method to lift tissue, but rather to complement other gripping methods such as suction.

1

INTRODUCTION

1.1. GRIPPING WITH LIQUIDS

On first thought, gripping with liquids sounds contradictory. Objects are usually clamped with rigid grippers or tweezers. However, an example from daily life shows that gripping with liquids is more common than you might have thought. Say, you just ate a cookie and crumbs were spilled on the table. What some people might do, is to wet one of their fingers and pick up the crumbs. Once the crumbs contact the liquid on the finger they remain attached through capillary forces.

Capillary forces have been exploited for technical applications to grip and manipulate millimeter-sized [1] or micrometer-sized objects [2, 3] and to align them in a two-dimensional [4, 5] or a three-dimensional configuration [6, 7]. Lifting an object by capillary forces is mostly done with a single liquid bridge which connects the target object to a probe. In this state the probe can be moved together with the object and as soon as the bridge is disabled, the object is released.

The main difference between capillary-based and other types of grippers is that in a purely capillary-based gripper no dry contact is established. Capillary-based grippers already exist but they are not commercially available, and can only lift objects up to a few grams. Figure 1.1 presents four indicative grippers from scientific literature. The top left image is a square shaped gripper which can pick up flat silicon chips. Three channels are present, the channel in the center for the liquid supply and the others to release the chip with a burst of air. The bottom left image is a conical concave shaped gripper which was designed as proof of concept to pick up ball bearings of a watch. The top right image is a gripper designed to pick, place and align flat components. The component is lifted with four liquid bridges. The bottom right image shows a gripper which can manipulate objects underwater using a bubble of air.

The value of capillary-based grippers lies in the possibility to automatically align the gripper with the lifted object. For example, a liquid bridge between two flat square plates will minimize the surface energy of the bridge by exerting a torque on the plates, causing alignment. A second advantage is that the stress concentration on the object is low.

In this work, the potential of capillary based grippers for soft-tissue manipulation in minimally invasive surgery is investigated. Specifically, laparoscopic bowel surgery was chosen, because with current instruments it remains difficult to atraumatically grip soft delicate tissues [10].

As stated earlier, capillary forces are used in technical systems only for gripping rigid objects with a micrometer or millimeter length scale, but not on macro-scale. The potential force that capillary-based gripping can generate on macro-scale, and whether capillary grip could be implemented in a surgical tool for gripping tissue is explained in this chapter. A theoretical background of capillary forces is preceded.

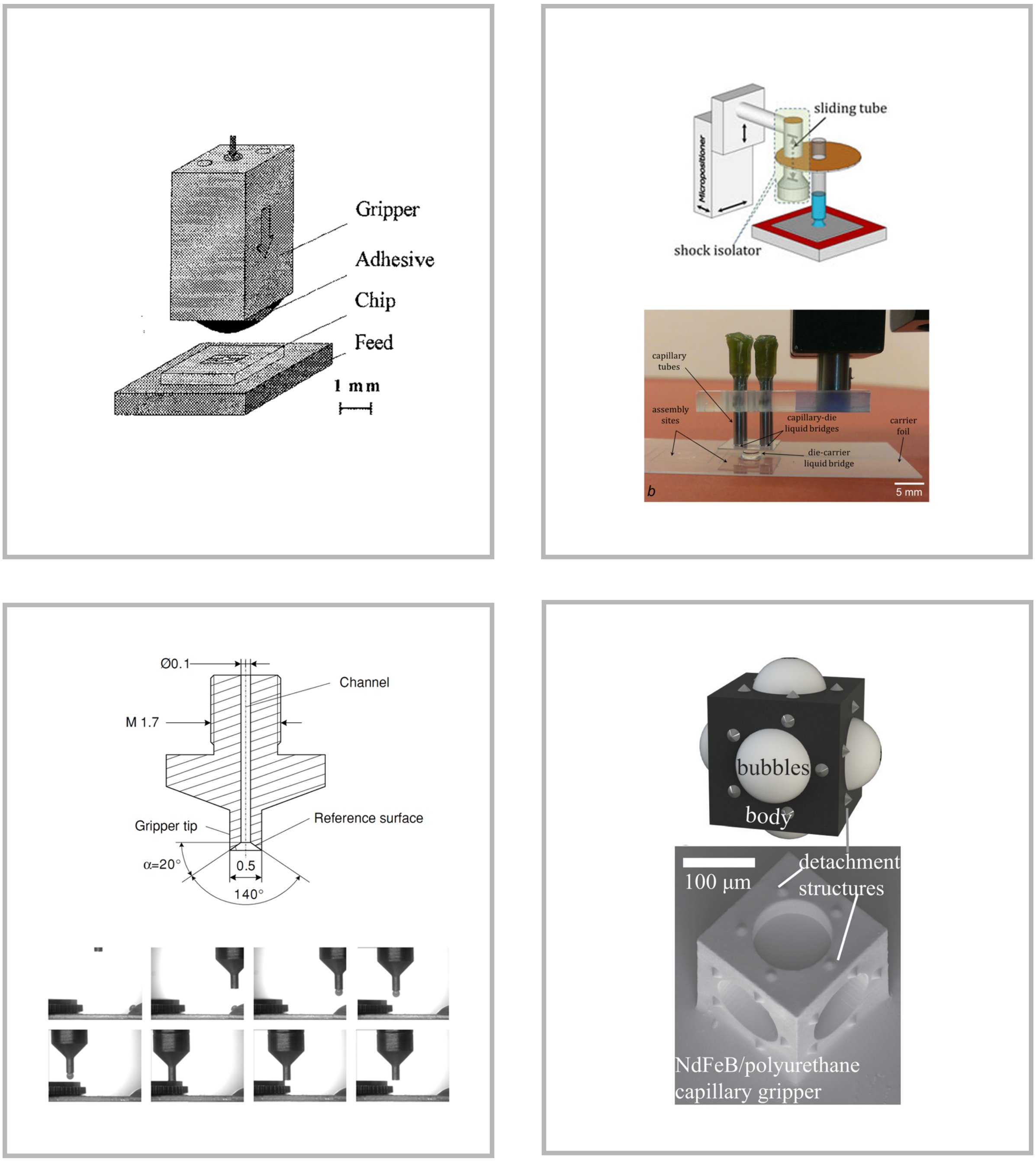

Figure 1.1: The top left image shows a gripper made by Bark et al. [8] in 1998, which was designed to pick up and align silicon chips. The bottom left image shows a gripper from Lambert et al.[1] from 2006 that is able to pick up and place watch ball bearings. The top right gripper can pick, place and align components (foil dies) and was made by Arutinov et al. [9] in 2015. The picture shown is the side view of the set-up. At the bottom right image, the 3D model shows a magnetically controlled untethered cubical gripper, capable of manipulating objects underwater using a bubble of air. This gripper was designed in 2016 by Giltinan et al. [3]. The image below depicts the actual gripper.

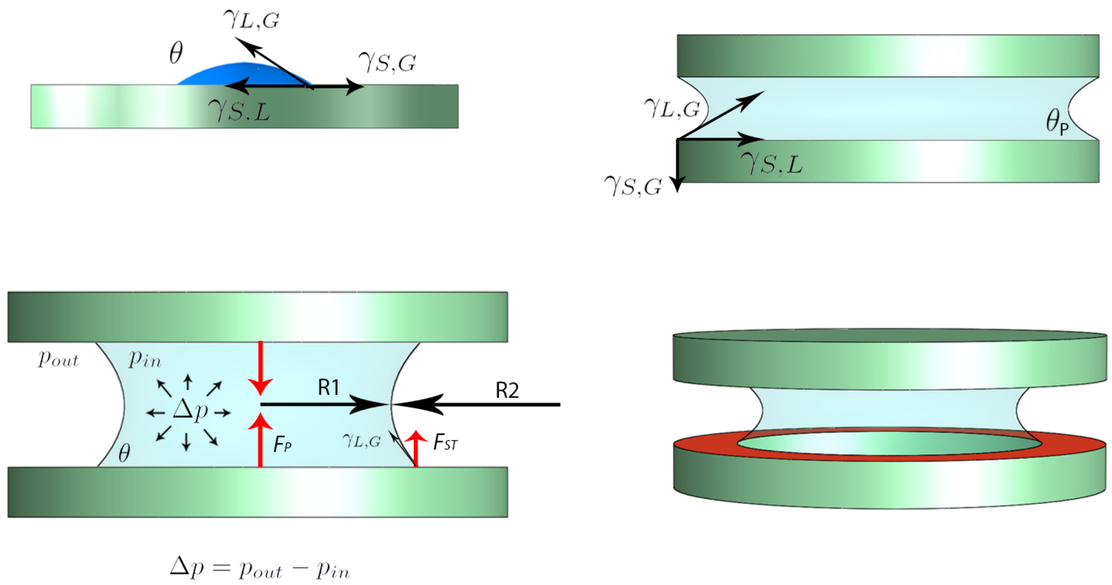

Figure 1.2: The interfacial tensions at the triple line are shown on the top left. The bottom left shows a parallel-plate system: R_1 and R_2 are radii of curvature which describe the meniscus profile, $\gamma_{L,G}$ is the surface tension along the liquid-gas interface, Δp is the pressure difference outside and inside the bridge, and θ is the contact angle between the surface and the liquid. The red arrows signify components of the capillary force. The Laplace force F_P acts on the wetted area on the plates, and the surface tension force F_{ST} acts along the perimeter of the wetted area. The bottom right image shows that the contact angle can be pinned due to a hydrophilic region surrounded by a hydrophobic material, marked in red. The top right shows contact pinning by the geometry of the disks. The wetted area is unable to expand its radius R freely in the pinned case. The horizontal force equilibrium of (1.1) does not apply anymore to the situation of the upper right since the contribution of $\gamma_{S,G}$ becomes zero.

1.2. ORIGIN OF CAPILLARY FORCES

Capillary forces originate in cohesive interactions of molecules. Suppose that a liquid bulk is floating in air, without gravity. At the surface of the liquid bulk, molecules experience fewer attractive interactions than those at the inside. The measure for the forces resulting from this imbalance is the surface tension γ [J/m^2 or N/m]. The liquid surface tension (or interfacial tension $\gamma_{L,G}$ between the liquid and gas) is the reason that the bulk will form a curved surface. The bulk eventually becomes a spherical droplet in order to minimize its surface area and reach the lowest energy state.

If the materials and liquids are assumed to be a continuum, the capillary force associated with a liquid bridge between two rigid bodies in air consists of two terms: the surface tension- and Laplace force. These terms are explained individually in the following sections.

1.2.1. SURFACE TENSION FORCES

When a liquid droplet contacts a perfectly flat horizontal surface, it forms a convex or almost flat shape, as shown in Figure 1.2 at the top left. The force equilibrium of equation (1.1) in the horizontal plane, describes this relation with the *equilibrium* contact angle θ as a function of the three interfacial tensions: the liquid-gas $\gamma_{L,G}$, liquid-solid $\gamma_{L,S}$ and the solid-gas $\gamma_{S,G}$ interfacial tension. How well the liquid spreads on the surface depends on the value of θ. From the top left image it can be seen that $\gamma_{L,G}$ has a vertical component acting along the contact perimeter of the droplet. This surface tension term is described in equation (1.2). With this vertical surface tension force component, the resultant axial force F_{ST} can be calculated as in equation (1.2), given that the droplet has a circular perimeter with radius R.

$$\gamma_{S,G} = \gamma_{L,S} + \gamma_{L,G} \cdot cos(\theta) \tag{1.1}$$
$$F_{ST} = \gamma_{L,G} \cdot sin(\theta) \cdot 2\pi \cdot R \tag{1.2}$$

1.2.2. LAPLACE FORCES

When a liquid droplet on a plate is contacted by a second plate from above, a liquid bridge is formed in between the two plates as shown at the bottom left of Figure 1.2. This model is called the parallel-plate model and assumes that both plates are perfectly smooth, parallel, axially symmetric and rigid, and that continuum mechanics apply. Gravity effects on the meniscus are neglected, which is justified for liquid bridges smaller than 2.5 mm for water [1]. In this parallel-plate model, the radius of the meniscus at its neck is R_1 and the curvature is described with R_2. In Figure 1.2, at the bottom left, the radius R_1 is positive and R_2 is negative. The Young-Laplace equation (1.3) defines the relation between the shape of the meniscus and the pressure difference between the in- and outside of the liquid.

$$\Delta p = p_{out} - p_{in} = \gamma_{L,G} \cdot \left(R_1^{-1} + R_2^{-1}\right) \tag{1.3}$$

Since the external pressure is often known, the internal pressure can be calculated from equation (1.3). The Laplace force is the resultant of the pressure difference acting over the wetted area $A_{wet} \approx \pi R_1^2$ on the plate, as in equation (1.4). The force can be attractive or repulsive, depending on whether the meniscus is concave or convex, respectively.

$$F_L = \Delta p \cdot A = \gamma_{L,G} \cdot \left(R_1^{-1} + R_2^{-1}\right) \cdot \pi R_1^2 \tag{1.4}$$

1.2.3. TOTAL CAPILLARY FORCE BETWEEN PARALLEL PLATES

Summing equation (1.2) and (1.4) results in a complete expression for the axial capillary force of a single circular liquid bridge between parallel plates of the same material:

$$F_C = F_{ST} + F_L = \gamma_{L,G} \cdot \left\{sin(\theta) \cdot 2\pi R + \left(R_1^{-1} + R_2^{-1}\right) \cdot \pi R_1^2\right\} \tag{1.5}$$

This theory does not only hold for liquid bridges, but it can be formulated in a more general way. A capillary bridge has three different interfacial tensions; other possible combinations such as a gas bridge in liquid, or a liquid bridge within a liquid are not treated in this work.

Equation (1.5) can be readily implemented if the meniscus shape is known, for instance, based on image analysis of a stable liquid bridge in an experimental set-up. Analytical solutions of forces resulting from bridges between standard geometries such as a spherical gripper tip and a plate, can be found here [11]. However, determining the right input parameters such as the liquid volume and the meniscus shape of the bridge for these analytic formulas without having experimental data, is difficult. Also, for non-standard geometries with asymmetric liquid bridges, the Young-Laplace equation (1.3) cannot be used to calculate the capillary force. The first tool for countering the problem of not knowing the meniscus shape is the the so-called double shooting method, described by Lambert in chapter 14 of his book [1], to numerically integrate the Young-Laplace equation. This method will be used in this work and is explained in chapter 2. The second tool is the Surface Evolver software [12] which can simulate asymmetric liquid bridges, but this software is not used in this thesis.

1.3. CALCULATING CAPILLARY FORCES FOR ADHESION

The principle to lift objects using liquid bridges is extended in this section. Instead of lifting a small object with a single bridge, the attainable adhesion force over a larger (flat) area is calculated assuming that multiple bridges are present. In 1.3.1 the adhesion of a single bridge is calculated, and in 1.3.2 the adhesion of multiple bridges over a larger area is calculated.

1.3.1. NORMAL ADHESION GENERATED WITH LIQUID BRIDGES

Adhesion of a single bridge perpendicular to the plates, as depicted in the left of Figure 1.3 is the capillary force F_C of equation (1.5) divided by its wetted area A_{wet} at the plate. Here A_{wet} is πR_1^2.

$$\frac{F_C}{A_{wet}} = \gamma_{L,G} \cdot \left\{2sin(\theta) \cdot R_1^{-1} + \left(R_1^{-1} + R_2^{-1}\right)\right\} \tag{1.6}$$

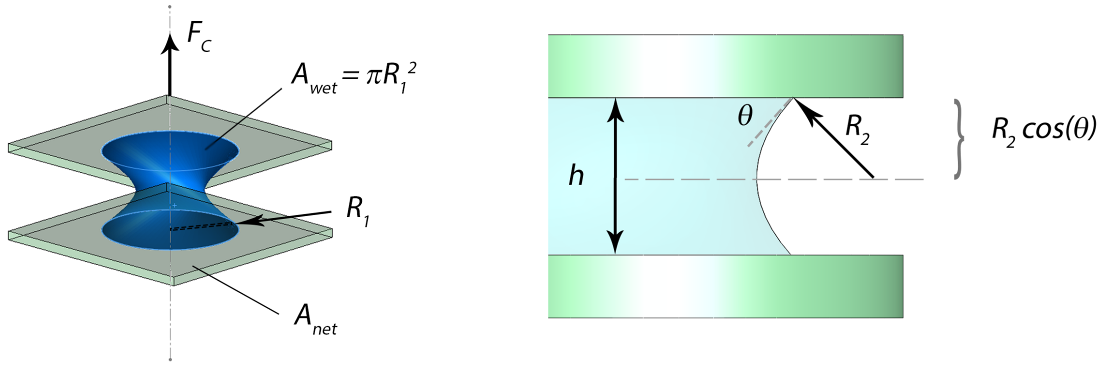

Figure 1.3: Left, an axisymmetric liquid bridge between parallel plates. The wet adhesion of this bridge is the ratio of its capillary force F_C to the wetted area A_{wet}. Right, the geometric relation that describes gap height h as a function of contact angle θ and radius R_2.

Equation (1.6) is simplified with the following assumptions to write it solely in terms of the bridge radius R_1. First, the gap height h between the plates is described by the relation $h = 2R_2cos(\theta)$ as done by [13] shown in the right of Figure 1.3. Secondly, the aspect ratio of the bridge h/R_1 is set to 100, as done by [14]. Then R_2 is written in terms of R_1. The simplified equation for capillary-based adhesion becomes:

$$\frac{F_C}{A_{wet}} = \gamma_{L,G} \cdot \left\{ \frac{2sin(\theta)}{R_1} + \left(\frac{1}{R_1} + \frac{100cos(\theta)}{R_1} \right) \right\} \tag{1.7}$$

Figure 1.3 shows the normal adhesion of a single liquid bridge as a function of the contact angle θ and the bridge radius R_1. The adhesion was calculated using equation (1.7) with an interfacial tension $\gamma_{L,G}$ of 30 [mN/m] in line with the parameters used by [14] and who's derivation is treated in the next section. It can be seen that the normal adhesion of a single bridge increases as the bridge radius R_1 decreases (keeping aspect ratio constant).

1.3.2. BENEFIT OF CONTACT SPLITTING

Since adhesion of a single bridge increases as the radius R_1 decreases, the following question comes to mind: could the total capillary force be enhanced by splitting the wetted area of a single contact into multiple small bridges, while keeping their aspect ratio the same?

Researchers Labonte et al. derived analytic equations to calculate in which regime of the contact angle θ contact splitting increases the total capillary force between parallel plates [14]. The top of Figure 1.5 depicts how contact splitting looks like and a part of the derivation is shown at the bottom of Figure 1.6. The rest of the derivation is explained here. Equating the capillary force of a single bridge F_C and the capillary force F_{CS} after contact splitting as stated in Figure 1.5 and then solving for the number of bridges n gives:

$$F_{CS} > F_C \;\; if \;\; n > \left(\frac{R_1}{h} \frac{2cos(\theta)}{2sin(\theta) - 1}(1-\phi) + 1 \right)^2 \cdot \left(\frac{1}{\phi} \right) \tag{1.8}$$

Where ϕ is the ratio of A_{wet} to total gripper area A_{net}, called "area coverage". Labonte et al. then describe the smallest radius R_1 of the bridge as a function of the variables h and θ:

$$2R_1 > \frac{h(1 - sin(\theta))}{cos(\theta)} \tag{1.9}$$

This size restriction of the bridge is implemented into equation (1.8) to obtain the maximum number of bridges n_{max} that can be placed between the parallel plates:

$$n_{max} = 4\phi \left(\frac{R_1}{h} \right)^2 \frac{1 + sin(\theta)}{1 - sin(\theta)} \tag{1.10}$$

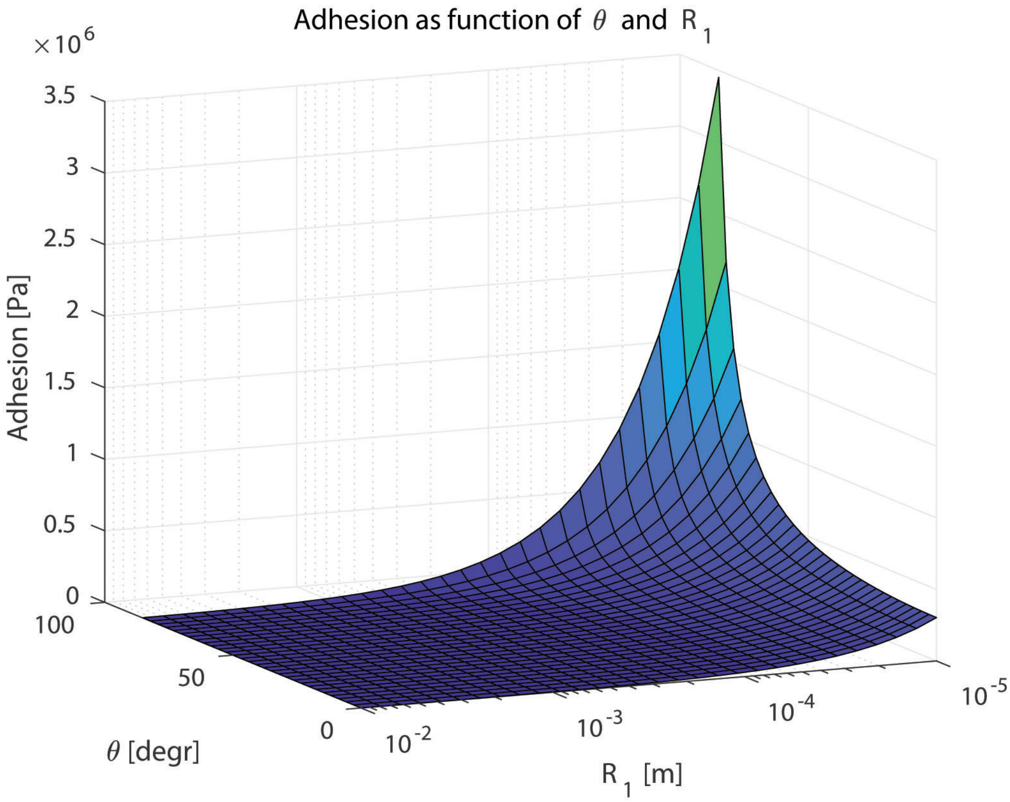

Figure 1.4: Normal adhesion of a single liquid bridge as function of contact angle θ and meniscus radius R_1 for a parallel-plate system. Values were calculated with equation (1.11) and $\gamma_{L,G} = 0.03$ [N/m].

The graph at the top of Figure 1.6 is a computational reproduction of Figure 7(a) from Labonte et al. [14]. The blue line is equation (1.8) and the red line is equation (1.10). The parameters used in the equations are: $\phi = 0.3$, $R_1 = 0.05$ [m], $R_1/h = 100$, $\gamma_{L,G} = 0.03$ [N/m]. The top plot shows that contact splitting is only beneficial with a contact angle higher than 50°. The lines in the middle graph are the calculated forces with (red) and without (blue) contact splitting. In the case of contact splitting, the number of bridges is the theoretical maximum of equation (1.10). The adhesion force is in this simulation only enhanced with contact splitting for contact angles higher than 60°. The bottom graph shows the value of the radius R_n which corresponds to the maximum number of bridges n_{max} as shown in the top and middle graph. We can conclude that for this simulation the radius of the bridges has to be (sub)micron to obtain a benefit from contact splitting.

De Souza et al. used the Surface Evolver software to simulate contact splitting for a parallel-plate system in [15]. The applied liquid volume V, disk radius R_1 and interfacial tension $\gamma_{L,G}$ are kept constant and the contact angle θ and the number of bridges n are varied. The axial force, or pressure or the work of separation could be maximized with a combination of variables θ and n. The force plot of Figure 1.7 shows that for mildly hydrophobic surfaces $\theta = 70^o$, and the values $V = 1$ [μL], $R_1 = 7.5$ [μm], $\gamma_{L,G} = 0.072$ [N/m], the axial force is roughly 0.2 and 1.5 [N] when the bridge is split into the maximum possible number of bridges, which is set by the separation distance of 15 μm between the plates.

There are currently no devices that perform capillary-based adhesion in the regime where contact splitting outperforms the axial force of a single bridge. Outside this regime, Vogel et al. designed a device [16] consisting of a porous gripper plate which can form multiple liquid bridges onto a flat target surface, as shown in the left of Figure 1.8. The top plate is placed onto the flat target surface and the spacers, denoted by (a), to fix the gap height between the plates. The liquid is pumped through the holes and an array of liquid bridges forms. Configurations with different gripper materials, pore diameters and number of pores have been tested. The volume is controlled actively, either with an electroosmotic pump or a manual syringe. The measured adhesion forces of the different device configurations are plotted against the bridge diameters in the right of Figure 1.8. The bridges with smaller diameters generate a higher net adhesion compared to the larger bridges. Net

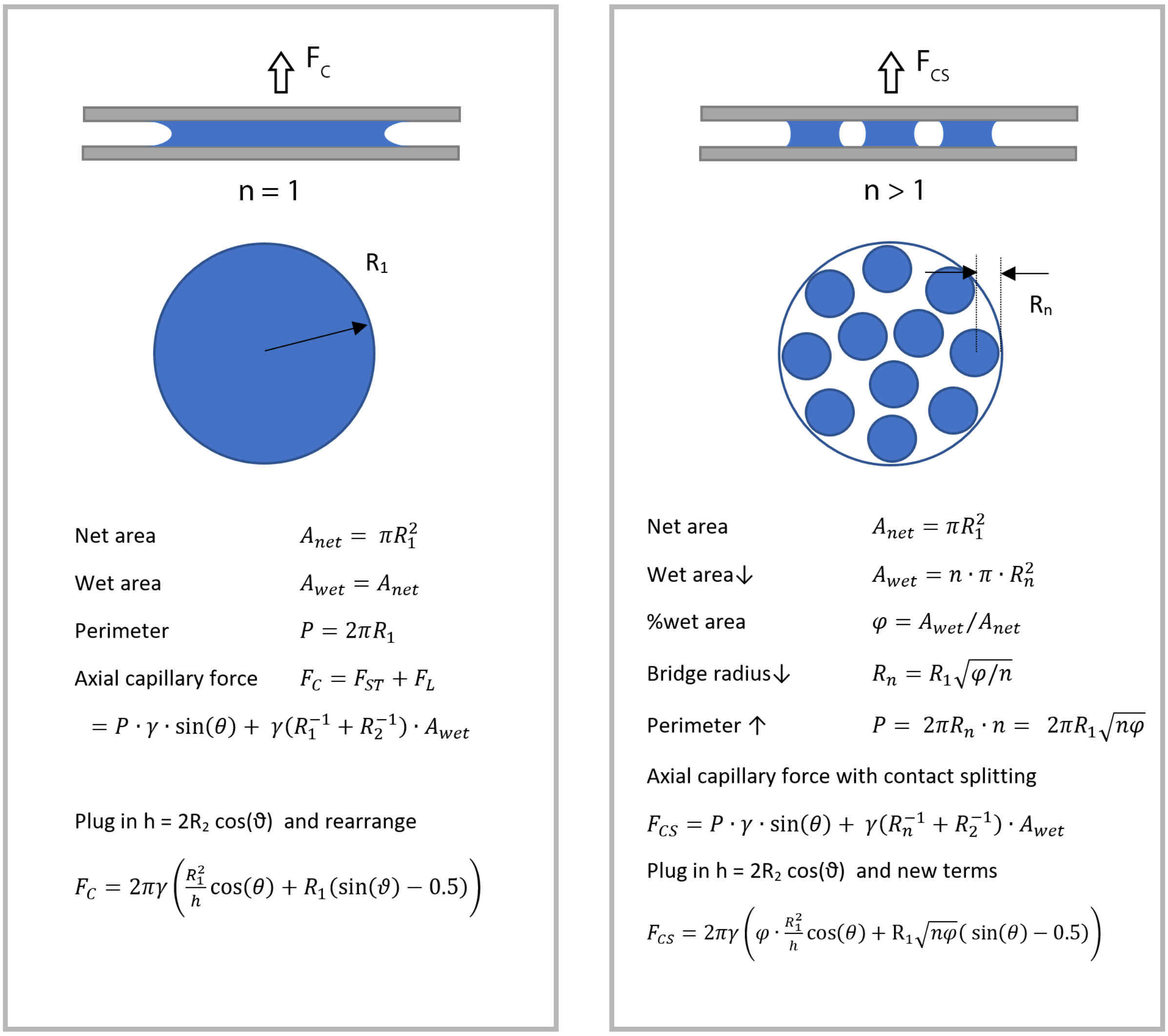

Figure 1.5: The images at the top show how a single liquid bridge is split into multiple small bridges. Bottom, the equations derived in [14] associated with both a single bridge and multiple bridges between parallel plates.

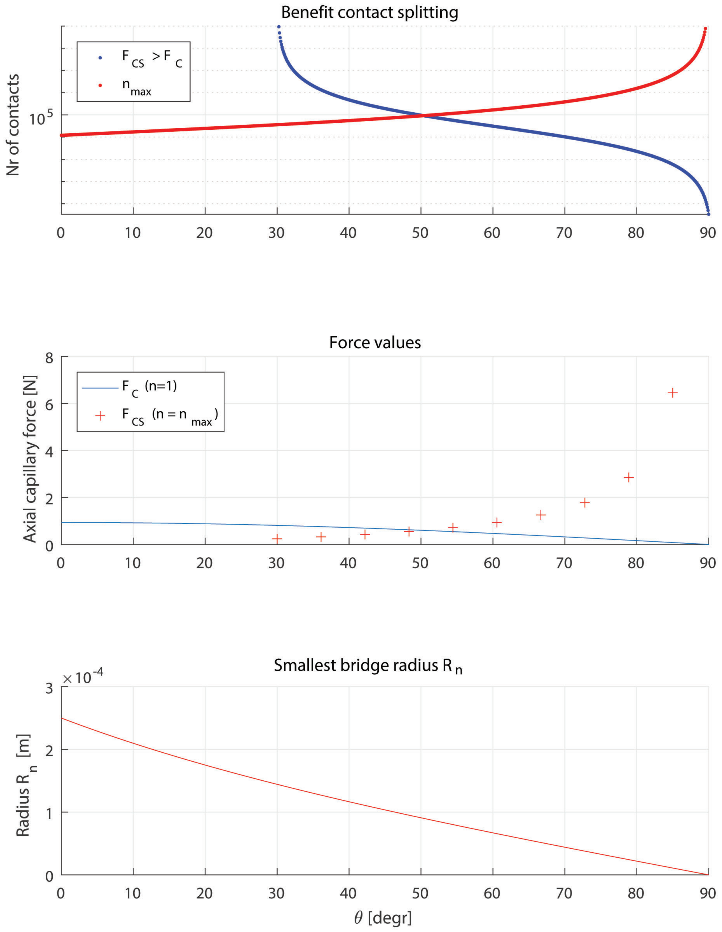

Figure 1.6: Top, contact angle regime where contact splitting leads to a higher force compared to a single liquid bridge, reproduction from [14]. Middle, force values of a single bridge (blue) or the maximum possible number of bridges (red). Bottom, the smallest possible bridge radius R_n as a function of the contact angle θ.

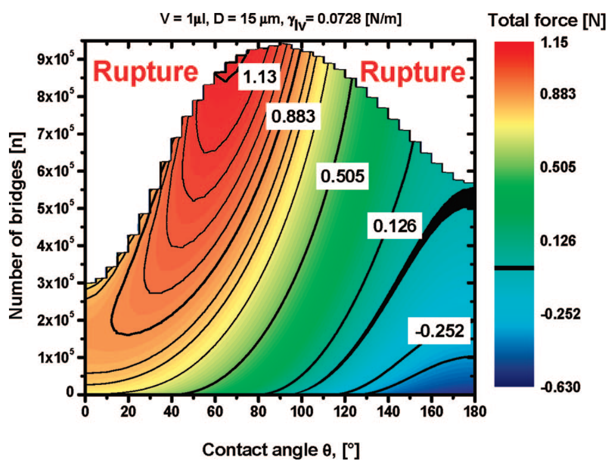

Figure 1.7: Surface Evolver simulation map adapted from [15] which shows the increase in axial capillary force due to contact splitting for a parallel-plate system. The symbols at the top are: the liquid volume V, the distance between the plates D and the liquid-vapor surface tension $\gamma_{L,V}$.

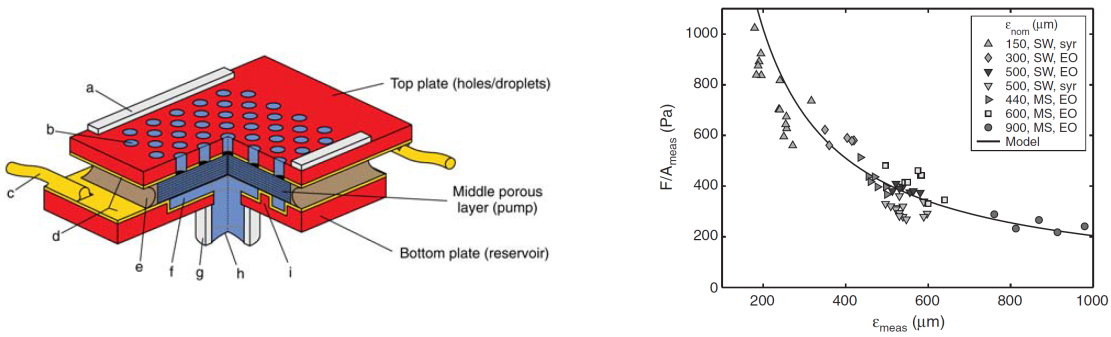

Figure 1.8: Left, schematic cut through image (not to scale) of the capillary-based adhesion device adapted from [16]. Right, the average measured bridge diameter ϵ_{meas} is plotted against the ratio of the measured total force divided by the area of all the bridges.

capillary-based adhesion with multiple similar axisymmetric bridges can be then calculated as:

$$\sigma_{capillary} = \frac{F_{bridges}}{A_{net}} = \frac{N \cdot F_{1bridge}}{A_{net}} = \frac{F_{1bridge}}{A_{wet}} \cdot \phi \tag{1.11}$$

Where the term $\phi = 0.6$. The model that fits the data points on the right of Figure 1.8 is derived from (1.11). This model neglects the surface tension contribution to the capillary force.

1.4. SIZE LIMITS OF CAPILLARY BRIDGES

In order to design a new gripper that can pick up larger objects and generates a higher adhesion compared to the existing ones, down scaling of the liquid bridges, bridge size limits and phenomena occurring at (sub)micron scales need to be taken into account. These topics are discussed in this section.

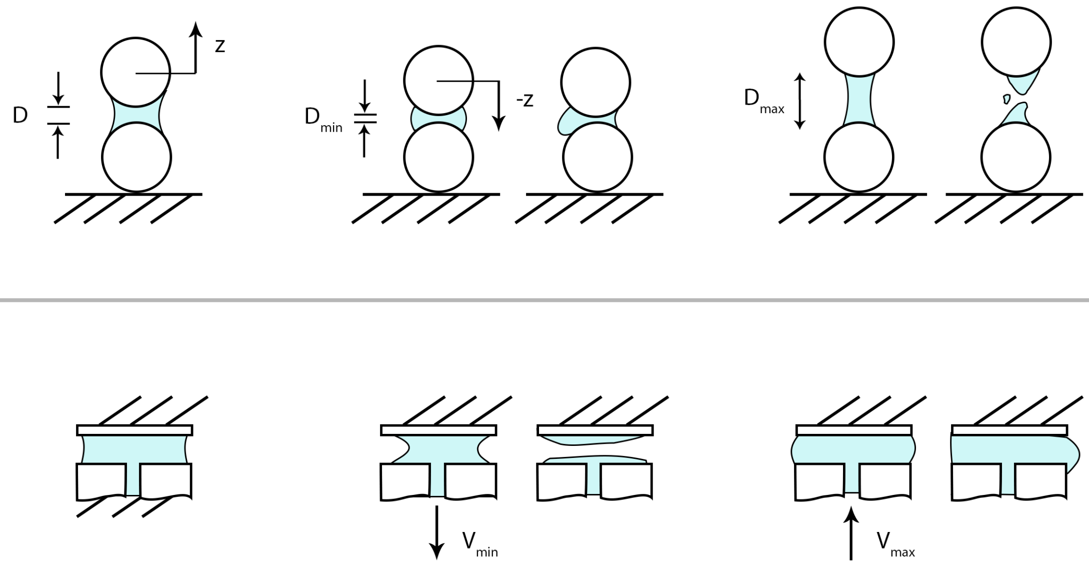

Figure 1.9: Experimental methods to test size limits of a liquid bridge, shown in the top and bottom images. Top, a liquid bridge of fixed volume is present between two rigid spheres. The gap height is varied to find the minimum and maximum separation distance. Bottom, a liquid bridge is established between two parallel plates with constant gap height. Through a channel the liquid volume is decreased or increased to find the minimum and maximum volume stability limits, respectively.

1.4.1. VOLUME AND SEPARATION DISTANCE

The most obvious factors that determine the length at which a capillary bridge is stable, are the volume of the bridge, the distance between gripper and object and their dimensions. Simply put, very small grippers cannot hold large volumes, and a large gap between gripper and object cannot be bridged with a small volume. Maximum and minimum lengths of capillary bridges can be identified experimentally by holding the bridge volume constant while slowly varying the bridge length, or vice versa. Both methods are shown in Figure 1.9.

By plotting each experimentally determined size limit as a function of dimensionless gap height D* and dimensionless volume V*, the stability regime of a capillary bridge can be visualized. Such a visualization is shown in Figure 1.10 for parallel disks. For every Bond number, as defined in equation (1.12), such a stability regime exists. As the Bond number increases, the stability regime becomes smaller.

$$Bo = ((\rho_{bridge} - \rho_{surround}) \cdot g \cdot R^2)/\gamma_{L,G} \tag{1.12}$$

Where ρ_{bridge} is the density of the capillary bridge, and $\rho_{surround}$ is the density of the surrounding medium. The gravity constant is g, the radius of the parallel disks is R and the liquid-gas interfacial tension is $\gamma_{L,G}$.

In addition to the experimental method, the numerical integration of the Young-Laplace equation as described in [18] can be used to determine accurately at what length the bridge ruptures. With an analytic fit to the numerical data, a simple expression of the maximum separation distance can be obtained. A overview of these numerical approaches, as well as recent advances on the subject of capillary bridges is written by Lian et al. [19].

The rupture distance is defined as the distance at which a liquid bridge becomes unstable and collapses. This is the maximum length of a capillary bridge. By numeric integration of the Young-Laplace equation Lian et al. [20] found that the relationship between the rupture distance for a liquid bridge between equal rigid spheres can be expressed as:

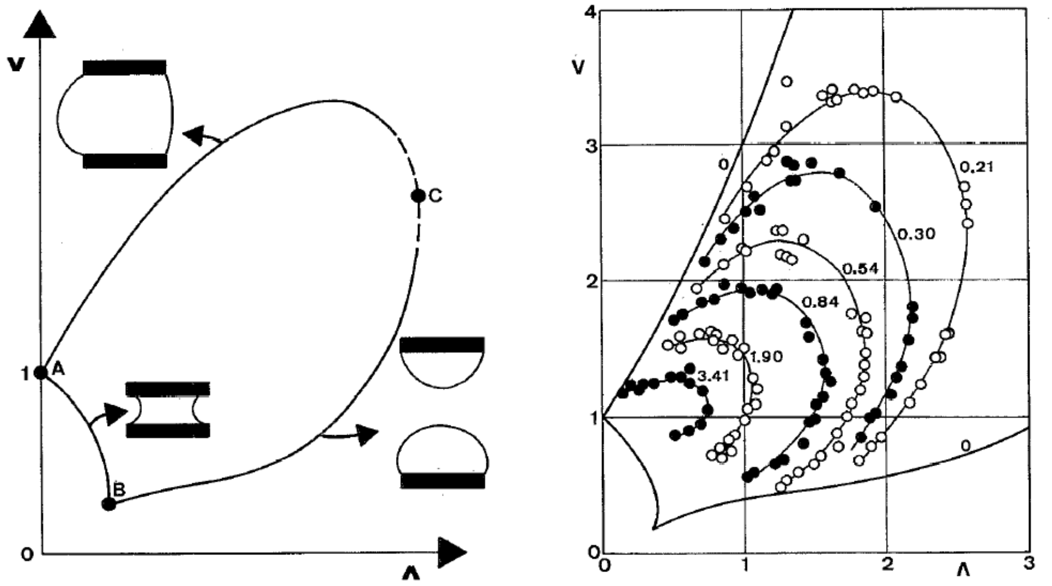

Figure 1.10: Stability regimes of a capillary bridge between equal parallel disks. The horizontal axes represent the dimensionless gap height $D_{disk}* = D/2R$. The vertical axes represent the dimensionless volume $\Lambda_{plates}* = V/(2\pi R \cdot D)$. The left graph indicates the stability curve has three parts. A-B is the detachment of the interface from the edges of the disk. B-C is the minimum volume stability limit. C-A is the maximum volume stability limit. The right graph shows that with increasing Bond numbers, the stability regime decreases. Radius of the disks were 0.25-5 mm and the working fluid was water. Adapted from [17]

$$\frac{2S_c}{V^{1/3}} = \frac{2S_c^*}{V^{*1/3}} = \left(1 + \frac{\theta}{2}\right) \tag{1.13}$$

Where $2S_c$ is the rupture separation distance, shown as D_{max} in Figure 1.9, V is the liquid volume between the spheres and θ is the contact angle. The relationship is applicable for contact angles smaller than 40°. The asterisk means that the term is normalized by the sphere radius.

The minimum length of a capillary bridge is not clearly defined. It seems that for capillary bridges with nanometer lengths, the assumption of continuum mechanics would crumble. However, according to molecular dynamics simulations by Cheng and Robins [21] of a liquid bridge between parallel plates, the Young-Laplace equation is valid up to bridge lengths of 4 nanometer. Since van der Waals forces become exponentially larger as the gap between the plates decreases, it is recommended to calculate the contribution of van der Waals forces with respect to the capillary forces at the (sub) nanometer length scale.

1.4.2. GRAVITY

Capillary length λ_C is a function of the gravity constant g [m/s^2], the density of the liquid ρ [kg/m^3] and the interfacial surface tension $\gamma_{L,G}$ [N/m]:

$$\lambda_C = \sqrt{\gamma_{L,G}/\rho g} \tag{1.14}$$

If the bridge length exceeds λ_C, the meniscus will be deformed due to the gravity acting on the large liquid volume. The meniscus cannot be described with a mean constant curvature anymore. This means that the Young-Laplace equation will become inaccurate and, when calculating the capillary force with numeric methods, the weight of the liquid needs to subtracted.

1.4.3. CONDENSATION AND EVAPORATION

Capillary condensation can affect the size of a capillary bridge, depending on the liquid type, gap height between gripper and object and the environmental conditions. The phenomenon of capillary condensation is described by Butt et al [11]. In this process, molecules of the surrounding gas keep condensing into the meniscus. An equilibrium state is reached when the Kelvin equation is equal to the Young-Laplace equation, as in (1.15).

$$\frac{R \cdot T \cdot \ln(p_{in}/p_{out})}{V_m} = \gamma_{L,G} \cdot (R_1^{-1} + R_2^{-1}) \tag{1.15}$$

Where R is the ideal gas constant 8.314 [J mol^{-1} K^{-1}], T is the temperature [K], p_{in} is the pressure inside the bridge, and p_{out} the pressure of the surrounding gas [Pa], V_m is the molar volume of the liquid [m^3/mol]. The Young-Laplace equation on the right hand side of equation (1.15) has been introduced earlier in equation (1.3).

Assuming that the liquid bridge is water and the surrounding gas is air, the ratio of p_{in}/p_{out} is equal to the relative humidity RH of air. Assuming also that $R_2 << R_1$, an expression can be found for R_2, which is called the Kelvin radius.

$$R_2 = r_K = \frac{\gamma_{L,G} \cdot V_m}{R \cdot T \cdot \ln(RH)} \tag{1.16}$$

Kelvin radii, for different liquids at 25 degrees Celsius are given in [11], ranging between 0.5–2 nm. The same work explains a general expression of the meniscus formation process and more about the kinetics of formation and rupture. This point about condensation and evaporation is made, because the choice of the liquid and the environment affect what the minimum size of a bridge can be.

1.5. GOAL OF THE THESIS

The literature treated in sections 1.3.2 and 1.4 suggests that it is theoretically possible to enhance capillary forces by contact splitting. Secondly, it seems possible to use capillary forces to lift large flat surfaces if an array of liquid bridges is used. The research question of the thesis I initially started with was: *"Can a purely capillary-based device provide enough grip to manipulate bowel tissue?"*

The reasoning behind this specific application is that gripping soft slippery tissues during laparoscopic surgery requires forces in the order of Newtons [10] which induces a risk of tissue damage when using conventional laparoscopic grippers that rely on tissue pinching. Capillary-based grip might be a promising alternative for atraumatic tissue gripping, but such a method has not yet been applied to lifting tissue and no clear design rules are available for applying capillary-based grip on macro scale.

The goal of the thesis was to test capillary-based adhesion of a gripper tip on a tissue phantom and investigate the relation between the measured adhesion and the chosen gripper tip dimensions.

In Chapter 2 the capillary forces for a chosen gripper tip shape are modelled and the dimensions of the gripper are proposed. Chapter 3 describes the fabrication method of the gripper, the test method of pilot tests and the method to experimentally evaluate the performance of the gripper on a glass substrate and a tissue phantom. The results of the pilot tests and experiments are presented in Chapter 4. The results are discussed in Chapter 5, followed by the conclusions and recommendations of the thesis. Appendix A presents a flowchart with the chosen gripper tip shapes from those listed in the literature review. The MATLAB scripts are included in Appendices B, C and D. The literature review made prior to the thesis is included as a separate document.

2

SELECTING THE GRIPPER SHAPE AND PREDICTING ITS CAPILLARY FORCE

2.1. HOW GRIPPER SHAPE AFFECTS CAPILLARY FORCES

From Chapter 1 we know that the capillary force a gripper can exert on a surface is a function of the properties of the liquid ($\gamma_{L,G}$), the liquid volume V, the contact angles θ and the size and shape of the gripper itself. Keeping liquid type, liquid volume and the materials constant, we want to know how the gripper shape and size affect the capillary force. Regarding the shape, Figure 2.1 shows at the left a flat gripper shape (parallel-plate system), and on the right a parabolic tip, both with contact angles of 30°. To accommodate the same liquid volume of the plate-system in the one with the parabolic tip, the meniscus must be stretched. Consequentially, the vector F_{ST} changes in orientation towards the axial direction which improves the contribution of the surface tension force to the capillary force. However, the radius R_2 increases too, which lowers the Laplace force. Regarding the size of the gripper, if R_2 » R_1, the Laplace term dominates the surface tension term in the equation (1.5) of the total capillary force. Suitable tip shapes are selected from the set of gripper shapes found in the literature review made prior to this thesis. The selection criteria, and the final choice are given in the following section.

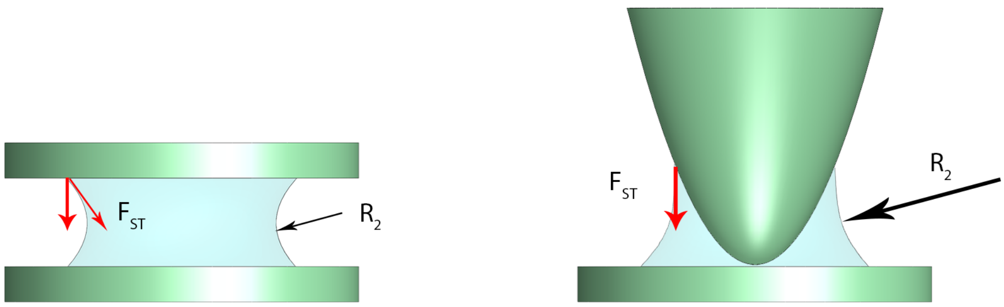

Figure 2.1: Left, flat gripper with a liquid bridge between the tip and the object. Right, a parabolic shaped gripper with a liquid bridge of a similar volume. The tip shape can alter the contribution of the surface tension force F_{ST} in the axial direction. However, if R_2 increases, the Laplace force F_L will decrease.

2.2. SELECTION OF THE GRIPPER TIP SHAPE

Since the possible gripper shapes are virtually endless, we restrict ourselves to those found in the literature review. This is done because the literature provides dimensions and force data, which is a good starting point to determine the gripper dimensions. The gripper tip must satisfy the following requirements:

1. The force of the liquid bridges can be calculated with the Young-Laplace equation, in order to set the dimensions of the gripper and compare its performance with the calculated values from theory. Therefore axially symmetric tip shapes are chosen.

2. The %wet contact area ϕ needs to be maximized, as shown in Figure 1.5 and equation 1.11. Therefore tip shapes are chosen which can function without spacers that fix the gap height between the gripper and the substrate

3. In case multiple liquid bridges are introduced, they must not fuse together. Therefore, tip shapes are chosen which allow the liquid to remain at the perimeter of the tip after the liquid is squeezed out of the contact area.

4. The gripper can grab flat objects and the array of tips can be manufactured with the facilities available at the workshops on the campus in Delft.

As shown in the flowchart of Figure A.1 in Appendix A, only the spherical shape strictly meets all the requirements. However, as shown in Figure 2.2, variations of the spherical and conical tip shapes are possible. Figure 2.3 shows that for similar menisci, a spherical shape generates a higher adhesion compared to the conical shape. The forces are calculated with the equations found in [11]. The sphere has a radius of 1mm, the angle β between the conical tip and the substrate is 20° and the contact angles are $\theta = 0°$ at the surfaces.

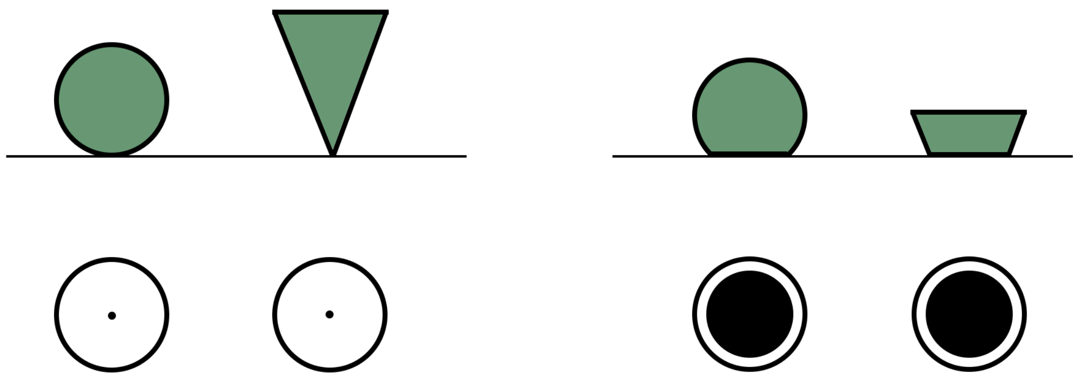

Figure 2.2: Left, a spherical and conical tip in contact with a rigid flat substrate. Beneath, the projected contact areas are shown. Right, the contact area of the flattened spherical and conical tips is much larger compared to the point contacts shown on the left.

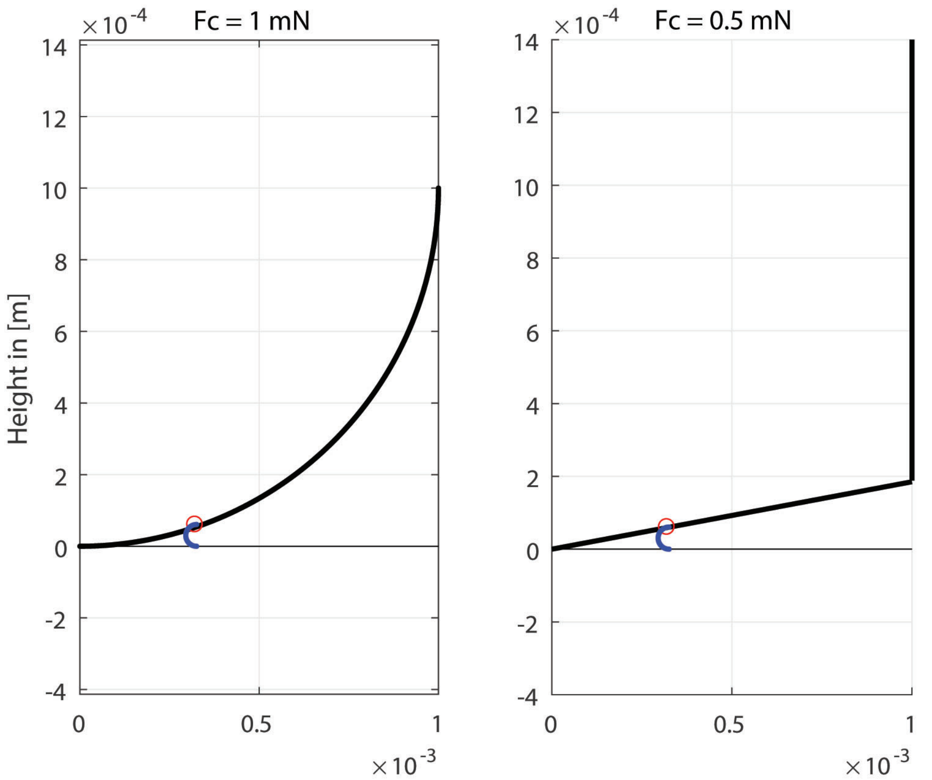

Figure 2.3: Left, a spherical tip in contact with a flat surface. The red circle is the starting point of the meniscus and the blue line is its profile. Right, a conical tip in contact with a flat surface. For similar menisci, the spherical shape generates a higher adhesion compared to the conical shape. The analytic equations can be found in [11]. Input parameters were: $\gamma_{L,G}$ = 0.072 [N/m], $\theta_1 = \theta_2 = 0°$, D = 0 [m], b = 0.32e-3 [m], $\beta = 20°$, $\phi = 79.327°$

Only looking at the adhesion properties, the best choice would be the spherical shape. However, if the cone is flattened the adhesion will increase and the static friction is expected to increase due to the enlarged contact area. Manufacturing such a flattened cone is also easier compared to a flattened sphere, because standard drill tools can be used. Therefore the flattened conical shape is chosen for the gripper tips. The concept design of the gripper with flattened conical tips is shown in Figure 2.4. An array is chosen because we want to investigate the relation between pillar size and the adhesion, and whether contact splitting is beneficial. In addition, the gripper must be able to exert a friction force to generate grip. In the case of dry contact, the friction force scales with the contact area. In the next section the dimensions of the tip are determined.

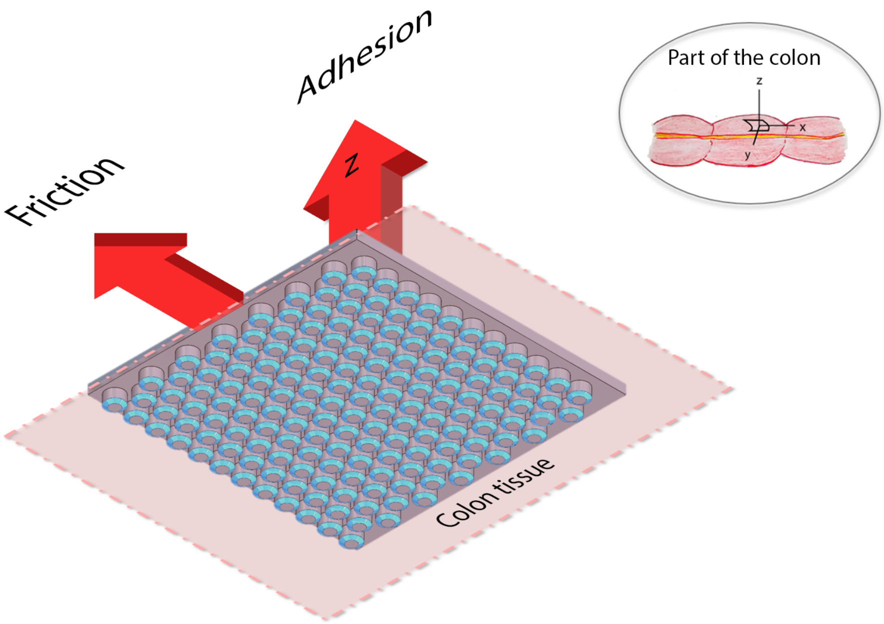

Figure 2.4: Impression of the underside of the gripper which is in contact with colon tissue. Top right, a part of the colon. The functionality of the gripper tips is twofold: the perimeter of the tip guides the capillary bridges which are effective for adhesion in the z-direction. Secondly, the contact area of each conical tip exerts friction forces on the tissue.

2.3. ATTAINABLE CAPILLARY FORCES WITH CONICALLY SHAPED TIPS

In the previous section a conical shape was selected as the best option. A flattened cone, however, is not found among the standard gripper tip shapes for which the capillary forces of an axially symmetric liquid bridge can be calculated based on existing models (e.g., [11]). This section presents the method which was used to calculate the capillary forces generated by a conically-shaped gripper.

2.3.1. FINDING REALISTIC INPUT PARAMETERS

This section determines the input parameters for the script ConicalPlate.m to calculate the capillary force of a conically-shaped gripper. To do so, an estimation of the gripper dimensions is first made with the script Prototype_Dim.m, based on which grippers can actually be fabricated.

The flattened conical parts will be made by drilling holes to a specified depth into a plate - a method that poses limitations to the achievable tip diameter. The available fabrication method of 3D metal printing was investigated, but the surface quality and resolution of the prototypes was not good enough when printing millimeter-sized, high aspect ratio pillars. A photolithography method such as SU-8 can produce high aspect ratio structures [22], but it requires expensive masks. Apart from screenprinting, photolithography is not my personal expertise and it is outside the budget of this project. Therefore drilling was selected as the most suitable fabrication method. The drilling depth determines the cone height L_2. For a constant cone height L_2 a larger opening angle corresponds to a larger contact area. With a larger contact area between the gripper tips and the substrate, a higher friction force can be generated. Therefore, spotting drills with the largest opening angle α available (120°) were chosen, with diameters D_1: 2, 1 and 0.5 millimeter respectively. This range is used so that the relation between pillar size and adhesion can be tested. The %wet area ϕ is set to 0.6 similar to [16] and the %contact area ζ is set to 40% because then the pillar height L_2 is within the manufacturing tolerance of 0.1 millimeters.

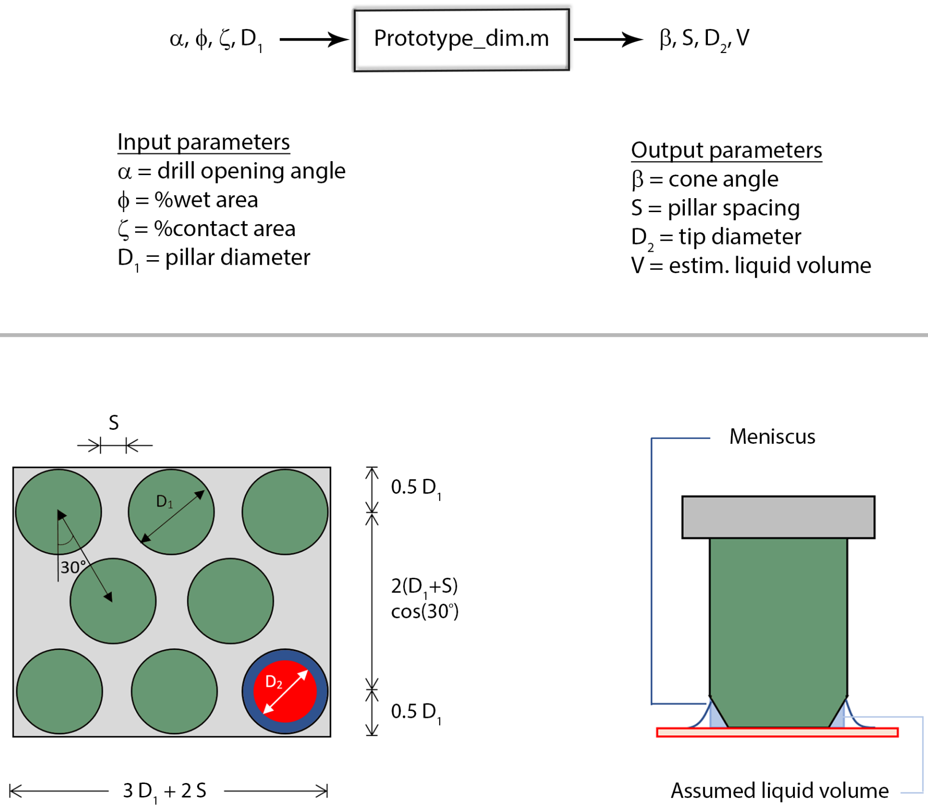

Figure 2.5: Schematic input and output of the MATLAB model Prototype_dim.m which estimates the dimensions of the pillar structures and the applied liquid volume per tip. Left, 2D bottom view of 8 hexagonally packed pillars with diameter D1 on a baseplate. The pillars are green in colour and the plate is in grey. The red area is the contact area with the liquid meniscus situated at the perimeter of the conical tip of diameter D2. Right, meniscus at perimeter of a tip in contact with tissue. The estimated volume of the liquid wedge does not follow the shape of the meniscus.

The script Prototype_dim.m, see Appendix B, estimates the dimensions of the pillar structures and the volume of a liquid bridge. The input and output parameters are listed in Figure 2.5. The script calculates the spacing S between the pillars based on the hexagonal packing of 8 pillars on a baseplate, as shown in the bottom left of Figure 2.5. The %wet area ϕ is linked to the diameter D_1 and the % contact area ζ is linked to diameter D_2. The liquid bridge volume is assumed to be a circular wedge, as shown in the bottom right of Figure 2.5.

The input parameters for Prototype_dim.m, as shown in Figure 2.5, are:
$\alpha = 120°$, ϕ=0.6, $\zeta = 0.4$, and $D_1 = [2, 1, 0.5]$ mm

The calculated output parameters are:
$\beta = 31°$, $S = [0.4\ 0.2\ 0.1]$ mm, $D_2 = [0.408\ 0.8171\ 1.633]$ mm and $V = [9e\text{-}4\ 7.2e\text{-}3\ 5.77e\text{-}2]$ mm^3

These estimated dimensions will be used in the next section to simulate the capillary force a liquid bridge generates.

2.3.2. CALCULATING THE CAPILLARY FORCES

With the estimated dimensions of the gripper tip given in 2.3.1 and choosing the liquid and the grippers' material properties, the capillary forces can be calculated. Water is selected as liquid because it has a high surface tension in air ($\gamma_{L,G}$ = 0.072 [N/m] @ 20 °C) and it is safe to use on tissue. The static contact angle θ_{gri} at the gripper tip is set to be mildly hydrophobic: 70° based on recommendations for a parallel disk system [14, 15]. The static contact angle θ_{obj} at the plate is slightly hydrophilic: 45° based on the contact angle of water on 15 wt.% gelatin [23]. For a laparoscopic gripper H. de Visser found that the maximal pull force exerted by the surgeon on the instrument is 5N and the pressure due to the pinch force that lead to tissue damage was calculated to be in the range of 0.9-3.3 MPa for 2 mm hemispherical tips [10]. The only source, to my knowledge, that refers to lifting bowel tissue in the out-of-plane direction is done using suction [24]. However, the actual force on the tissue could not be determined.

Although the desired adhesion force for the gripper is not known yet because no force damage limits are available for the out-of-plane direction, 1N was chosen because this value is below the applied compression and pull forces found by de Visser. The second reason is that at this force level the available S-beam loadcells can be used for the data collection.

To calculate the force of a liquid bridge between the conical tip and a flat substrate, I used chapter 8 of Lamberts' book [1] and the work of Arutinov et al. [9] as guidance. Here, the Young-Laplace equation introduced earlier in (1.3) is written in more general terms: the radius of the meniscus profile is written in terms of height z, instead of R_1 and R_2 as shown in Figure 2.6.

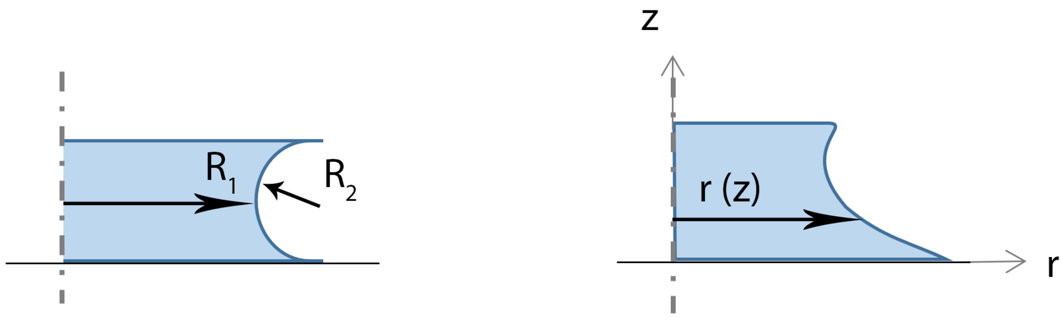

Figure 2.6: Left, the neck of the meniscus is R_1 and the curvature is R_2. Right, the meniscus radius is descibed in terms of the height z. The dotted vertical line is the axial symmetry line of the liquid bridge.

The result is a second order non-linear differential equation:

$$\frac{\Delta p}{\gamma} = \frac{1}{r\left(1+\dot{r}^2\right)^{0.5}} - \frac{\ddot{r}}{\left(1+\dot{r}^2\right)^{1.5}} \qquad with\ \dot{r} = \frac{\partial r}{\partial z}\ and\ \ \ddot{r} = \frac{\partial^2 r}{\partial z^2} \tag{2.1}$$

This equation can be rewritten into first order ordinary differential equations (ODEs):

$$Y' = f(Y)\ \ with\ Y = \begin{pmatrix} u \\ v \end{pmatrix} = \begin{pmatrix} r \\ \dot{r} \end{pmatrix} \tag{2.2}$$

Taking the derivative of Y with respect to the height z leads to:

$$Y' = \begin{pmatrix} \dot{u} \\ \dot{v} \end{pmatrix} = \begin{pmatrix} v \\ f(u,v) \end{pmatrix} \tag{2.3}$$

Rewriting the equation (2.1) in terms of u and v, and bringing $\dot{v}$ to the left hand side gives:

$$\dot{v} = -\frac{\Delta p}{\gamma}(1+v)^{1.5} + \frac{(1+v^2)}{u} \tag{2.4}$$

Now that the expression for $\dot{v}$ is known, the set of ODEs in (2.3) can be solved by numerical integration between height $z = P_y$ to $z = 0$ in MATLAB with the ode45 solver and the boundary conditions as specified in Figure 2.7. The double shooting approach [25] is used with shooting variables pressure difference Δp and point P on the meniscus, because both are yet unknown. The steps of this approach are shown in Figure 2.8 on the left, and on the right the iterations of the menisci are shown. The solution is accepted when the calculated volume of the mensicus profile was within the 5% error margin of the input volume.

Boundary conditions

z = Py

Slope $\frac{dr}{dz} = \begin{cases} 1/tan(\theta_{gri}+\beta) & if\ (\theta_{gri}+\beta) \neq \frac{\pi}{2} \\ 0 & if\ (\theta_{gri}+\beta) = \frac{\pi}{2} \end{cases}$

z = 0

Slope $\frac{dr}{dz} = \begin{cases} -1/tan(\theta_{obj}) & if\ \theta_{obj} \neq \frac{\pi}{2} \\ 0 & if\ \theta_{obj} = \frac{\pi}{2} \end{cases}$

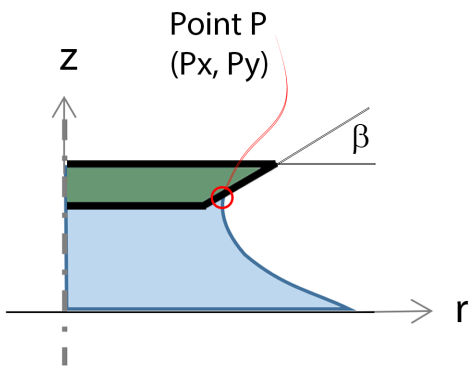

Figure 2.7: Boundary conditions of the meniscus profile between the surface of a conical gripper and a flat substrate.

The required gripper areas, calculated with the ConicalPlate.m model for three geometries, are presented in Table 2.1. The dimensions of the baseplate should be equal for all geometries, because this limits the number of introduced variables when testing them in the experimental set-up. With a baseplate area of 30x30 millimeters, gripper **D2** generates 0.31 N, **D1** generates 0.67 N and **D05** generates 1.52 N. These values are within the measuring range of the available load cells for this project. The proposed baseplate area of 30x30 millimeters is validated in the next paragraph.

Table 2.1: Required baseplate areas for the grippers to generate 1N adhesion, calculated with the ConicalPlate.m script.

	D2	**D1**	**D05**
Diameter pillar [mm]	2	1	0.5
Baseplate area [mm^2]	3200	1500	660
Length of gripper [mm]	56.7	38.5	25.6

2.3.3. TOWARDS A GRIPPER DESIGN

VALIDATION OF THE CALCULATED GRIPPER AREA

The gripper area values of Table 2.1 are verified with a simple calculation based on adhesion values from literature. Assuming that $\phi = 0.6$, the normal adhesion force of a square gripper [8] or a gripper with an array of liquid bridges [16] is both approximately 1 kPa, which is the same as 1 mN/mm^2. Generating 1 N of force with an adhesion of 1 kPa requires a gripper area of 1000 mm^2. Since the gripper area is square, the length of the sides is $\sqrt{1000} = 32$ mm. Therefore the chosen gripper area of 30x30 mm^2 seems reasonable.

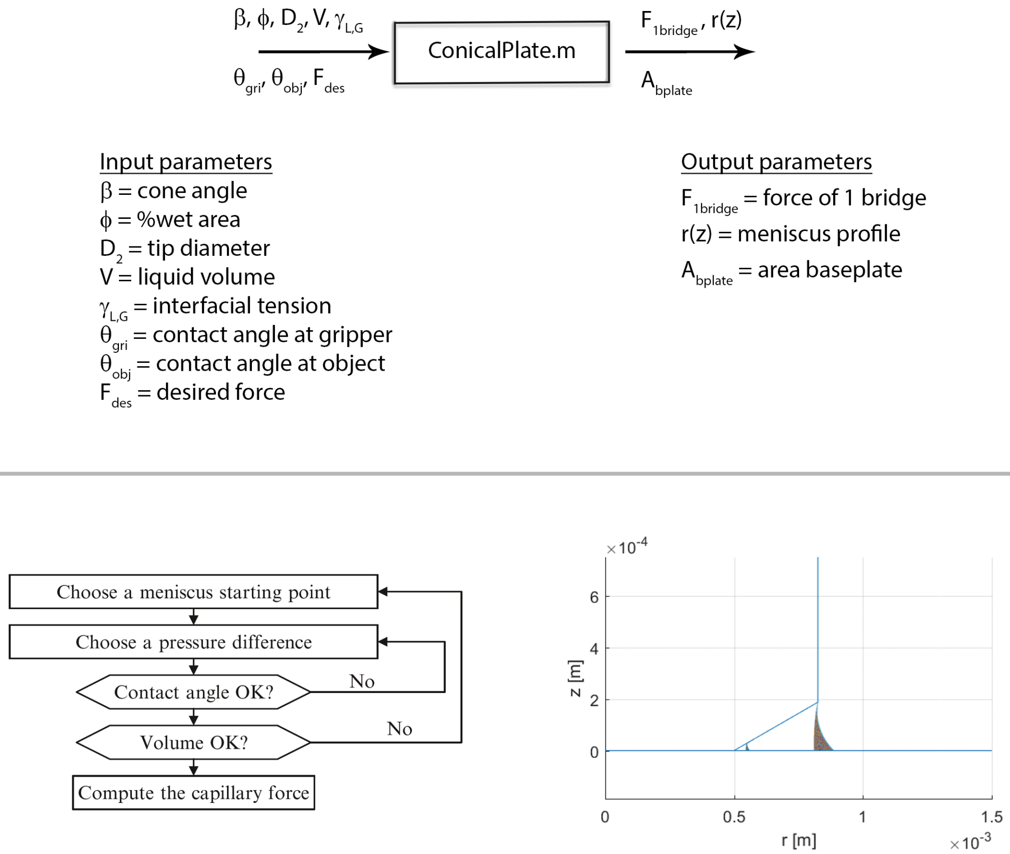

Figure 2.8: Schematic input and output of the MATLAB model ConicalPlate.m which calculates the meniscus shape between a conical gripper and a plate for the specified boundary conditions and input parameters. Bottom left, schematic of the iterations of the method, adapted from [1]. Bottom right, example graph of the calculated menisci profiles for 2 starting points on the grippers' surface using the double-shooting approach.

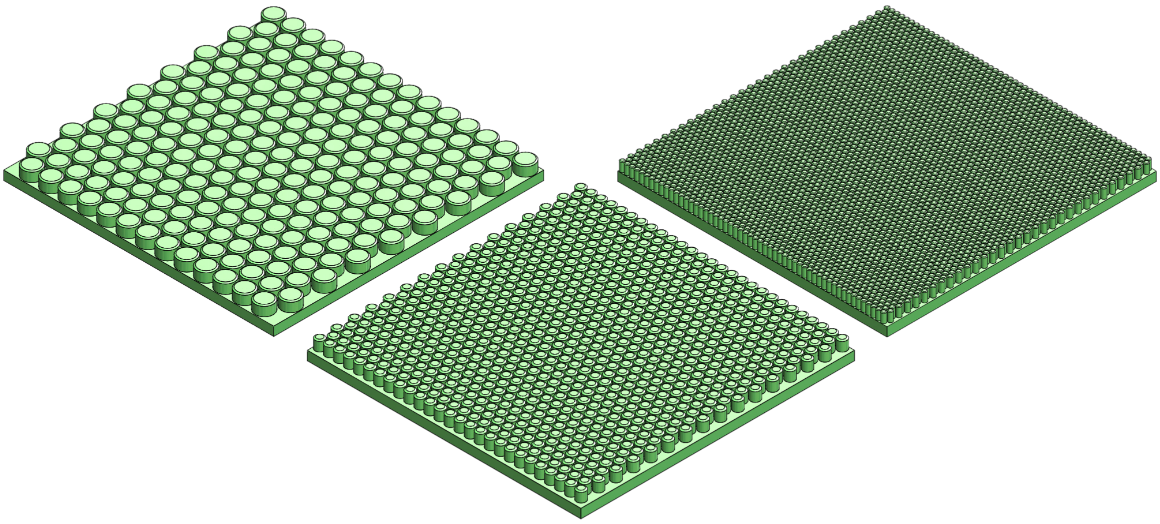

Figure 2.9: Isometric views of the pillar structures on a 30 by 30 millimeter baseplate with pillar diameters 2, 1, and 0.5 millimeters, shown in the order from left to right.

DIMENSIONS OF PILLAR STRUCTURES

Three pillar structures with the estimated dimensions from 2.3.2 and the previous section are made in Solidworks. Spacing S and the number of pillars n are adjusted to fit the array of pillars into the baseplate area of 30 by 30 millimeters and achieve the desired %wet area ϕ of 0.6. Then, the cone height and diameter of the tip were chosen to match the %contact area ζ of 0.4. Figure 2.9 depicts the pillar structures and Table 2.2 lists their dimensions. In the next chapter, the fabrication method for these pillar structures will be specified, as well as how their adhesion performance can be assessed.

Table 2.2: Dimensions of the pillar structures in the CAD model.

	D2	**D1**	**D05**
Cone angle β [°]	31	31	31
Diameter pillar [mm]	2	1	0.5
Diameter tip [mm]	1.652	0.795	0.403
Height tip [mm]	0.105	0.062	0.029
Number of pillars n	168	725	2822
ratioContact ζ [%]	39.1	42.2	41.0
ratioWet ϕ [%]	58.6	63.6	61.6
Spacing S [mm]	0.435	0.184	0.102

2.4. RESEARCH QUESTION AND HYPOTHESIS

The research question for this work as stated in 1.5, was: *"Can a purely capillary-based device provide enough grip to manipulate bowel tissue?"*. However, the proposed method of gripping tissue using forces on the tissue in the out-of-plane direction, is uncommon. Therefore, we focus the effort of this research on how adhesion can be maximized for the gripper. The friction properties of the resulting gripper shapes are evaluated, but this is a secondary objective in this research.

The hypothesis will be: *"On a mildly hydrophobic substrate, for a constant gripper area and % wet area, adhesion increases with decreasing pillar diameter."*

3

MATERIALS AND METHODS

3.1. FABRICATION OF THE MOULDS

Pillar structures are made according to the dimensions stated in Section 2.3.3. The fabrication of the master is described in this paragraph. The master is the negative of the array of pillars and is a part of the complete mould. The three masters used to cast the pillar structures in are made from an aluminum block, each with a total surface of 40 by 40 millimeters. An array of holes of diameter D_1 are drilled to drilling depth L_1 into the block. The in-plane configuration of the holes to one another is hexagonal and the distance between the holes is given by the spacing S. With wire Electric Discharge Machining a 0.5-millimeter-thick sheet is sliced off. The calculated dimensions of the masters are listed in Table 3.1. A 3D visualization and a section view of the master are depicted in Figure 3.1.

Another part of the mould are the square frames. The function of the frame is to join the pillars to the same base. The frames are cut out of a 2-millimeter-thick aluminum sheet with a laser cutter to the following dimensions: an outer area of 40 by 40 millimeters and an inner square part of 35 by 35 millimeters. The frame is shown in Figure 3.2.

Table 3.1: Dimensions of the three masters. Their names begin with the base diameter, followed by the total area of the gripper.

	D2_30x30mm	*D1_30x30mm*	*D05_30x30mm*
Angle β [°]	31	31	31
Depth L_1 [mm]	0.395	0.438	0.471
Depth L_2 [mm]	0.105	0.062	0.029
Diameter D_{base} [mm]	2	1	0.5
Diameter D_{pillar} [mm]	1.652	0.795	0.403
Number of holes [n]	168	725	2822
Plate thickness [mm]	0.5	0.5	0.5
Spacing S [mm]	0.435	0.184	0.102

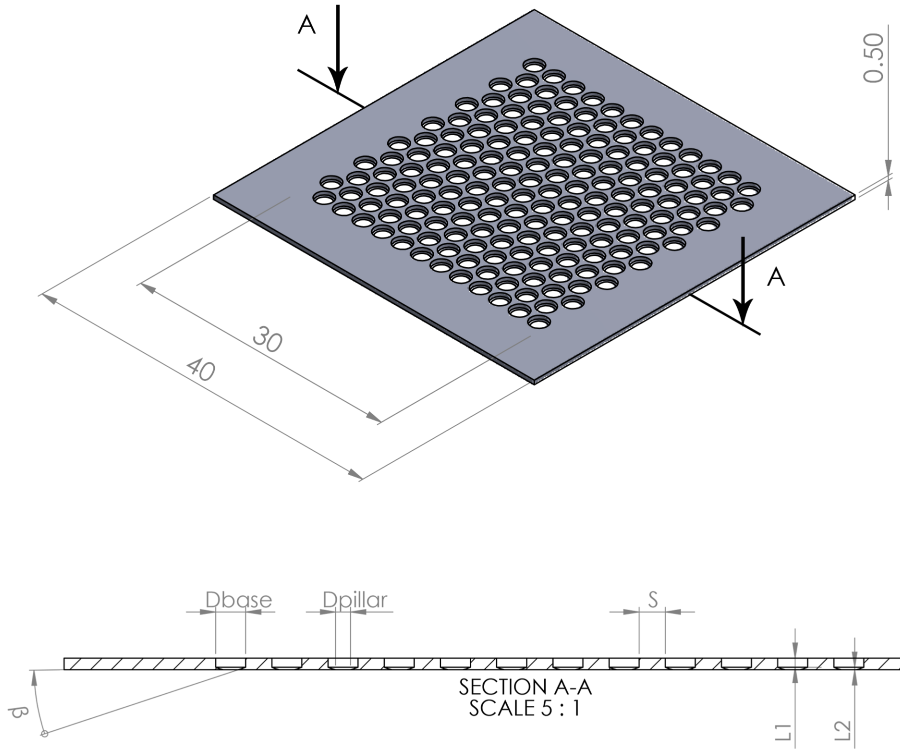

Figure 3.1: Top, the master *D2_30x30mm* used to cast the pillar structures in. Below, the section view of that master. Since the pillar structure is the negative of the master, the diameters of the mould are named D_{base} and D_{pillar} corresponding to the pillar dimensions. The spacing between the pillars is denoted by S and the cone angle is given by β.

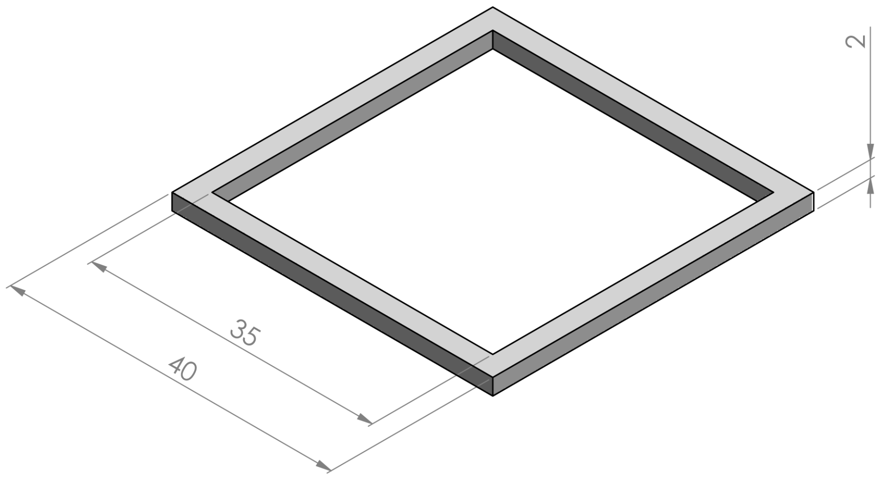

Figure 3.2: The square frame of aluminum which is placed on top of the master during fabrication. The units of the dimensions are listed in millimeters.

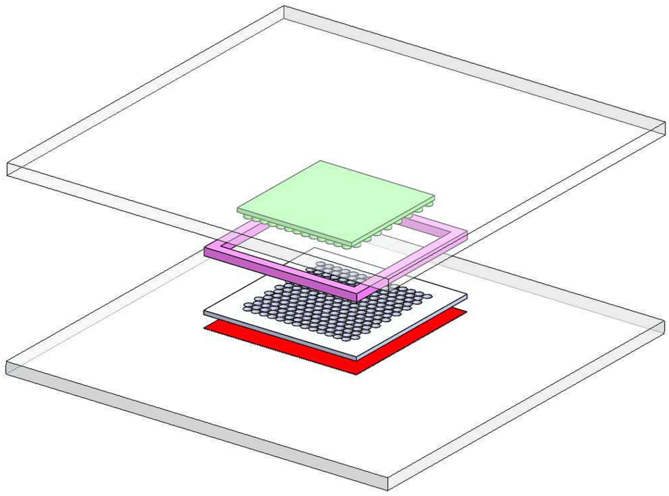

Fabrication steps
1. Cleaning of master
2. Mixing PDMS
3. Degassing PDMS
4. Tape off underside mould
5. Fixate mould
6. Pouring of PDMS
7. Degassing PDMS in mould
8. Top off mould with PDMS
9. Cover with glass plate
10. Place weight on top
11. Curing
12. Release glass plates and frame
13. Cut to 30x30 mm size

Figure 3.3: Right, exploded view of the mould which is used to cast the silicone (PDMS) in. The parts listed from the bottom to the top are: the glass plate (transparent), scotch tape (red), the master with an array of holes (white), the frame (pink) and the cured PDMS pillar structure (green) and the glass plate on top (transparent). Right, step-by-step fabrication of the gripper.

3.2. FABRICATION OF THE PDMS GRIPPERS

The right part of Figure 3.3 lists a brief summary of all fabrication steps. In the paragraphs below, the steps are explained in detail.

A mould is required to cast the pillar structures in, because the starting material is a viscous liquid that will be cured. Before fabrication of the gripper tip can start, a cleaning step is required to make sure that the mould is free from oil and other contaminants. The mould is cleaned with a soap solution, rinsed with water, cleaned in an ultrasonic bath during 5 minutes and dried with nitrogen gas. After the cleaning step, the conical part of the master is taped off with scotch tape, to prevent leakage during the degassing step. Next, the master is fixated on top of the smooth glass plate with the conical part facing downward, and the square frame is placed on top of the master, aligned properly and fixated with tape.

Curing agent and liquid polydimethylsiloxane (Sylgard 184, Dow Corning) hereafter abbreviated as PDMS, is weighted on an electronic balance and mixed in a ratio of 1:10 to amount to a total volume of approximately 10 mL. PDMS is chosen because its stiffness can be tuned easily by adjusting the mixing ratio and the material is safe to use on tissue. The liquid PDMS is degassed for about 5 minutes and poured in a thin stream into the mould. Entrapped air in the holes is removed with a second degassing step. After this step, some more liquid PDMS is poured into the mould until it is topped off again. A clean glass plate is placed on top of the frame using a tilting motion. This step ensures that the top side of the gripper tip will become flat. Figure 3.3 depicts an exploded view of the complete mould.

The complete mould, sandwiched between the glass plates, is placed inside an oven with a 2 kg weight on top as shown in Figure 3.4. The PDMS is cured at a temperature of 67 °C for two hours. After curing and cooling down to room temperature, the frame is carefully detached and the PDMS pillar structure is gently peeled along the edges from the master with a spatula, as depicted in Figure 3.4. In the case that the 35x35 mm frames were used, the PDMS pillar structure is cut to the size of 30 by 30 mm with a metal ruler and a snap-off utility knife.

The adhesion performance of the pillar structures will be compared with a flat reference sample. The method of fabrication for the flat sample is almost the same as for the pillar structures. The only difference in the fabrication method is that the master is left out. Instead, the underside of the frame was taped off with scotch tape. Figure 3.5 depicts the four final grippers.

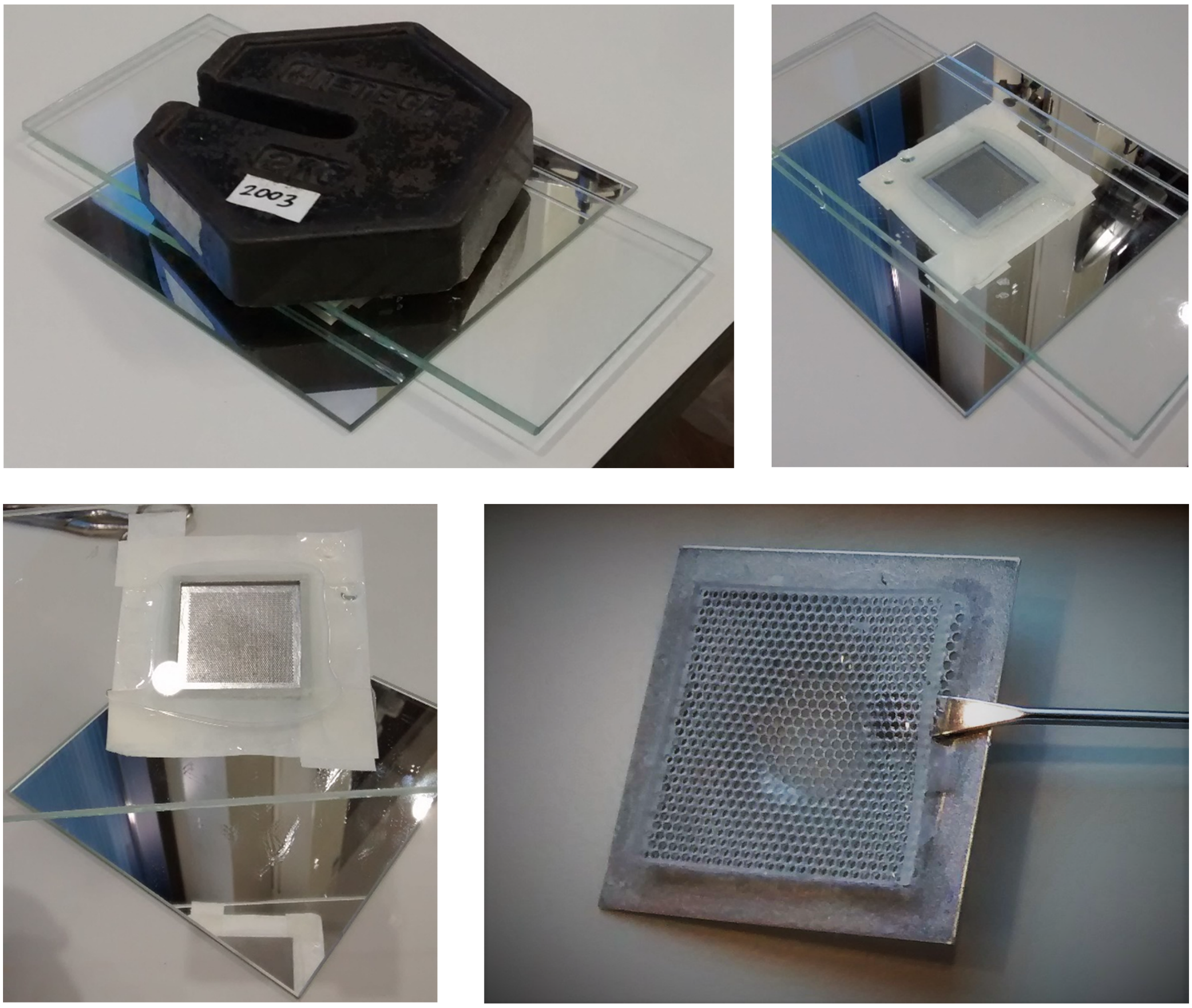

Figure 3.4: Photos of the fabrication process. Top left, the cured PDMS pillar structure is taken out of the oven. The mould has been sandwiched between two glass plates and a weight was placed on top. Top right, the weight is removed. Bottom left, the mould is detached from the bottom plate. Bottom right, the master *D1_30x30mm*. The 30 by 30 millimeter square frame and the tape at the underside have been removed. The PDMS pillar structure is gently peeled off the master along the perimeter using a spatula.

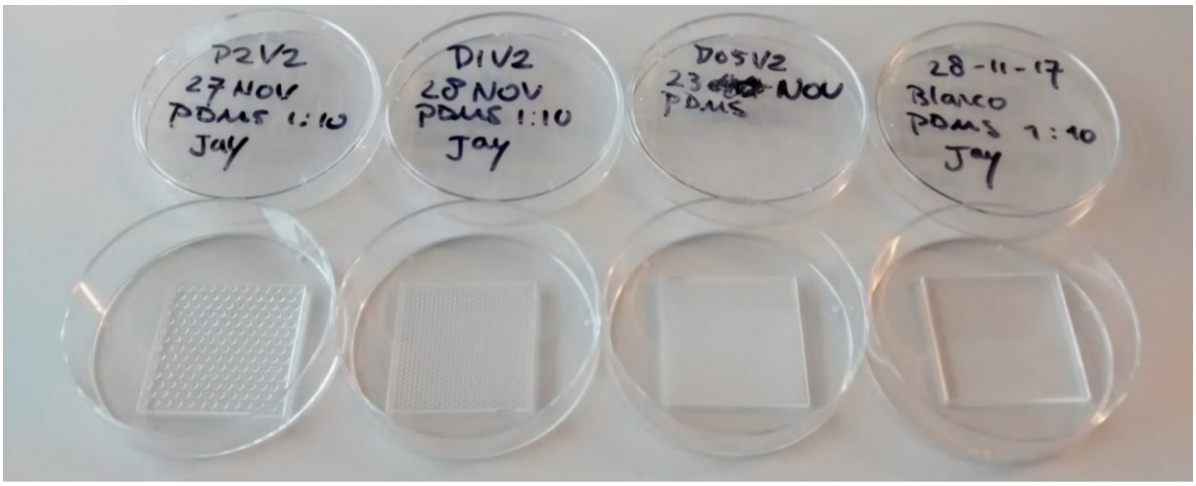

Figure 3.5: The four gripper geometries. From left to right, the pillar structures with diameters of 2, 1, and 0.5 millimeter respectively. The flat gripper on the right is the reference with which the pillar structures are compared.

3.3. ADHESION AND FRICTION MEASUREMENTS

An experimental setup was developed in order to measure the friction and adhesion of the four fabricated grippers. Since neither a standard experimental setup nor protocols were available, a series of pilots were conducted to improve the experimental setup and to determine which test conditions should be varied. In section 3.3.1 below, the aim of the pilots is explained. The experimental setup and procedures of the pilots 1 to 10 is not described, because no quantitative data is presented for these pilots and secondly, to keep the report concise. In sections 3.3.2 and 3.3.3 the setup of the friction and adhesion experiment is explained, for which quantitative data will be presented.

3.3.1. AIM OF EACH PILOT

Table 3.2 presents an overview of the conditions which have been tested for the eight adhesion and the three friction pilots. Each dot represents if the test condition was applied. The aim of each pilot is discussed in the next paragraph.

Table 3.2: Overview of the test conditions for all adhesion and friction pilots. The pillar structures are D2, D1, D05 and Fl is the flat reference sample. The PVA substrate is the mock-up tissue. No liquid is (-) and Gly stands for glycerol. Preload means that the gripper was pressed against the substrate prior to testing. Plasma means that the gripper underwent a plasma cleaning procedure to make the PDMS temporarily hydrophilic. Gripper placement with 1-step means that the gripper was attached to the connector, wetted and placed onto the substrate prior to the test. The 2-step condition means that the gripper was wetted and placed onto the substrate. Then, the connector was attached to the grippers' top side before testing. Video means that camera footage was taken during the test.

Adh. Pilot	Geometries				Substrate		Liquid			Retraction speed mm/s				Preload	Plasma	Fluid application		Video
Nº	D2	D1	D05	Fl	Glass	PVA	-	H2O	Gly	0.1	0.5	1	2			1-step	2-step	
1		•		•	•		•	•		•			•	•		•		
2		•		•	•		•	•		•			•			•		
3		•			•			•		•	•	•	•			•		
4		•		•	•		•	•				•			•	•		
5	•	•	•	•	•	•	•	•			•			•		•		
6			•	•				•	•		•						•	
7	•	•	•	•	•			•		•	•			•			•	•
8	•	•	•	•	•		•	•		•				•			•	•

Fri. Pilot	Geometries				Substrate		Liquid			Retraction speed mm/s				Preload	Plasma	Fluid application		Video
Nº	D2	D1	D05	Fl	Glass	PVA	-	H2O	Gly	0.1	0.5	1	2			1-step	2-step	
9		•		•		•	•	•		•			•			•		
10		•		•	•		•	•				•				•		
11	•	•	•	•	•	•	•	•			•					•		

1. The aim of the first pilot is to try out the adhesion setup and the measuring protocol for one pillar structure and the flat sample. Also, a suitable retraction speed is investigated.
2. The aim of the second pilot is to use the same test conditions as the first pilot to investigate if a newly fabricated gripper generates a higher adhesion force.
3. The aim of the third pilot is to investigate which retraction speed should be selected for the adhesion experiment. With a higher speed the measurements take less time, therefore more measurements can be taken. However, the contribution of viscous forces to the measured adhesion force is expected to increase.
4. The aim of the fourth pilot is to investigate if a more hydrophilic gripper exerts a higher adhesion force and whether this condition should be included in the experiment. To test this, the PDMS gripper was given a plasma cleaning treatment.
5. The aim of the fifth pilot is to apply a constant preload using a compression spring between the connector and the gripper. A second goal was to start testing on PVA to investigate if the pillar structures outperform the flat sample.
6. The sixth pilot has three aims. First, to test the 2-step gripper placement method. Second, to investigate how large viscous forces are with respect to the capillary forces using water and glycerol as liquid. Third, to test a new fluid application method: stamping the gripper on a wet cloth instead of dipping the gripper into the liquid.

7. The aim of the seventh pilot is to show the benefit of the 2-step gripper placement method and to reduce the spread in the data. Measures taken to reduce the spread: applying a constant preload with a 200-gram weight, using another connector and including a side-view camera in the setup.

8. The aim of the eighth pilot is to reduce the degrees of freedom of the connector to only a vertical translation to prevent the rotation and tilting of the gripper during lifting. To achieve this, a rigid 3D printed connector was directly secured to the force sensor.

9. The aim of the ninth pilot is to try out the friction setup and measuring protocol. The difference in friction forces between the dry and wet condition is investigated.

10. The aim of the tenth pilot is to find out how the tests on PVA should be conducted and to find which retraction speed should be selected for further friction tests.

3.3.2. FRICTION PILOT 11

EXPERIMENTAL DESIGN

We varied the following conditions in the friction experiment: the four gripper geometries, as shown in Figure 3.5, and two substrates: glass and PVA. The order of conditions is randomized. Each condition is tested ten times.

SUBSTRATES

Glass was used as reference material, and Polyvinyl alcohol (PVA) hydrogel as the tissue phantom. To make the hydrogel, ten grams of hydrolized PVA is dissolved into 90 grams of water at 95 °C whilst stirring continuously, as shown in the left of Figure 3.6. The dissolving takes half a day. The solution is then poured into a mould and undergoes 2 freezing cycles overnight, to increase the stiffness of the substrate. The mould, shown in Figure 3.6 on the right, is 3D printed from PMMA and parafilm is placed inside the mould to aid the release of the substrate. Three PVA substrates were prepared in this way.

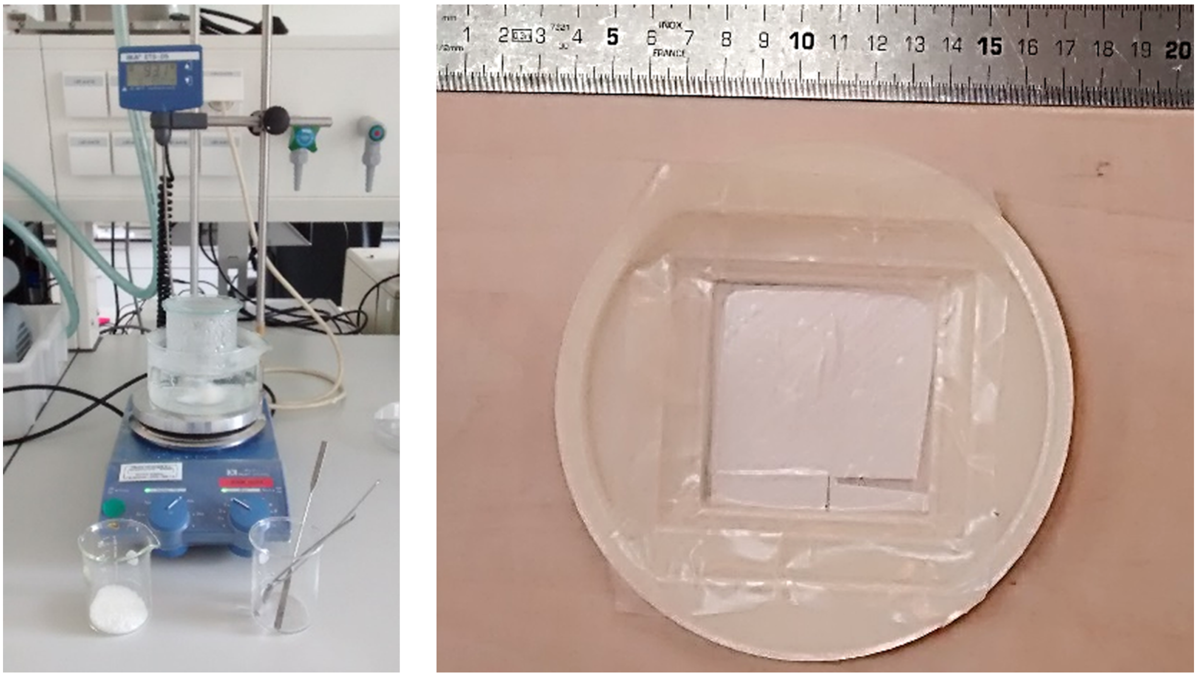

Figure 3.6: Left, dissolving the dry PVA into water to a 10 wt% solution. Right, the mould to cast the PVA solution in.

EXPERIMENTAL SET-UP

The friction set-up is shown in Figure 3.7. A force sensor is fastened to an aluminum block on the carriage of the vertically oriented linear stage (Aerotech, ACT115). A hook, situated below to the force sensor, connects a wire via a pulley to the friction-connector. The friction-connector is an aluminum plate which has double sized tape secured to its underside. The pulley system is secured to the baseplate. The gripper tip is located beneath the friction-connector and is in contact with the substrate. In the case that PVA is used, the substrate is fixated with a frame onto a lab jack. In the case that glass is used, a glass plate is fixated on top of a lab jack.

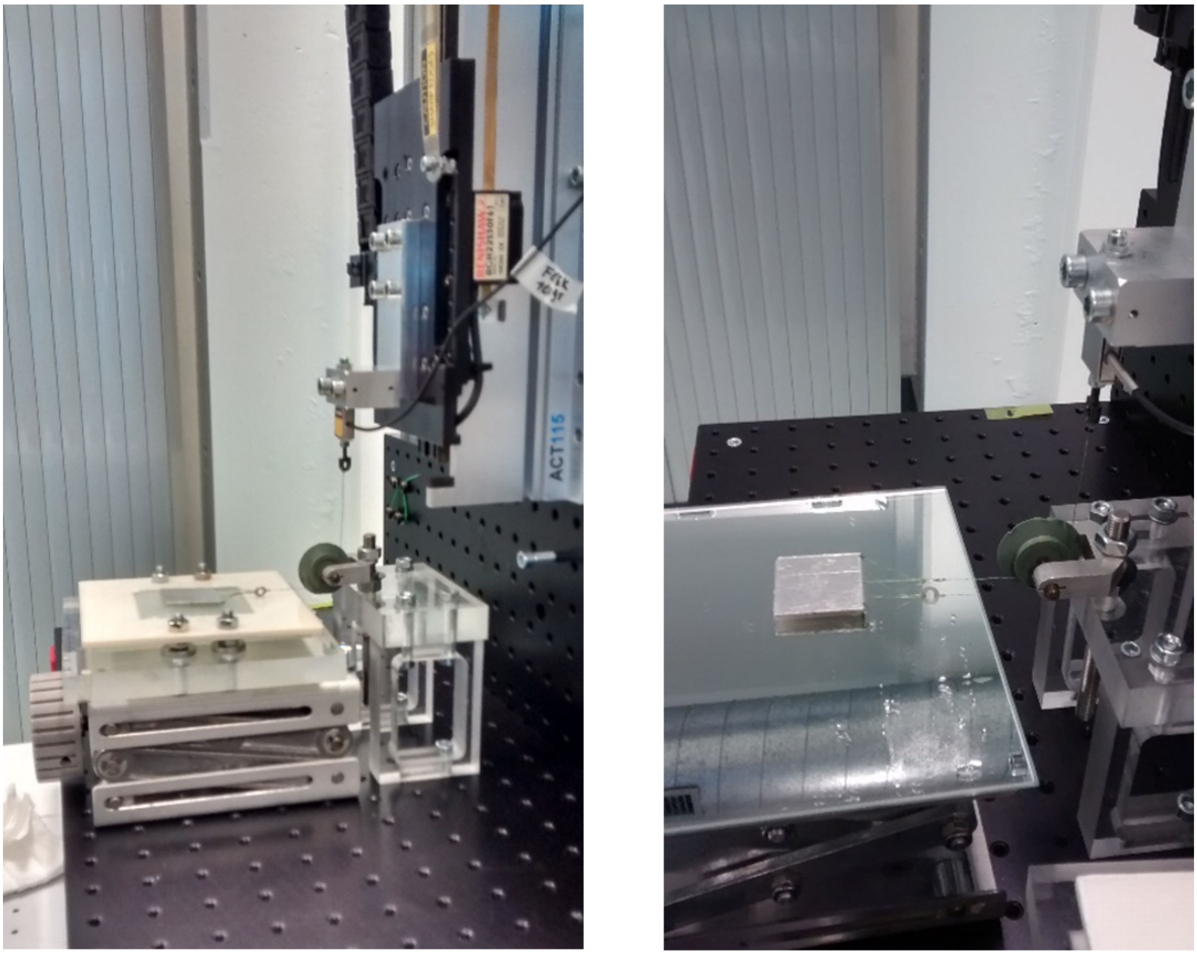

Figure 3.7: Left, side view of the friction set-up with the PVA substrate as mock-up tissue. Right, glass as substrate.

MEASUREMENT PROTOCOL

The table with the pulley is bolted directly underneath the force sensor. The PVA substrate is fastened with the frame on top of the lab jack and is bolted such that the center of the table is in line with the table with the pulley. For the tests on glass, the PVA substrate on top of the lab jack is replaced by a glass plate. The gripper is attached to the friction connector and the wire is secured to this connector. The height of the pulley system is adjusted such that the wire will pull the connector in a horizontal direction. The gripper, attached to the connector, is dipped into a Petri dish filled with demi water. Two steps are made on the glass substrate. The desired substrate is put into position and the gripper is placed on top. The linear stage is raised to the initial position (no tension on the wire). Then the measurement is started. The linear stage is moved up with 1 mm/s while recording the force data. After the measurement, the remaining liquid is removed. In the case that a measurement is done on PVA, the substrate is swapped.

3.3.3. ADHESION EXPERIMENT

EXPERIMENTAL DESIGN

We varied the following conditions in the adhesion experiment: the four gripper geometries, as shown in Figure 3.5, and the two substrates. The order of conditions is randomized per substrate. Each condition is tested ten times.

SUBSTRATES

Glass was used as reference material, and gelatin as tissue phantom. Although the PVA hydrogel used in the pilot tests is a better candidate for representing bowel tissue since it is slightly hydrophilic, gelatin was selected here. Gelatin remains transparent after curing whereas the PVA hydrogel becomes opaque. To verify that liquid bridges are present in the contact area between the substrate and the gripper, and thus that capillary forces are measured, a regular camera will be used. With the transparent substrate of gelatin the contact area can be visualized from below, but with the PVA hydrogel this is not possible. To make the gelatin substrate, dissolve gelatin powder (Dr. Oetker, product no. 1-50-230004) in water at a temperature of 60 degrees °C whilst stirring continuously for ten minutes to obtain a 10 wt.% solution. Pour five grams of the solution into a 55-millimeter Petri dish. Three gelatin substrates are prepared and cured in the fridge overnight.

EXPERIMENTAL SET-UP

The schematic drawing in Figure 3.8 depicts the set-up. An aluminum block is bolted to a vertically oriented linear stage (Aerotech, ACT115). A 2 lb load cell (FUTEK, LSB200) is bolted between the block and the 3D-printed connector. Double sided carpet tape is applied to the underside of the connector. Two lab jacks are secured to a baseplate and support a glass plate, as shown in the picture.

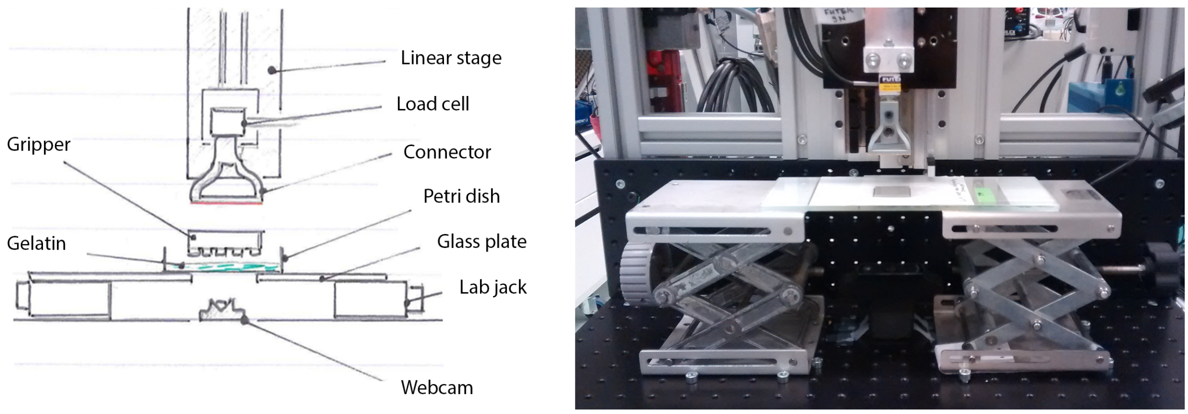

Figure 3.8: Left, schematic drawing of the experimental set-up. The set-up consists of a glass plate resting on top of two labjacks. A webcam is located below the plate. The load cell is bolted onto the vertically oriented linear stage and the 3D-printed connector is secured to the load cell. Double sided carpet tape is applied to the underside of the connector. For the experiments on gelatin, the gelatin-filled Petri dish is secured on the glass plate with double sided tape as shown in the schematic drawing. For the experiments on glass, the surface is taped off as shown in the picture on the right, except for a square region in the center which is the 'landing zone'.

For testing on glass, the surface is taped off except for a square 'landing zone'. The PDMS gripper is placed in this spot during the experiment. For testing on gelatin, a gelatin-filled Petri dish is secured on top of the glass plate with double sided tape, as shown in the schematic drawing.

A webcam (Logitech, C920) located below the glass plate captures the detachment of the gripper during the experiment. Figure 3.9 depicts snapshots of this detachment process on glass and gelatin. The linear stage and load cell provide the force-displacement data. Another camera (Panasonic, DMC-FZ7) captures the liquid footprint left on the substrate at the end of each test, as shown in Figure 3.10.

The gripper is first wetted and placed on the substrate, and is picked up by the connector during the downward stroke of the stage. A preload of about 3 Newtons is applied to make the top side of the gripper adhere to the connector during the upward stroke.

Controlling the exact preload was not possible with this setup. The contact between the gripper and the

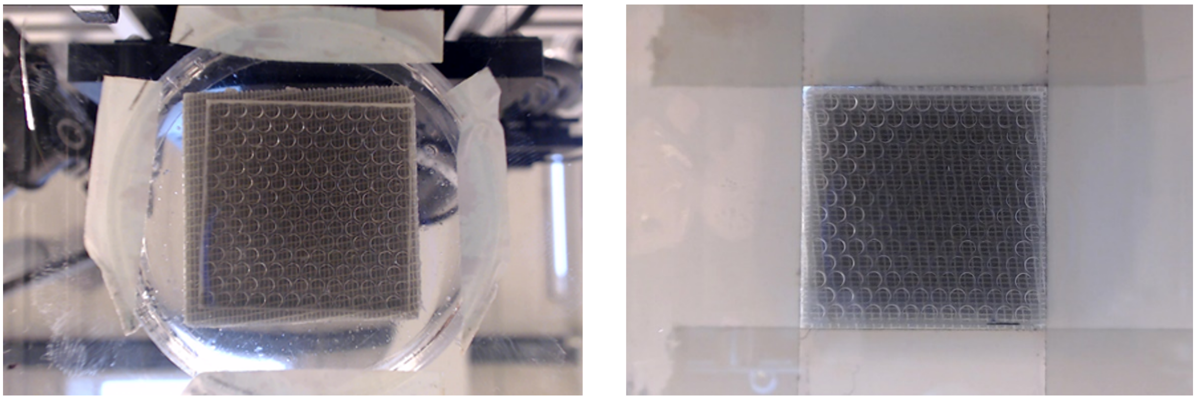

Figure 3.9: Images of the contact between the D2 pillar tips and the substrate. Gelatin as substrate is shown on the left, and glass as substrate is shown on the right. Since the gripper is transparent, the connector and adhesive tape can be seen through the gripper.

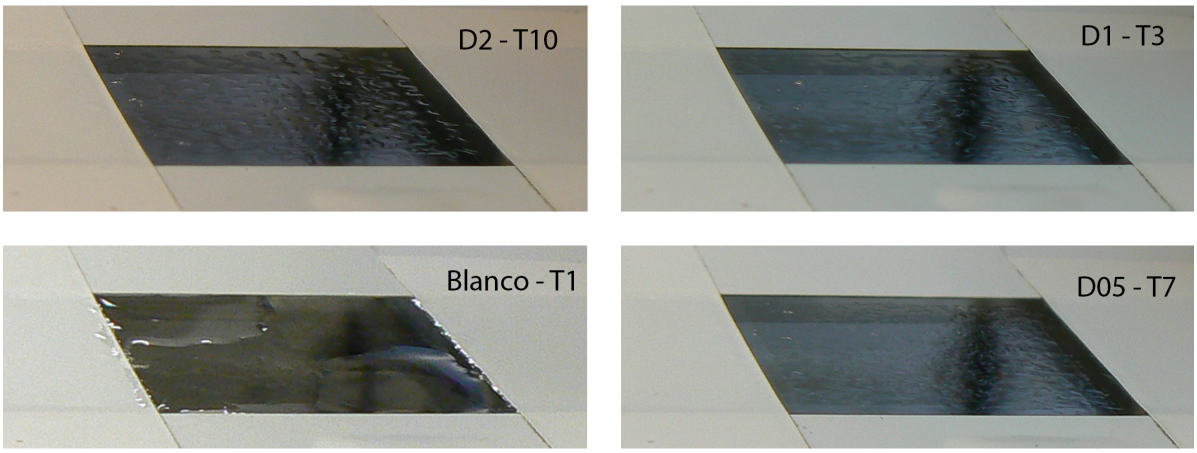

Figure 3.10: Footprints of water left behind on glass after an adhesion measurement finishes. The code in the top right corner stands for the geometry which was tested, followed by the test number.

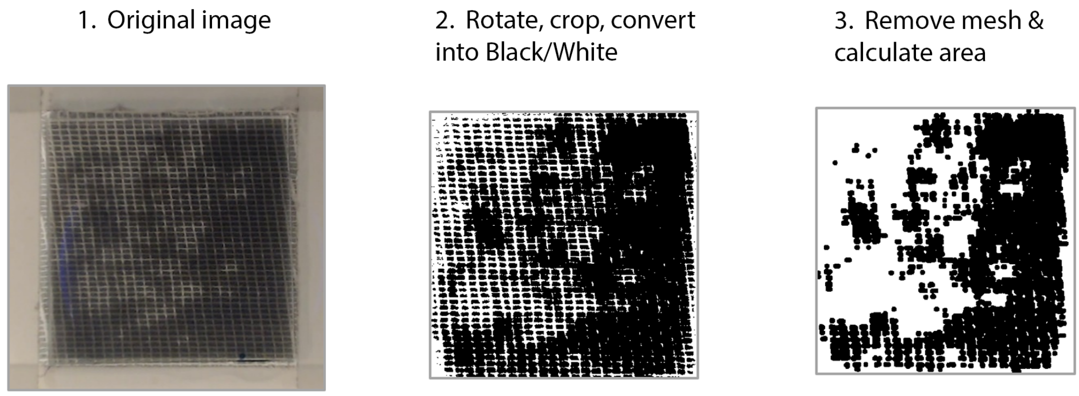

Figure 3.11: Steps taken in the script to estimate the contact area between the gripper and the connector. First, the original image is picked from the video footage during the preload phase. The left image is a blanco gripper on glass. Proper contact is established in the white regions. In the second step, the image is cropped along the gripper contours and converted into a black/white image. In the following steps, the mesh background is (partially) removed by growing and shrinking the black and white regions. The calculated contact area in this case is 484 of the 900 [mm^2] total area.

connector depends on the alignment of the gripper with the substrate and the preload settings. How well the gripper remains attached to connector is shown in the webcam images captured during the preload phase. These images are processed using a script to estimate the contact area, which is named 'connected area'. This measure describes the pressure distribution between the gripper and the connector. The steps of the script are shown in Figure 3.11, namely: convert the region of interest to black and white pixels, erode and dilate to grow and shrink regions in order to remove the mesh background. The full script can be found in Appendix D.

PROTOCOL FOR THE GLASS SUBSTRATE

The glass plate is cleaned with ethanol and a fiber-free tissue. After the cleaning step, the pillar structures of the gripper are stamped onto a wet cloth inside a flat case. When testing the flat gripper, 3 droplets are placed on the substrate using a disposable pipette and the gripper is placed on top of the liquid. The amount of fluid for the flat gripper is chosen such that no dry spots are present in the contact and that the liquid is not squeezed out of the contact during the test.

The height of the linear stage is set to 20 millimeters, leaving a gap between the gripper and connector. Now the height of both the labjacks is adjusted independently such that the adhesive tape under the connector makes uniform contact with the gripper. The webcam feed is used to guide this height adjustment process. When this process is finished, the linear stage is moved up. The gripper is now detached from the connector and the remaining liquid on the surfaces is removed. At this point the set-up is prepared for the actual measurement.

Measurement

Perform the same cleaning step and apply the liquid as described earlier on. Place the gripper on the substrate and lower the stage to an initial height of 21 millimeters, leaving a gap of 1 millimeter in between the connector and gripper. Select the value of the downward vertical stroke such that the connector applies a preload to the gripper and start the force measurement simultaneously with the webcam video. After the stroke is completed, move the stage up and take a photo of the liquid footprint left behind on the substrate, as shown in Figure 3.10.

PROTOCOL FOR THE GELATIN SUBSTRATE

For the gelatin substrate, the protocol is similar to the tests conducted on the glass substrate. The difference is that for gelatin, a gelatin-filled Petri dish is secured on top of the glass plate prior to the measurement, as shown in Figure 3.8 and 3.9. The three prepared gelatin substrates are swapped after each test to keep them cool.

4
Results

4.1. Pilots

To improve the experimental set-up and to decide which conditions should be investigated, a series of of eleven pilots were conducted: eight are adhesion tests and three of them are friction tests, see Table 3.2. Since for most of the pilots only 3 measurements were done, only qualitative results will be described here. An exception is friction pilot 11, which has 5 measurements per condition and for which quantitative data are presented. Below, the most important observations are listed.

1. In the first pilot the adhesion of D1 and the flat sample is evaluated on glass. The wet and dry conditions are tested and the retraction speeds 0.1 and 2 mm/s are used. A preload was manually applied to the gripper by pressing it onto the substrate. The fluid remaining on the substrate after the test was only present at the perimeter of the gripper, but not at the center. This fluid distribution is caused by the uneven thickness of the gripper.

2. In the second pilot, the same conditions are tested as in pilot 1. The difference is that the grippers were made with a 35x35 frame in the mould instead of a 30x30 frame. The newly made grippers had a better fluid distribution. The adhesion of the gripper D1 with H2O at 2 mm/s increases compared to the first pilot.

3. In the third pilot, the adhesion of gripper D1 is evaluated on glass with water as liquid using four different retraction speeds: 0.1, 0.5, 1 and 2 mm/s. After securing the gripper to the connector and retracting it from the glass substrate, they are not lifted off perpendicularly to the surface. The connector, whose motion is not constrained to a single degree of freedom, tilts and rotates during retraction. The tilting and rotating also happened in the first two pilots. At a retraction speed of 0.1 mm/s, the tilting and rotating of the connector can be observed as 2 peaks in the force-time data. At higher retraction speeds the connector tilts less and only a single peak is recorded in the force-time data.

4. In the fourth pilot, the effect of a plasma cleaning treatment on the adhesion of gripper D1 and the flat sample is investigated on the glass surface in the dry and wet condition. The retraction speed 1 mm/s was used. A plasma cleaning treatment on the PDMS gripper only seems to increase adhesion for the dry tests, based on the results (3 data points per tested condition). Therefore plasma cleaning is not considered as a test condition in the final adhesion experiment.

5. In the fifth pilot, the adhesion of all four grippers was tested on the substrates glass and PVA, in the dry and wet condition at a retraction speed of 0.5 mm/s. Similar to the previous pilots, the gripper is wetted by dipping it into Petri dish filled with demi water. The difference in the setup compared to the previous pilots was the connector, which can apply a preload with a spring. The preload value was about 0.5 N on glass and 0.4 N on PVA. The preloads are not constant due to different stroke lengths. Also, the gripper is still not lifted off parallel to the surface, because the tilting and rotation motions are not constrained. The measured maximum adhesion values per gripper have a large spread. The two observations mentioned (preload not constant and no parallel liftoff), and a lack of control over the applied liquid volume are the suspected causes for the large spread in the data. Consequently, no

relationship could be found between the diameter of the pillar structures and the measured adhesion. The flat sample outperformed the pillar structures.

6. In the sixth pilot, the adhesion of D05 was compared to the flat sample, using water and glycerol as liquid and a retraction speed of 0.5 mm/s. Compared to the previous pilots the gripper placement method differs. In this pilot, the gripper is stamped onto a wet cloth, placed onto the substrate and then the connector is attached. Although the surface tension of glycerol is lower than water (60 versus 72 mN/m), the adhesion of the geometries D05 and the flat sample with glycerol was higher compared to using water. This means that viscous forces were present. The viscous effect for the flat sample was larger compared to D05.

7. In the seventh pilot, the adhesion of all four grippers was tested on glass with retraction speeds of 0.1 and 0.5 mm/s. A constant preload was applied using a weight of 200 grams and a camera at the side of the setup was used to judge whether the measurements were valid. Pilot 7 was tested with similar conditions to pilot 5. Differences in the method were the gripper placement method (2-step), the constant preload and the connector which was used. In pilot 7 the connector was pulled up with one wire in the center, instead of 4 wires at each corner. Comparing the results of pilot 7 with pilot 5, the adhesion on glass at a retraction speed of 0.5 mm/s improved more than twofold. However, the spread in the force values increased as well. Still, the new connector tilted as well, so the improvement in adhesion is likely caused by the gripper placement method.

8. In the eighth pilot, the adhesion of all four grippers was evaluated on glass with a retraction speed of 0.1 mm/s, with the condition dry or H2O. Every condition was tested five times. A 3D-printed rigid connector was used to constrain the tilting and rotating motions that occurred during the previous adhesion pilots. A webcam was added to the setup to observe the contact area between the gripper and substrate. Out of 40 measurements only 8 were valid, because the gripper peels off the connector during retraction. With the webcam videos was observed that the top side of the gripper did not uniformly adhere to the connector. This is likely to be the cause of the peeling. During the peeling, a front of liquid bridges detaches, instead of all bridges at once. Using calipers, a 0.1 millimeter difference in thickness of the grippers was measured. For the final adhesion experiment, the grippers will be manufactured with a flat top side, because the goal is to ensure uniform contact between the grippers' top side and the connector.

9. In the ninth pilot, the friction forces of D1 and the flat sample were measured on a glass substrate. The grippers were pulled across the surface with speed of 1 mm/s, and the test conditions for the liquid were dry and H2O. The gripper placement method was in a single step, and the liquid was applied by dipping the gripper together with the connector in a Petri dish filled with water. Two steps were applied on the glass substrate prior to the test. The friction of grippers D1 and the flat sample in the cases without liquid shows stick-slip behavior on glass. With a liquid present, no stick-slip is observed.

10. In the tenth pilot the friction forces of D1 and the flat sample were measured on the PVA substrate. The grippers were pulled across the surface with speed of 0.1 and 2 mm/s, and the test conditions for the liquid were dry and H2O. The gripper placement method is similar to pilot 9. When comparing the wet and dry condition for the flat sample on PVA, a higher speed leads to a higher friction. However the effect of speed on friction is larger for the dry case compared to the wet case. The friction values recorded with the gripper D1 in the wet and the dry case are almost similar. The PVA substrate was not properly clamped, so for the following pilot, the PVA substrate is clamped with a frame. The way to rule out relaxation effects of the PVA in new tests is to use three substrates and swap them after each measurement.

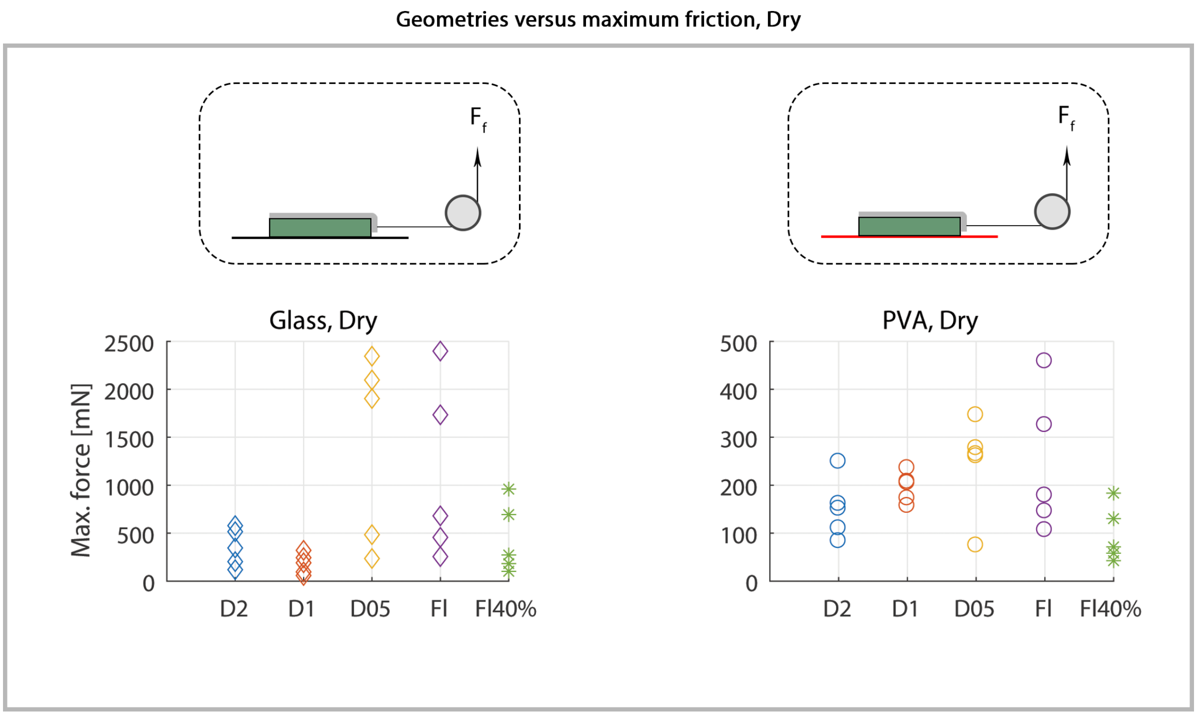

Figure 4.1: Top, schematic drawings of the friction test. Bottom, graphs of the maximum friction forces before the gripper starts sliding across the substrate, plotted for each geometry. No liquid was applied. Fl40% is not a geometry, but a correction such that the contact area of the flat sample matches the pillar structures. The substrates are Glass and PVA. The PVA hydrogel is clamped with a frame during the friction tests. No preload was applied while performing the friction tests.

11. In the eleventh pilot the maximum static friction forces are tested on the substrates glass and PVA. The applied retraction speed is 0.5 mm/s and each condition (Dry, H2O, Glass, PVA, 4 geometries) is tested five times in a random order. The test results in the dry case and the wet case are presented in Figure 4.1 and 4.2, respectively.

    11.1. **Geometries versus maximum friction (dry)**
    On glass, the maximum static friction values for D2 are between 119 – 578 and for D1 between 59 – 321 mN. For D05 two clusters are shown. The lowest values are 236 and 484, and the highest values are 1904 and 2345 mN. The flat reference sample has also two clusters with the lower values 256 and 680, and the highest values are 1734 and 2398 mN. The effects observed for the tests on glass are the following. First, D05 and Fl have two clusters. Second, assuming equal contact area, D2 has the highest mean friction among the grippers except for the high clusters.

    On PVA, the measured friction values of D2 are between 84 – 249 and for D1 between 157 – 236 mN. For D05 most of the values are between 261 – 349, but a value of 75 mN was also measured. For the flat sample the values in the lower range are 107 – 179 and in the higher range 326 and 549 mN. The effects observed for the tests on PVA are the following. First, the ranking of the mean friction values of the grippers with pillars is from low to high: D2, D1, and D05. Second, the average friction of D05 and Fl is comparable: 245 and 243 mN.

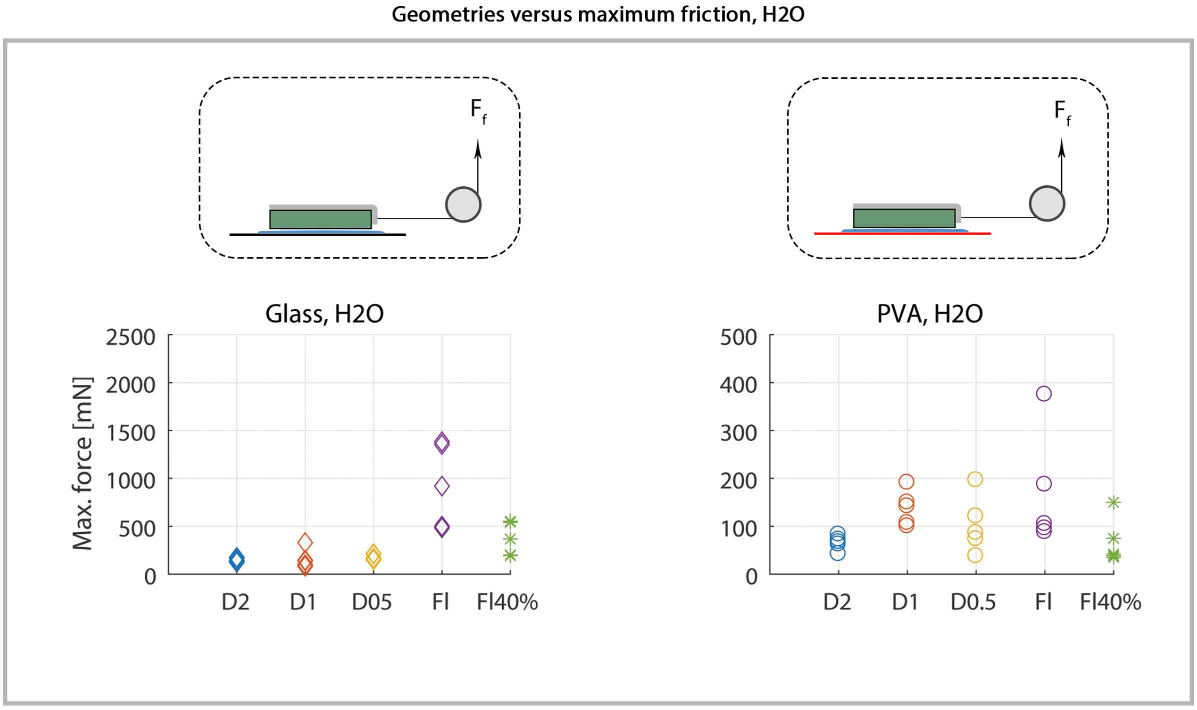

Figure 4.2: Top, schematic drawings of the friction test. Bottom, graphs of the maximum static friction forces with H2O as liquid, plotted for each geometry. Fl40% is not a geometry, but a correction such that the contact area of the flat sample matches the pillar structures. The substrates are Glass and PVA. The PVA hydrogel is clamped with a frame during the friction tests. No preload was applied while performing the friction tests.

11.2. **Geometries versus maximum friction (H2O)**

On glass, the measured friction values for D2 are between 125 – 176 and for D1 between 83 – 146, with 330 mN as maximum value. For D05 the values are between 125 – 215, and for the flat sample the values range between 484 – 1383 mN. The effects observed for the tests on glass are the following. The grippers with pillars: D2, D1 and D05 have mean friction values close to each other. The flat sample generates a higher friction compared to the other grippers, even when corrected for the contact area.

On PVA, the friction values of D2 are between 42 – 83, for D1 between 100 – 191, and for D05 between 38 – 197 mN. Three of the data points for the flat sample are between 88 – 105 and two values are further apart: 187 and 375 mN. The effect observed for the tests on PVA is that the average friction of D1 lower is compared to the flat sample, but with a correction for the area (Fl40%), the average friction of D1 is higher.

Comparing friction values on PVA (Dry & H2O)

When comparing the friction on the PVA substrate for the dry and wet case, the same trend in average friction values can be observed. The order of the grippers, from low to high generated friction is: D2, D05, D1. However, D05 performs relatively worse with the liquid compared to the dry case.

4.2. ADHESION EXPERIMENT

4.2.1. APPLIED PRELOAD

The preload that has been applied prior to the adhesion measurement is plotted per gripper in Figure 4.3 for both substrates.

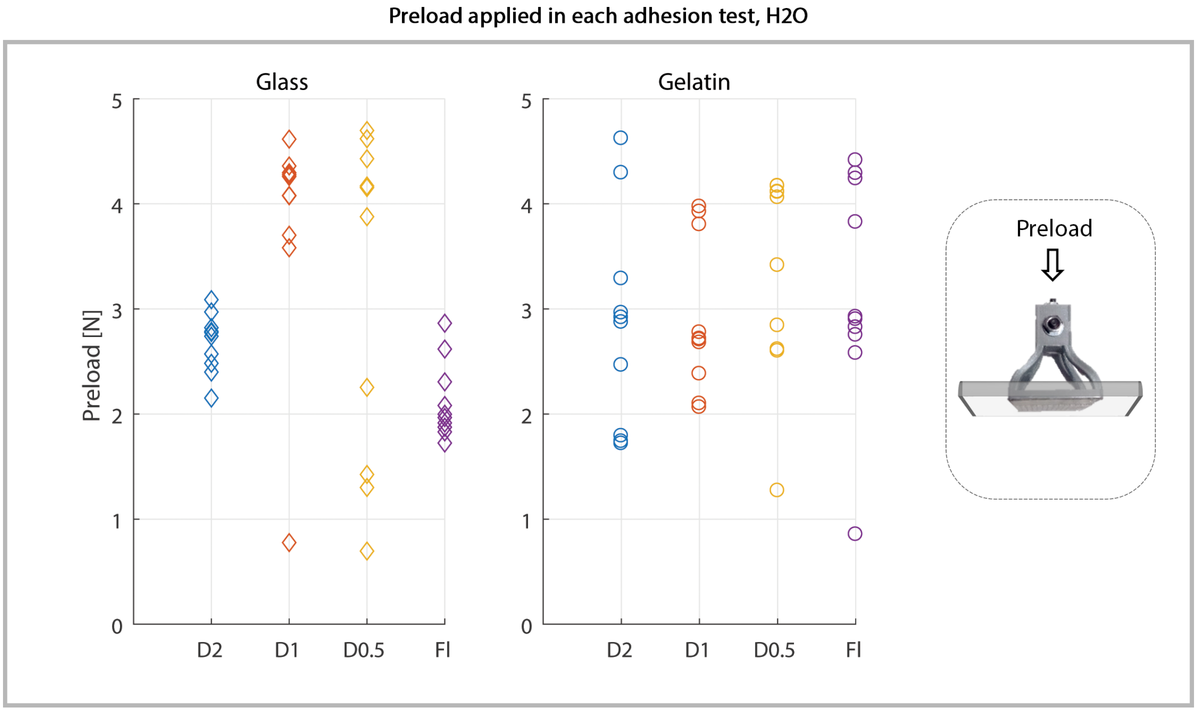

Figure 4.3: Preloads applied during the adhesion tests, for both substrates. The image on the right shows how the preload was applied on the gripper, namely, by pressing the connector downwards perpendicular to the substrate's surface.

Preload applied in each adhesion test

On glass, the applied preloads for D2 are between 2.1 - 3 N. For D1 the values are between 3.6 - 4.6, except for a low preload value of 0.8 N. With D05 the values have a larger range. Six values are between 3.9 - 4.7 N and the other values are 0.7, 1.3, 1.4 and 2.3 N. For the flat sample the values are between 1.7 - 2.9 N.

On gelatin, the applied preloads for D2 are between 1.7 - 4.6 and for D1 between 2 - 4 N. The values for D05 are between 2.6 - 4.1, except for the value 1.3 N which is outside this range. Preloads applied to the flat sample are between 2.6 - 4.4, except for a low preload of 0.9 N.

The effects of the substrate on the applied preloads are the following. First, for most of the applied preloads on glass the difference between minimum and maximum preload is about 1 N, whereas on gelatin the preload values lie further apart. Second, the averages of the preloads per gripper for gelatin are closer to each other, compared to the mean values for glass.

4.2.2. MAXIMUM ADHESION FORCE

The maximum adhesion values are extracted from each force measurement. These adhesion values are plotted against the gripper geometries in Figure 4.4 for both substrates.

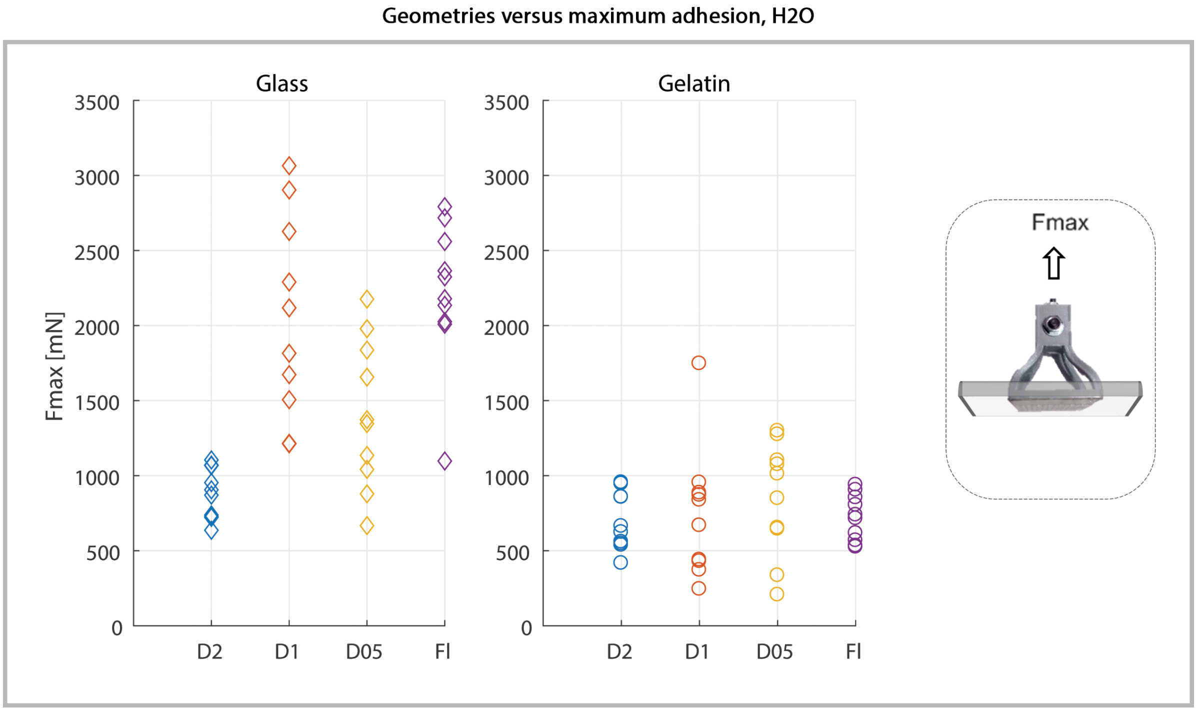

Figure 4.4: Maximum adhesion forces on both substrates for each geometry, with water as liquid. Left graph, results of the adhesion experiment on the glass substrate. Right graph, results on the gelatin substrate. The image on the right shows how the maximum adhesion force Fmax was measured, namely, by retracting the connector perpendicular to the substrate's surface.

Geometries versus maximum adhesion (H2O)

On glass, the maximum adhesion forces measured with water as liquid are for D2 between 637 - 1276 mN. The values for D1 are between 1213 - 3065 and for D05 between 667 - 2176 mN. The values for the flat sample are between 2009 - 2792 and a lower value of 1098 mN was measured outside this range.

On gelatin, the maximum forces for D2 are between 418 - 956 mN. Most of the values for D1 are between 245 - 955, but a high value of 1747 mN was measured as well. For D05 the range in values is 207 - 1299 and for the flat sample between 526 - 940 mN.

The effects of the substrate on the measured adhesion values are the following. For all grippers, the adhesion on gelatin becomes lower compared to the tests on glass, and the spread in the adhesion values decreases as well. Especially D1 and the flat sample perform significantly worse on gelatin compared to glass. On glass, D1 and the flat sample have the highest mean adhesion compared to D2 and D05, but on gelatin there are no clear effects of the gripper shape on the mean adhesion.

4.2.3. CONTACT AREA BETWEEN CONNECTOR AND GRIPPER

The graphs of Figure 4.5 present the connected area values for each adhesion measurement. This area Ac is located between the grippers' top side and the connector, as indicated in the image on the right.

Geometries versus connected area between gripper – connector

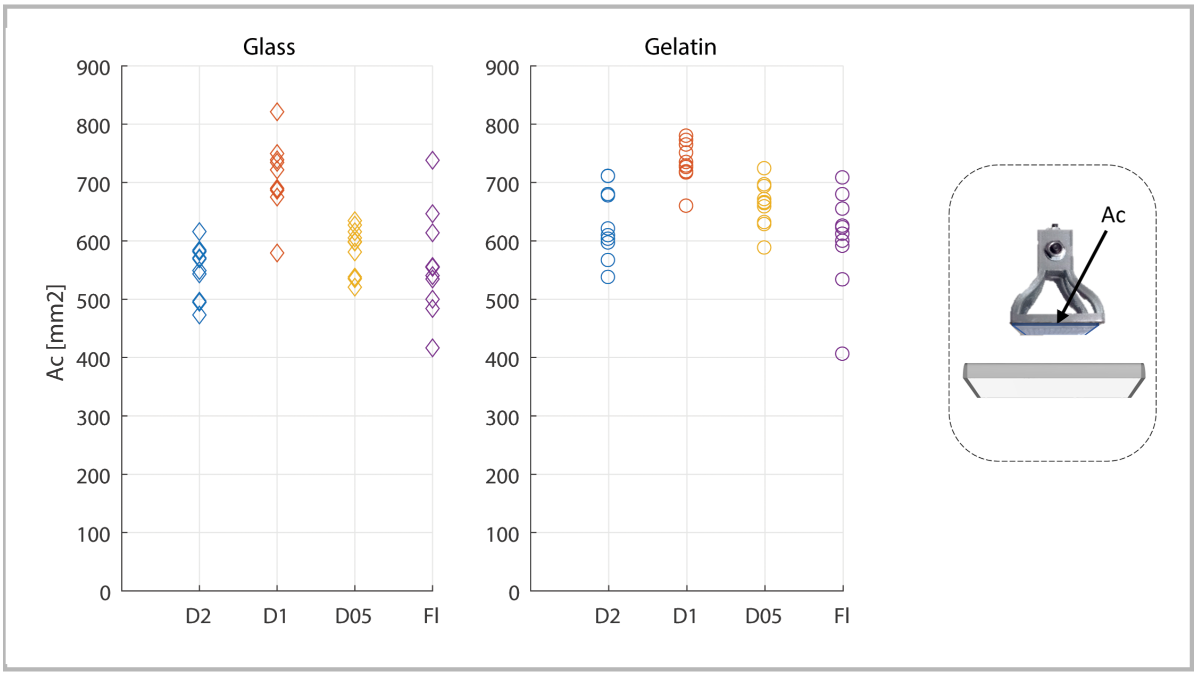

Figure 4.5: Left graph, connected area Ac calculated from the images taken during the adhesion experiments on glass. Right graph, the values for the gelatin substrate. The arrow in the image on the right points to the area Ac, which is located between the grippers' top side and the connector.

Geometries versus connected area

On glass, the connected area values of D2 are between 473 – 616 mm^2. The values for D1 are in the range of 675 – 750, except for 579 and 821 mm^2 which are outside this range. For D05 the values are between 521 – 635 mm^2. Eight values for the flat sample are between 484 – 647, the two remaining minimum and maximum values are 417 and 738 mm^2.

On gelatin, the values for D2 are between 537 – 710 mm^2. The values for D1 are between 716 – 779, except for 659 mm^2. For D05 the values range between 587 - 723 mm^2. The flat sample has values between 590 – 707 and two lower values: 405 and 533 mm^2.

The effect of the gripper shape on the connected area for both substrates are: the mean of the Ac values of D1 is the highest followed by D05, the flat sample and D2. Secondly, the connected area Ac of all the grippers becomes higher on gelatin compared to glass.

4.2.4. EXERTED PRESSURE BY THE GRIPPER ON THE SUBSTRATE

The local pressure exerted by the gripper on the substrate is shown in Figure 4.6, assuming multiple equal liquid bridges. The global pressure exerted by the gripper on the total area of 30 by 30 millimeters is shown in Figure 4.7.

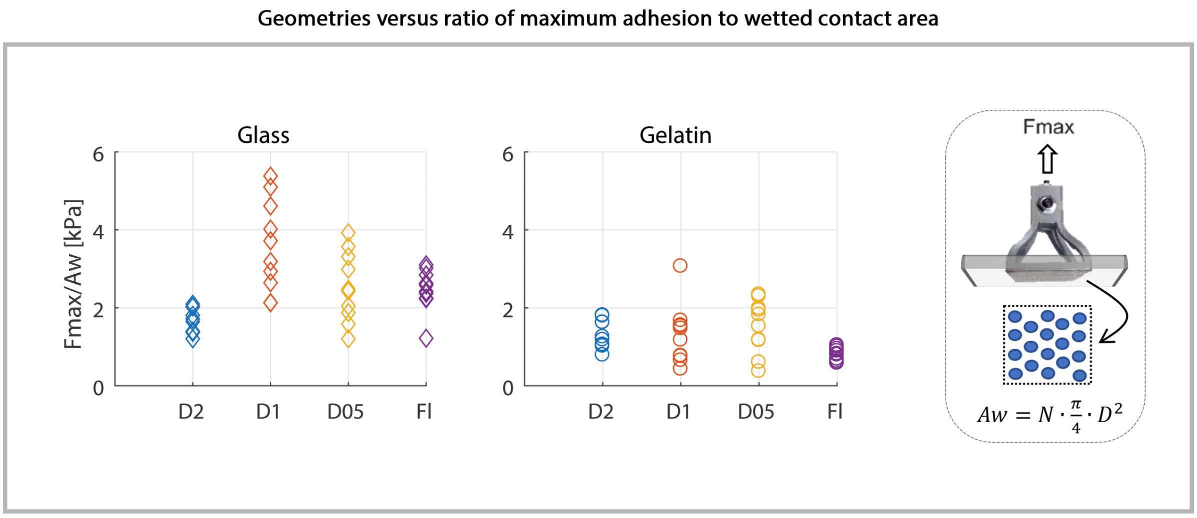

Figure 4.6: Calculated pressure that the gripper exerts on the substrate through the liquid bridge(s). Left graph, results of the adhesion tests on glass, the right graph is for the gelatin substrate. The image at the right shows what the ratio Fmax/Aw along the y-axis of the graphs mean, namely: Fmax is the maximum adhesion force and Aw is the total wetted area on the substrate. The formula on the right is the calculation for the wetted area, with N being the number of pillars and D the tip diameter. For the flat sample Aw is its total surface.

Geometries versus ratio of maximum adhesion to wetted contact area

On glass, the calculated pressure that the gripper exerts through the liquid bridges is for D2 between 1.2 - 2.0, for D1 between 2.1 - 5.4 and for D05 between 1.2 - 3.9 kPa. The flat sample has values between 2.2 - 3.1 and a lower value outside this range of 1.2 kPa.

On gelatin, the values for D2 are between 0.8 - 1.8 kPa. For D1 the pressure is between 0.4 - 1.7 and with a high value of 3 kPa. The gripper D05 has values between 0.4 - 2.3 and the flat sample has values between 0.6 - 1.0 kPa.

As also observed in Figure 4.4, the strongest effect of the gripper shape on the calculated pressure is that D1 performs worse on gelatin compared to glass. On gelatin D05 generates the highest mean pressure.

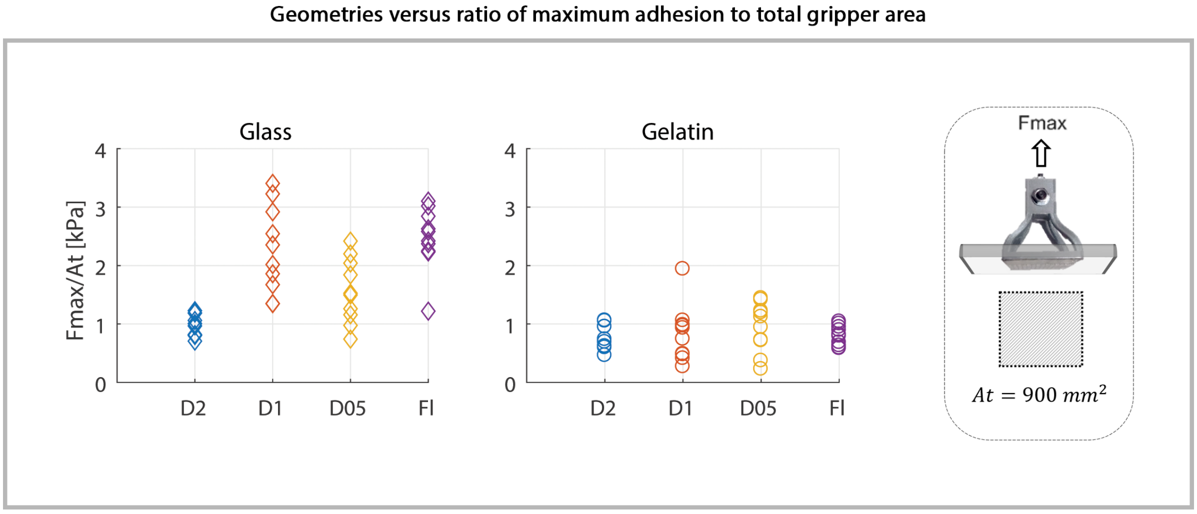

Figure 4.7: Global pressure that the gripper exerts on the substrate. Left graph presents results of the glass substrate, on the right for the gelatin substrate. The global pressure value is the maximum adhesion force Fmax, divided by the total area At of the gripper, as shown in the image.

Geometries versus ratio of maximum adhesion to total gripper area
On glass, the ratio of the maximum adhesion to the total gripper area (global pressure), is for D2 between 0.7 – 1.2, for D1 between 1.3 - 3.4 and for D05 between 0.7 - 2.4 kPa. The flat sample has values between 2.2 - 3.1 and one lower value of 1.2 kPa. The effects observed for the tests on glass are that D2 has the lowest mean pressure, followed by D05. The mean pressure exerted by the flat sample is higher compared to D1, but D1 has higher maximum values.

On gelatin, the global pressure values for D2 are 0.5 - 1 and for D1 between 0.3 – 1, except for the 1.9 kPa value of D1 that jumps out. The values for D05 range between 0.2 - 1.4 and for the flat sample between 0.6 - 1 kPa. The effects observed for the tests on gelatin are as follows. D05 generates the highest mean pressure of 0.94 kPa compared to the other gripper shapes D2, D1 and Fl, whose values are respectively 0.77, 0.83 and 0.80 kPa. The flat sample performs the most consistent. No clear difference is observed between the shapes D2 and D1. The gripper D05 has the highest and lowest pressure values among the gripper shapes, assuming that the 1.9 kPa value of D1 is an outlier.

5
Discussion

In this chapter the results of the adhesion experiments are first discussed in relation to the hypothesis. Then I provide arguments in which cases the measured forces are capillary forces. The findings of friction pilot 11 are presented in the next section. Hereafter, the limitations of the adhesion experiment are discussed. The chapter closes with recommendations regarding future experiments and the implementation of capillary-based adhesion in a surgical gripping tool.

5.1. Hypothesis

On a substrate of gelatin, for a constant gripper area and wet contact area, the measured adhesion does not increase with decreasing pillar diameter as Figure 4.4 shows. Although the geometry D05 with the smallest pillars did generate the highest mean adhesion, the spread in the measured values is so high for all geometries that the evidence to reject or accept the hypothesis is just not strong enough. The possible suspects for the spread in the adhesion forces are the fabrication method and the measurement method. These issues are discussed in section 5.4 about the limitations.

5.2. Main findings of the adhesion experiment

5.2.1. Did we measure capillary forces?

The PDMS which the grippers are made of, is sticky and the flat tips adhere very well to the smooth glass substrate without a liquid being present. This section provides evidence that the measured forces are predominantly capillary forces for the glass surface for D2 and D1. On gelatin, it could not be confirmed that adhesion was dominated by capillary forces.

Evidence: camera footage and force measurement

<u>Glass substrate</u>

The webcam-images in Figure 5.1 show that with D2 multiple bridges were lifted at the same time, and the fluid was well distributed over the pillars. The connected area A_c is concentrated at one side of the gripper, which could lead to the gripper peeling off the connector. In the case that peeling was observed with the naked eye, the measurement was excluded.

The force measurement corresponding to Figure 5.1 is presented in Figure 5.2. The maximum preload is applied at approximately 14 seconds and it takes roughly 2.5 seconds at the retraction speed of 0.1 mm/s to achieve the peak adhesion. After the peak adhesion at + 3.5s most bridges have collapsed and the adhesion decreases to zero. In Figure 5.3 the drop in force is plotted for all tests in higher detail, where the blue line represents T5. The assumption that all pillars are wetted as shown in Figure 5.1 is true for most measurements for D2 and D1. However, some tests show an uneven distribution of fluid in the footprint. Problems with the fluid distribution for specific tests are listed in Table 5.1 and Figure 5.4 provides examples of these issues.

An overview of the force measurements on glass over time, is shown in Figure E.1 in Appendix E.

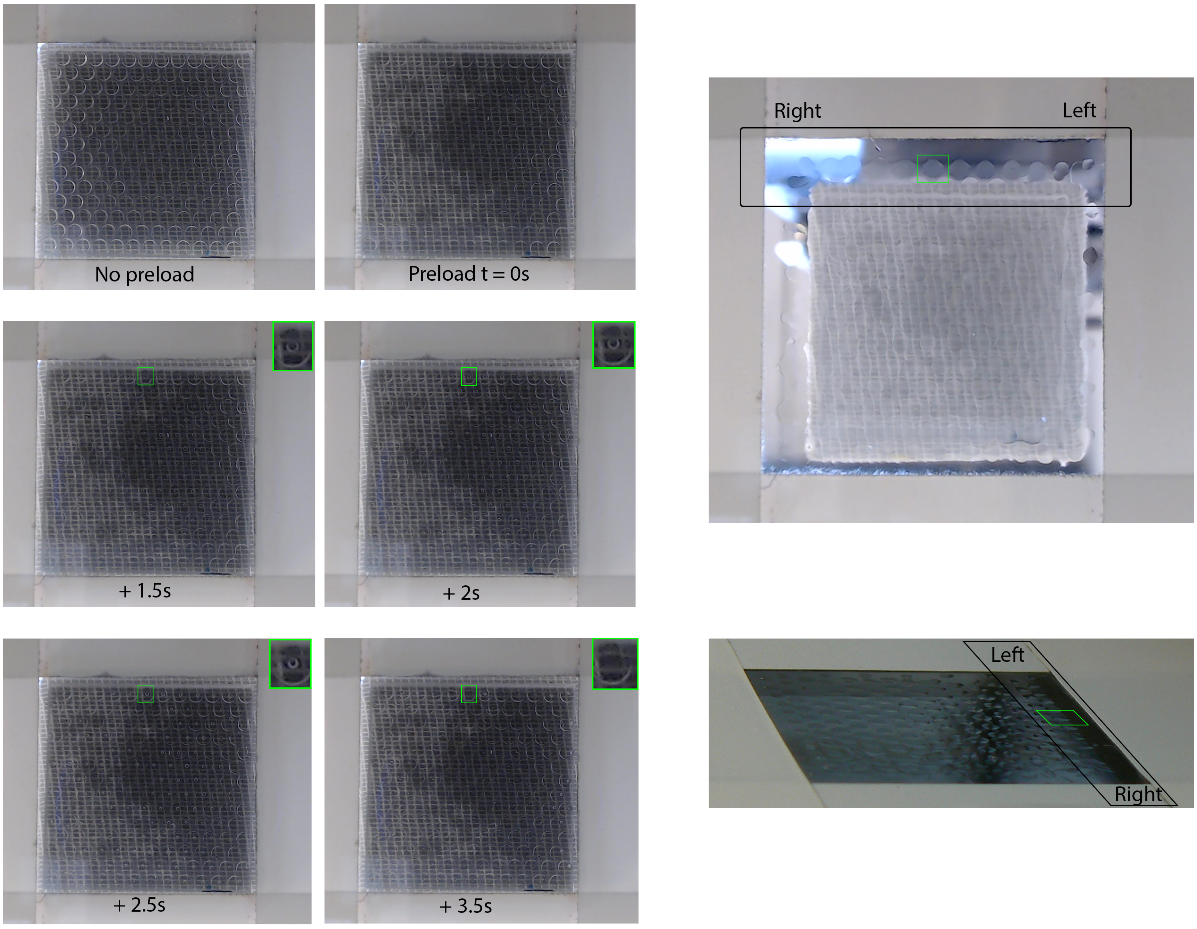

Figure 5.1: Left, slideshow of the webcam-images over time during the adhesion experiment with gripper D2 on glass (test 5). The webcam is located below the glass plate. The wetted pillars are in contact with the glass when the preload is applied. The mesh of the adhesive tape can be seen through the gripper. The light region is where the adhesive tape makes good contact with the grippers' top side. The inserts with the green frames are magnifications of one pillar to show the liquid bridge in detail. Top right, webcam-image of the footprint after the measurement is finished and the linear stage is raised. Bottom right, photo of the substrate taken from above with the camera.

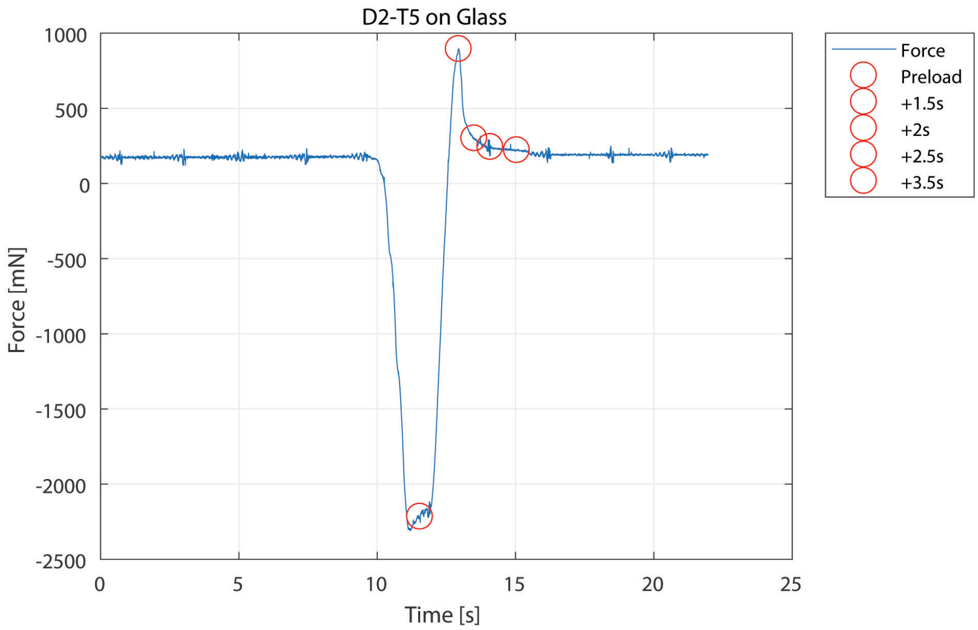

Figure 5.2: Force measurement of D2 on glass (test 5) over time. The red circles roughly indicate the times given in Figure 5.1.

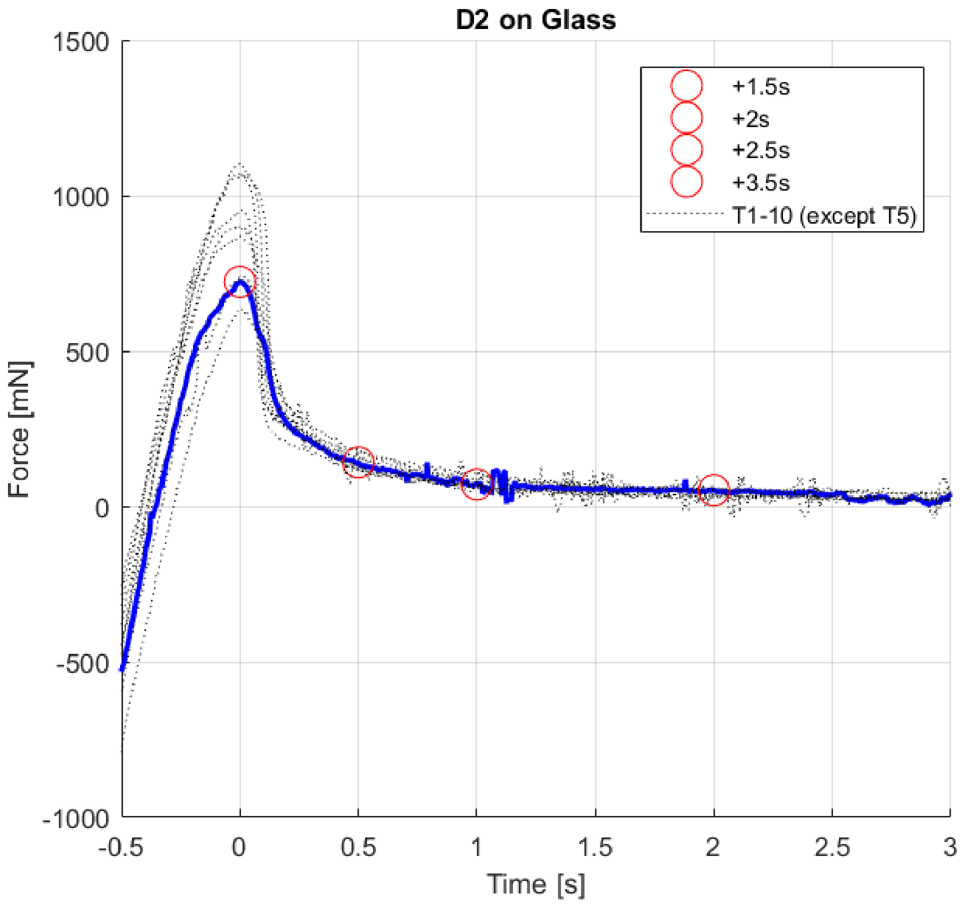

Figure 5.3: Force measurements of D2 on glass over time. The blue line represents T5. The graphs have been shifted in time such that the maximum adhesion force occurs at 0 seconds. The red circles indicate the times given in previous Figures 5.1 and 5.2.

Table 5.1: Issues with fluid distribution for adhesion tests on glass judged by the footprints.

Problem	Grippers and trial numbers
Too much liquid	D1 (T6, T8) D05 (T4, T6, T9)
Some droplets fused together	D2 (T1, T3, T6) D1 (T2) D05 (T8)
Not enough liquid, dry spots	D1 (T4, T9)

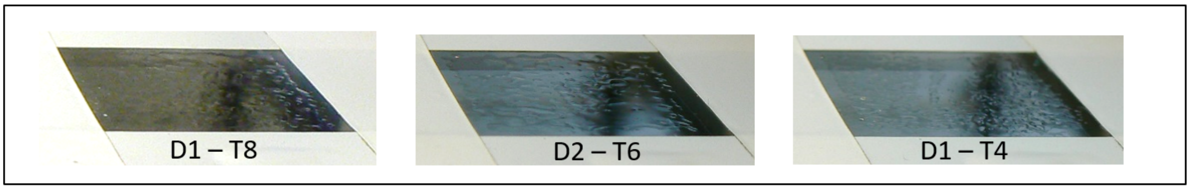

Figure 5.4: Left, the footprint of D1-T8 for which too much liquid was applied. Middle, the footprint of D2-T6 which shows droplets that have fused together. Right, the footprint of D1-T4 which shows dry spots at the upper part of the image. Brightness has been increased for clarity.

<u>Gelatin substrate</u>
With the gelatin substrate the footage of the contact is less clear compared to the glass substrate. The first reason is that small air bubbles are present in the gelatin. Secondly, distinguishing the difference between a liquid footprint and an imprint due to the applied preload is hard, especially for the pillar structures D1 and D05. Figure 5.5 presents an example of a liquid footprint and an imprint. The third reason is that it is hard to judge from the webcam images whether liquid bridges are present for the pillar structures. The clearest example for D2 (test 1) is shown in Figure 5.6. For most measurements however, the gripper does not lift off parallel to the surface because the applied preload was not uniform. Therefore, the evidence for measuring capillary forces on gelatin is considered to be weak. An overview of the force measurements on gelatin over time, is shown in Figure E.2 in Appendix E.

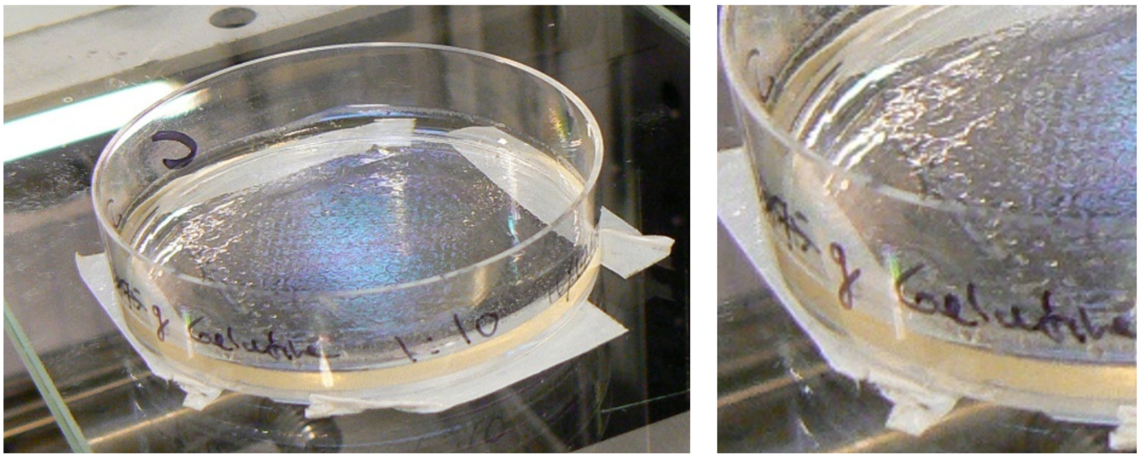

Figure 5.5: Left, photo of the footprint of D2 on gelatin (test 8). In the Petri dish droplets are present as well as an imprint in the gelatin caused by the preload. Right, a close-up of the photo. Discerning the footprint from the preload imprint is hard.

CONTRIBUTION OF VAN DER WAALS FORCES?

According to the following calculation there is no expected contribution of van der Waals forces to the adhesion, assuming that the pillars do not form dry contact.

In the lab I weighted the mass of liquid footprints for D1 on glass, which was between 5 and 30 mg. Assuming that 5 mg of water was present in the contact during adhesion – evenly spread over the 725 pillars – the liquid volume per pillar would be 0.007 mm^3. In the video footage, the liquid remained concentrated at the pillars and was not squeezed out of the contact. Therefore, if we assume that the liquid bridge between pillar and substrate is cylindrical, the required height to fit the volume is 1e-5 m. This height between the PDMS and the substrate is at least two orders of magnitude higher than the interaction distance of van der Waals forces [1].

CONTRIBUTION OF VISCOUS FORCES?

Here we estimate the value of viscous forces relative to the capillary forces for D1 on glass. During the retraction phase of the adhesion measurement, the fluid in the contact between the pillar and the substrate starts flowing. If we model this as two rigid parallel disks, equation (5.1) for Stefan adhesion can be used [26].

$$F_V = \frac{3\pi\mu R^4}{2h^3}\frac{dh}{dt} \tag{5.1}$$

Where the dynamic viscosity μ for water at 20 °C is 1.005 mPa ·s, the retraction speed dh/dt is 0.1 mm/s, the radius R of D1 is 0.5 mm and the height h between the disks is assumed to be 1e-5 m in line with the previous section. The calculated viscous force per pillar is 3e-5 N and the total viscous force for all pillars is 2e-2 N, which is two orders of magnitude lower than the measured adhesion values on glass 4.4. The contribution of viscous forces can therefore be neglected at this low retraction speed.

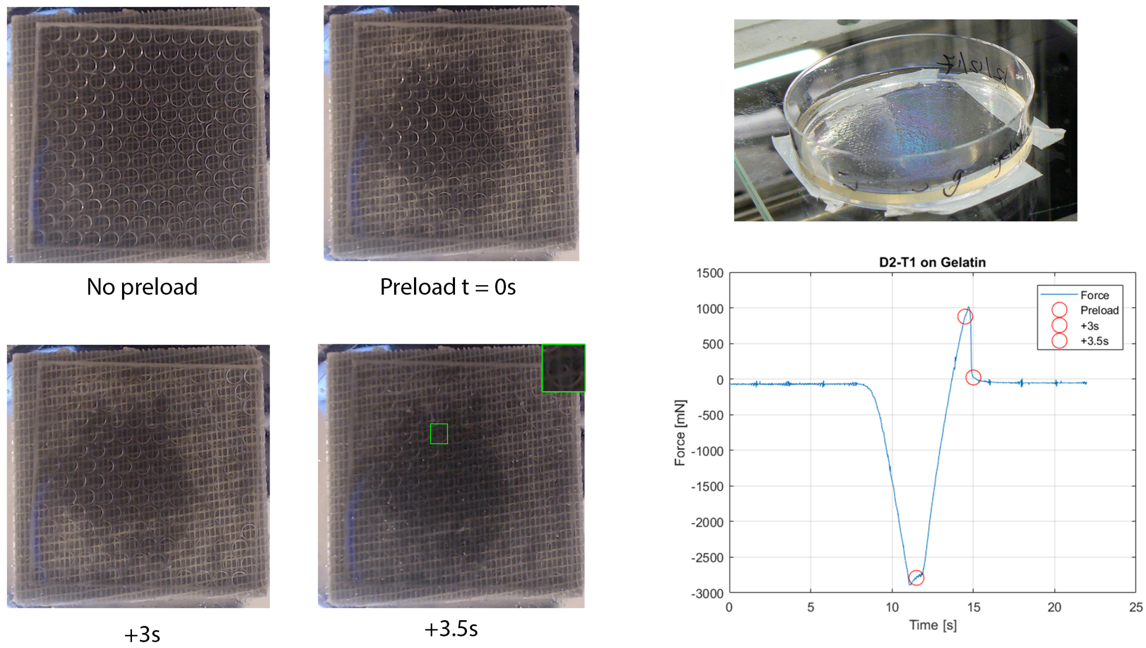

Figure 5.6: Left, slideshow of the webcam-images over time during the adhesion experiment with gripper D2 on gelatin (test 1). The inserts with the green frames are magnifications of one pillar to show the liquid bridge in detail. Top right, the footprint on gelatin. Bottom right, force measurement of the test on gelatin over time. The red circles roughly indicate the times shown at the left of the figure.

ACCURACY OF THE CAPILLARY FORCE CALCULATIONS

<u>Glass substrate</u>

The calculated pressure of 1 kPa on glass in Section 2.3.3 with values from literature is only valid for D2, as is shown in Figure 4.7. The other grippers have higher values.

<u>Gelatin substrate</u>

The calculated maximum adhesion values on gelatin with H_2O and the measured values from Figure 4.4 are listed in Table 5.2 below. Here can be seen that the calculated value for D2 is too low and the value for D1 is off by 0.08 N. The calculated value for D05 is too high.

Table 5.2: Calculated and mean of measured adhesion values on the gelatin substrate with water as liquid.

Gripper	Calculated adhesion [N]	Measurements [N]
D2	0.31	0.70
D1	0.67	0.75
D0.5	1.52	0.85

The most likely explanations that the calculated values differ from the measurements are:

1. As stated earlier in this section, it is not sure that the measured adhesion on gelatin is dominated by capillary forces. Multiple bridges are visible in the video footage. However, they do not separate at the same time, but as a front travelling from the contours of area A_c to the outside perimeter of the gripper.

2. The accuracy of the calculation is questionable because of the used input parameters for the contact angle θ and liquid volume V. The contact angle at the gripper is too low, as explained in 5.4, and the liquid volume V per pillar was not verified experimentally. Also, the calculation does not take the effects of the substrate and gripper stiffness into account.

5.2.2. UNEXPECTED FINDINGS

<u>Glass substrate</u>

The performance of D1 on glass with water is higher than expected. The mean of the local pressures from Figure 4.6 are given in Table 5.3. The datapoints T4 (3.2 kPa) and T9 (2.1 kPa) with possible dry contact, see Table 5.1, are actually low in comparison to the other values. The photo of the footprint of T7 (5.4 kPa) was not clear enough to judge how the fluid was distributed.

Table 5.3: Calculated mean pressure of grippers on glass with water from Figure 4.6

Gripper	Mean pressure [kPa]
D2	1.7
D1	3.6
D05	2.5
Fl	2.5

The spread of D2 in the adhesion measurements on glass with water is much smaller compared to D1 and D05 because, most likely, more bridges of D2 are lifted at the same time.

<u>Gelatin substrate</u>

The adhesion from Figure 4.4 shows no clear effect of the gripper geometry. This could be explained by the low stiffness of gelatin and no connected area A_c at the center of the gripper, leading to peeling at the contact. Another point of attention is that gelatin is wet which makes controlling the liquid volume difficult.

5.3. MAIN FINDINGS OF THE FRICTION PILOT 11

Here we present the main findings of the friction pilot 11 in order of importance. Note that no preload was applied during this test whereas laparoscopic grippers apply a pinch force on the tissue.

1. The generated friction on PVA (H2O) of all data is on average 0.12 N. The best performing pillar structure is D1 with 0.14 N. The flat sample outperforms D1, but not when corrected for the contact area.

2. The best performing pillar structure on PVA in the 'dry' case is D05 and matches the friction generated by the flat sample.

3. On glass (H2O), the flat sample generates a much higher friction compared to the pillar structures.

5.4. LIMITATIONS OF THE ADHESION EXPERIMENT

This section describes the limitations of the measurement procedure, the gripper fabrication and the calculation of the adhesion force.

A weak point in the measurement procedure was that the applied liquid volume before testing was not actively controlled or measured. If the total liquid volume was measured and it was equally distributed over the pillars, then the volume per pillar would have been known. This volume could have been used to calculate the capillary force contribution to the adhesion force per pillar. Another point of attention in the measurement procedure is that the gripper is not lifted off parallel to the substrate due to small misalignment's between the substrate and the connector. Consequently, not all pillars broke contact during liftoff but a front of bridges detached concentrically or from one side of the gripper to the other. The mode of release depended on the connected area Ac between the grippers' top side and the connector. The connected area Ac was never 100%, even when relatively large preloads were applied to the grippers, as indicated in Figure 4.3. These large preloads may have lead to liquid being squeezed out of the contact, although this was not seen in the video footage. The preloads are not constant, which means that an undesired variable is introduced, possibly increasing the spread in the measured adhesion values. A final limitation of the adhesion measurement procedure is that gelatin as tissue phantom is acceptable for representing the stiffness of bowel tissue, but not its surface properties.

A flaw in the gripper fabrication was caused by the master. Due to the heat generated during the wire Electric

Discharge Machining – to slice off the master from an aluminum block – the conically drilled parts burned away, even at a lower energy setting. Therefore, grippers were not made according to the dimensions as stated in section 2.3.3. Using PDMS it was proven that grippers can be cast using the mould. However, the PDMS is too hydrophobic compared to the desired 70° equilibrium contact angle as given in Section 2.3.2. According to Table 3 in [27] PDMS has a contact angle of 113°.

The calculation of the capillary force did not closely match the measured adhesion values, but was within the same order of magnitude. The numerical integration of the Young-Laplace equation of Section 2.3.2 is too complex to understand what are the most important design parameters for a gripper, and it does not yet even incorporate stiffness or viscous forces. Also, the underlying assumption that the force generated by a single pillar is not necessarily true for a large array of pillars if they do not lift from the substrate simultaneously.

5.5. RECOMMENDATIONS AND FUTURE WORK

- When repeating this experiment, the amount of fluid deposited on the gripper has to be controlled in a better way, for instance by using the linear stage instead of manual application. It is advised to measure the fluid volume in the contact when calculating capillary forces. Apply a constant preload to reduce the spread in the adhesion results. If possible, use a lower preload to prevent liquid being squeezed out of the contact. Conduct the measurements on a more realistic tissue phantom such as PVA. Find a suitable gripper material – possibly Polyurethane [3, 28] – which is moderately hydrophobic.

- It is not recommended to use capillary forces as a dominant mechanism for lifting bowel tissue. The normal forces generated by the grippers on gelatin are not high enough. Instead, capillary forces could complement other gripping methods, e.g. suction [24]. No clear force damage limits are available for gripping tissue with out-of-plane forces.

- For re-designing a capillary-based gripper, investigate how the normal forces are transferred from the substrate through the multiple contacts to the instrument. With the current gripper structure, not all liquid bridges are lifted simultaneously. The suspected cause is that some pillars are lifted too high from the substrate, exceeding the separation distance of the bridge. To distribute the normal force in a better way, the bridges would need to become longer, which is not possible. If the pillars elongate (or bend), as shown in Figure 5.7, a too high local lifting of one pillar does not lead to separation of that bridge and the neighbouring bridges.

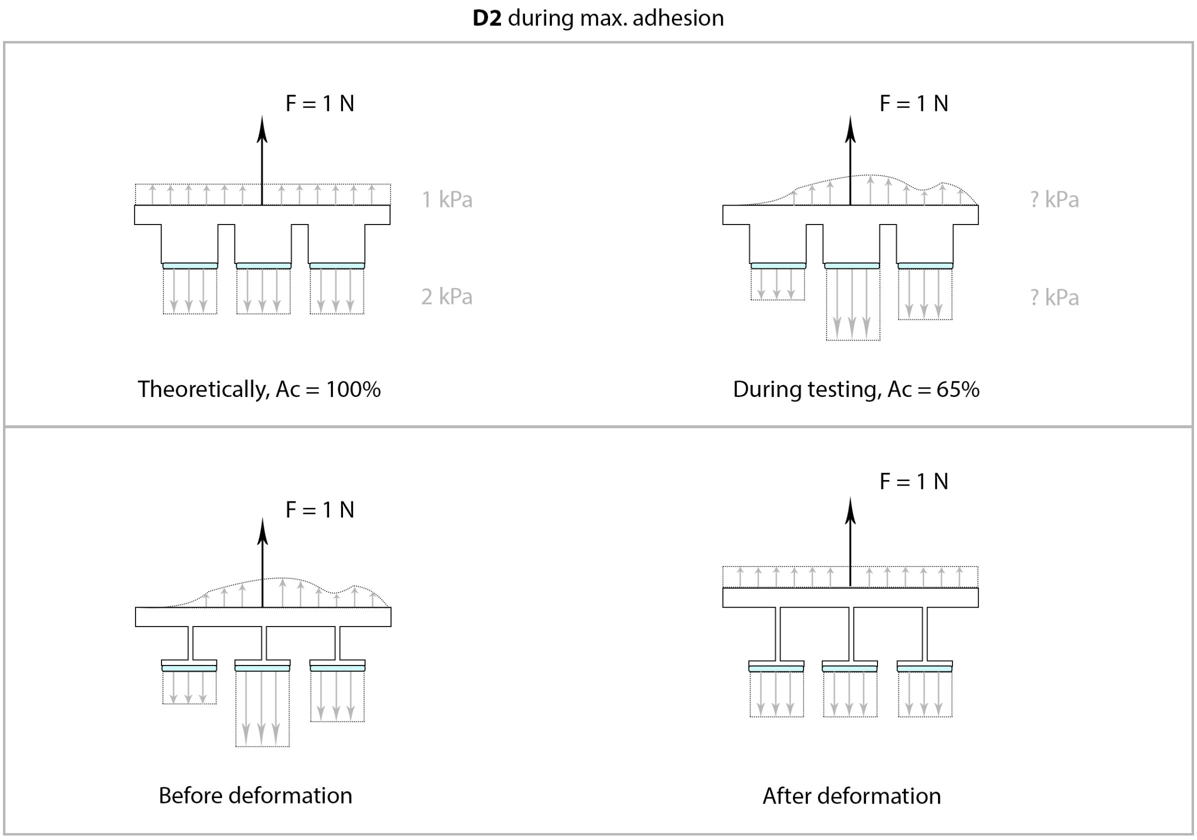

Figure 5.7: Top left, an equally distributed out-of-plane load leads to equal pressure at the contact between pillars and the substrate. Top right, for a unequal distributed load some pillars need to generate a higher adhesion force than is possible with liquid bridges. Bottom left, the pillar structure is fabricated such that the middle part can easily elongate or bend like a leaf spring. An unequally distributed load is applied. Bottom right, the load is distributed more equally after the pillars have deformed.

5.6. ARTIST IMPRESSIONS OF A CAPILLARY-BASED GRIPPER

Here in Figure 5.8 an existing babcock forceps is presented which is currently used in laparoscopic surgery for atraumatic tissue gripping. The concept versions of a capillary-based gripper are shown in Figure 5.9 and 5.10. Both require a vacuum to lift tissue. The first gripper is rigid and uses capillary-based adhesion to complement the suction force. The second gripper is elastic and can be draped on the tissue. Capillary forces forces are used to make the sealing ring stick to the tissue. By applying a vacuum the tissue folds between the pillars for improved friction. Shape grip is applied by pumping a fluid into the gripper tip.

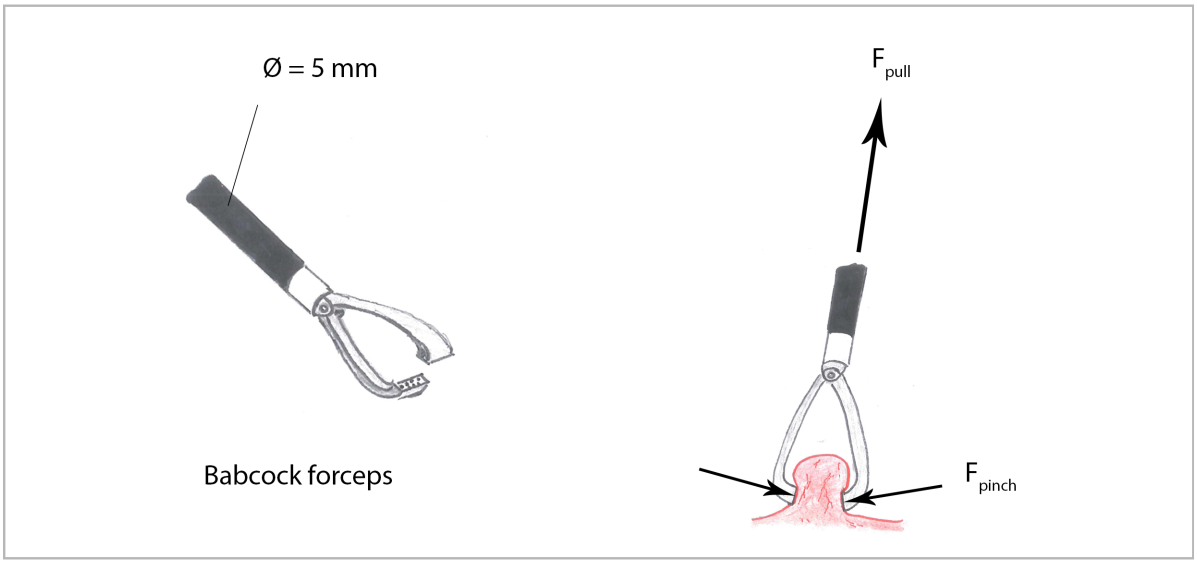

Figure 5.8: Top left, a typical babcock forceps used in laparoscopic surgery. The diameter of the instrument is 5 mm to fit through the trocar. The pinch force is applied by the surgeon before the tissue can be pulled, as shown on the right.

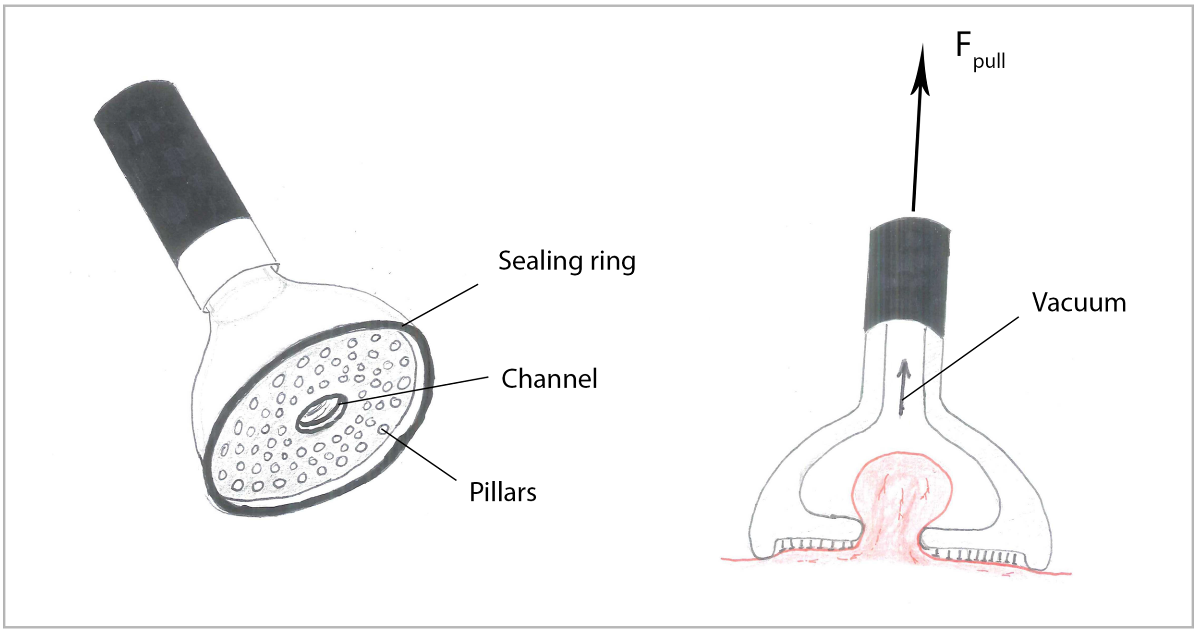

Figure 5.9: Left, a suction cup is shown which can be pulled into the shaft to be able to fit through the trocar. A sealing ring is located at the perimeter of the cup, and in the center a channel is present for applying the suction. Pillars between the channel and sealing ring will apply the capillary-adhesion. Right, a section view of the gripper when the vacuum is applied. The tissue bulges into the cup, and the pillars (as in Figure 5.7) form liquid bridges with the tissue.

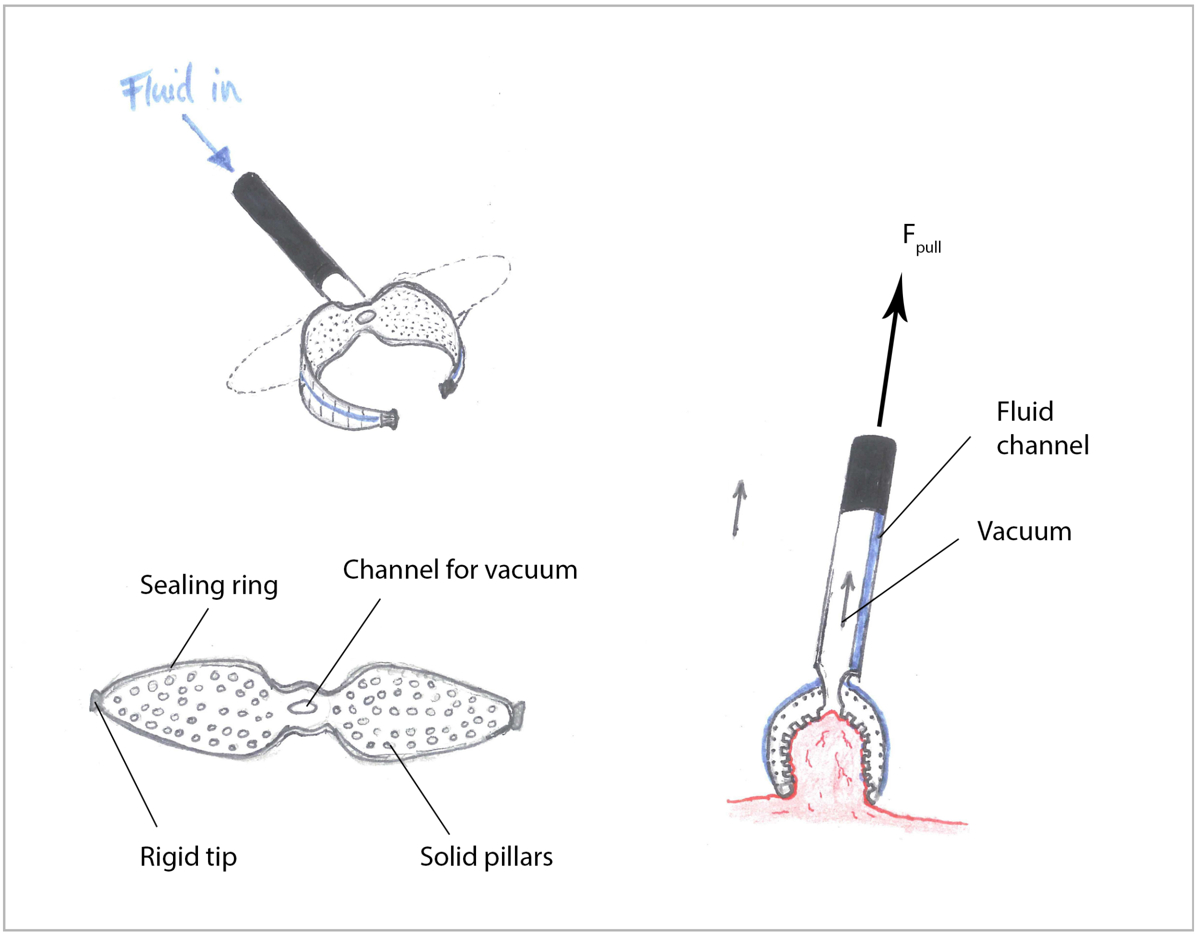

Figure 5.10: Left, the capillary-based gripper is made from a combination of elastic and stiff materials. The stiff fibers are used to improve the torsional stiffness of the gripper. The gripper closes when a fluid is inserted into the channel, which is located at the exterior part of the gripper. Close up, shows a channel for the vacuum in the center and at the perimeter a sealing ring. The tips are rigid and solid pillars such as **D1** from Chapter 3 are present at the grippers' surface. Right, by inserting a fluid the gripper closes. The pillars and the sealing ring make contact with the tissue, and stick through capillary forces. The vacuum is applied and the tissue is pulled between the pillars after which the tissue can be lifted.

A

FLOWCHART: CHOICE OF TIP SHAPE

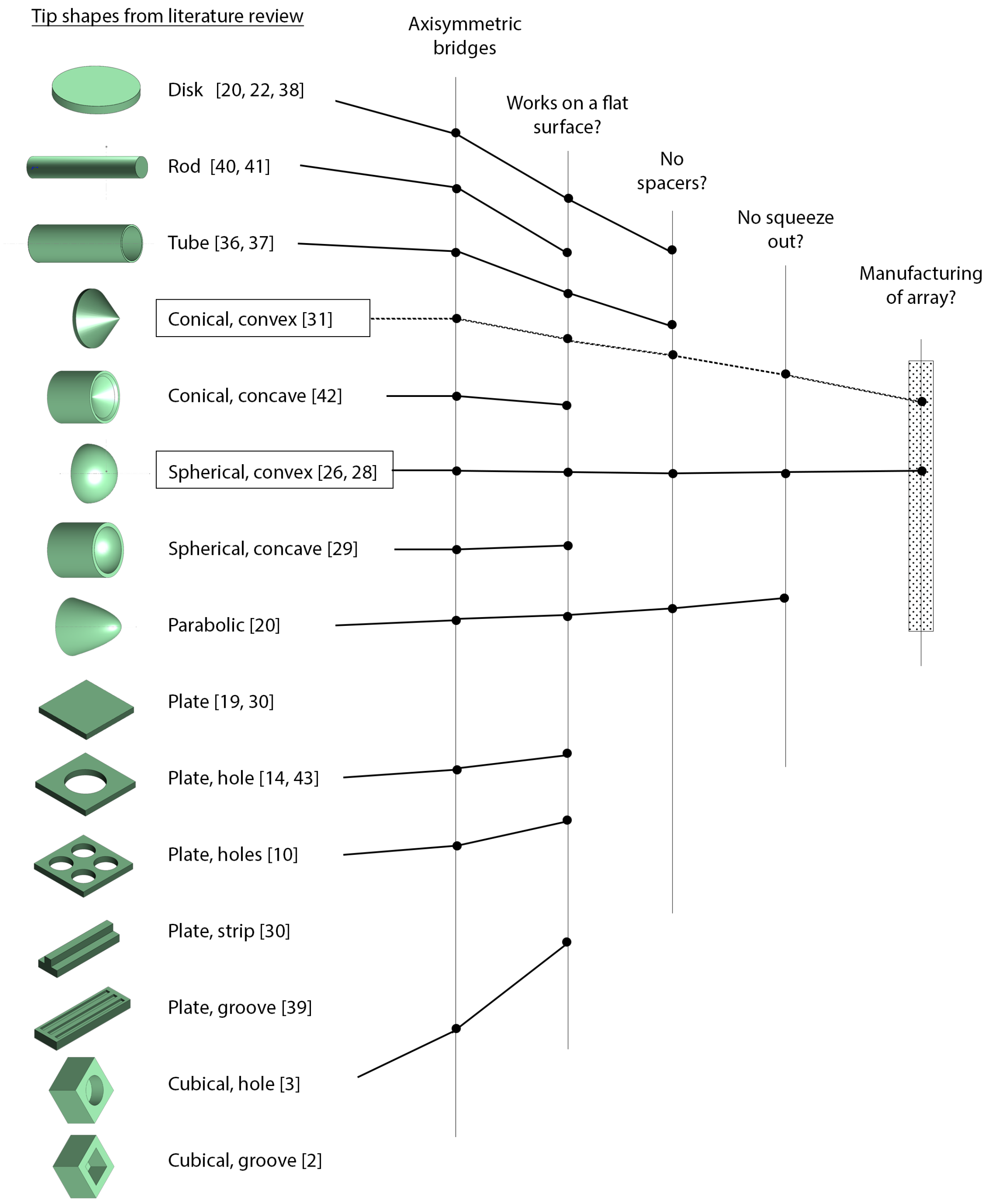

Figure A.1: Steps taken to select a suitable gripper tip shape from all the tip shapes found in the literature. Note that the references between brackets are listed in the literature review, not in this thesis.

B

MATLAB SCRIPT TO ESTIMATE THE DIMENSIONS OF THE GRIPPER

```
%%% Prototype dimensions
% This m-file calculates the dimensions of a structure with hexagonally
% packed pillars, with pillar to pillar distance S. The first calculation
% is based on a baseplate with 8 pillars. The second calculation is based
% on the solidworks file.

%% Parameters
alpha = 118*(pi/180);         % Angle of drill tip [rad]
beta = (pi-alpha)/2;          % Angle cone w. resp. to substrate [rad]
D1 = [0.5 1 2];               % Pillar base diameter [mm]
phi = 0.6;                    % Ratio wet area to baseplate area [-]

% xi should be smaller or equal to phi!
xi = 0.4;                     % Ratio dry area to baseplate area [-]

%% Pillar to Pillar distance S1      (in case Dbridge = D1)
% ABC formula
A = 2*phi*sqrt(3);
B = D1.*phi*(5*sqrt(3) + 2);
C = D1.^2 * phi * (3+3*sqrt(3)) - 2*pi.*(D1).^2;
D = B.^2 -4.*A.*C;

S1 = (-B+sqrt(D))./(2*A);       % Spacing between pillars [mm]

%% Flat cone diameter D2, and cone height L2
Abaseplate = (3.*D1+2.*S1).*(D1+2*(D1+S1)*0.5*sqrt(3));    %[mm2]
D2 = sqrt((xi.*Abaseplate)./(2*pi));     % Flat cone diameter [mm]
L2 = tan(beta)*0.5*(D1-D2);              % Height of cone [mm]

%% Calculating length of pillar L1
L1 = (D1.^4).^(1/3);

%% Volume of a single bridge
Vwedge = 0.25*pi*(D1.^2 -D2.^2).*L2*0.5;     %[mm3 = uL]
```

C

MATLAB SCRIPT FOR CALCULATING CAPILLARY FORCES

```
% The Conical_Plate.m script calculates the capillary force between a flat
% substrate and an array of conically shaped gripper tips.

% Msc. Thesis
% Jay van den Berg
% r.j.vandenberg@student.tudelft.nl
% 20-7-2017
% TU-Delft
% clear all; clc; close all;

%% Global parameters
global gamma_LG_ gap_ V_ tgri_ tobj_ Rtip_ Pxstart_ beta_ dPest_ dPincr_ dP_

%% Fixed parameters conical gripper
% assuming gravity effects on meniscus are negligible
% assuming the surfaces are rigid.

dPest_ = 10.5;                % Estimate for pressure difference
dPincr_ = 0.5;                % Pressure decrement value
gamma_LG_ = 0.072;            % Surface tension water-air interface [N/m]
gap_ = 0;                     % Gap between gripper and plate [m]
V = 1.5e-10;                  % Liquid bridge volume [1 = m3, 1e-3 = L]
tgri_ = 70*(pi/180);          % Contact angle at gripper [rad]
tobj_ = 45*(pi/180);          % Contact angle at bottom [rad]
Verror = 0.05;                % Acceptable error in volume calculation
beta_ = 30.*(pi/180);         % Angle of cone [rad]
Rtip_ = 0.5e-3;               % Tip radius [m]

%% Set Initial conditions
% Choose starting point P, where the mensicus touches the conical tip
Px = 0.55e-3;         % was 0.2e-3
Pxstart_ = Px;
Py = gap_ + (Px - Rtip_)*tan(beta_);

% Calculate meniscus slope in P [rad]
if tgri_+beta_ == pi/2
    drdz = 0;
```

```
else
    drdz = −1/tan(tgri_+beta_);
end

%% Boundary Conditions (B.C.'s)
% B.C. at the gripper
%       tgri_ is the contact angle at gripper [rad]
% B.C. at the object (plate)
%       tobj_ is the contact angle at the plate [rad]

%% Initial conditions: give y0 as output
y0 = [Px,drdz];              % Initial conditions for integration

%% Double shooting method
% Iteration j: Try dPest to find meniscus that agrees with contact angle at
% the objects side. Calculation takes place in function f_calc_meniscus.
% Iteration k: If the volume is too small, select starting point further
% from vertical symmetry axis r = 0. If the volume is too large, select a
% point with a smaller radius closer to the vertical symmetry axis.
iter = 2;
for k = 1:iter
   % Calculate Meniscus Shape & check B.C. at plate
   [y,z,dParray,tobj_calc_array] = f_calc_meniscus(Py, y0);
    r = y(:,1);                        % Radius of the meniscus.
    Vcalc = f_calc_vol_coneplate(r, z, Px, Py);
    V_calc_array(k) = Vcalc;
   % Select new starting point
    [Px, Py, y0] = f_calc_Pnew_coneplate(Px,Py,Vcalc,Verror,k);
end
Px_array(n) = Px;
Py_array(n) = Py;

%% Draw gripper and meniscus
figure
axis([−4*Rtip_ 4*Rtip_ −Py 4*Py])
grid on
hold on
line([−Rtip_ Rtip_],[gap_ gap_])
line([Rtip_ Px],[gap_ gap_+(Px−Rtip_)*tan(beta_)])
line([−Px −Rtip_],[gap_+(Px−Rtip_)*tan(beta_) gap_])
line([−4*Rtip_ 4*Rtip_],[0 0])
line([Px Px],[(Px−Rtip_)*tan(beta_) (Px−Rtip_)*tan(beta_)+1])
plot(r,z,'b')

%% Calculate the capillary force − 1 contact
R_at_object(n) = r(end,1);                        %Radius at plate [m]

% Calculate Laplace force
Awet(n) = pi*R_at_object(n)^2;       % Wetted area at plate [m2]
F_L(n) = dParray(end)*(Awet(n));     % [N]

% Calculate the Surface tension force (always attractive)
F_ST(n) = −2*pi*R_at_object(n)*gamma_LG_*sin(tobj_calc_array(end));    %[N]

% Calculate the Capillary force
F_C(n) = abs(F_L(n) + F_ST(n));    %[N]
```

```
end

%% Possible number of bridges
packing = 0.6;               % Ratio Awet to Atotal
F_desired = 1;               % Desired force [N]
N = F_desired/F_C;           % Number of bridges [-]
Anet = (Awet/packing)*N;     % Calculated gripper area [m2]
L = sqrt(Anet);              % Length of sides for a square gripper [m]
```

```
function [r,z,dParray,tobj_calc_array] = f_calc_meniscus(Py, y0)
%f_calc_meniscus Calculates the height z and radius r of the meniscus.
%   Input parameters Py is the y-coordinate [m] of the starting point P of
%   the meniscus, and y0 is a vector [Px, drdz] with initial conditions.

global tobj_ dPest_ dPincr_ dP_

% Parameters needed for calculation of contact angle at object (tobj_calc)
tobj_calc = tobj_+5; % Set this value to start the while loop.
j = 1;               % Do not change this value.
dP_ = dPest_;        % Set dP to estimated value (dPest often set to 10 Pa)

while tobj_calc>tobj_
   % Decrement pressure from estimated value.
    dP_ = dP_-dPincr_;

   % Integrate from z = Py to Liquid bridge height z = 0
   opts = odeset('RelTol',1e-3,'AbsTol',1e-6);
   [z,r] = ode45(@YoungLaplace,[Py 0],y0, opts);

   % Calculate contact angle at plate
   tobj_calc = f_calc_tobj_plate(z,r);  %[rad]

   % Save pressure array, and theta_obj array for plotting later
    dParray(j) = dP_;
    tobj_calc_array(j) = tobj_calc;

   % Increase step.
   j = j+1;
end
```

```
function [y_dot] = YoungLaplace(z,y)
%YoungLaplace This is the 1st order DE describing meniscus the profile
%   z = meniscus height, y = [u,v] u = r(z) meniscus profile, v = r_dot(z).
%   Global parameters end with an underscore, like: rho_

global  gamma_LG_ dP_

u = y(1);
v = y(2);

% By definition
u_dot = v;

% 2nd order eq. written down as a 1st order equation
v_dot = -(dP_/gamma_LG_)*(1+v^2)^1.5 + (1+v^2)/u;

% Now define y_dot
```

```
y_dot = [u_dot; v_dot];
end
```

```
function tobj_calc = f_calc_tobj_plate(z,r)
%f_calc_tobj_plate calculates contact angle between meniscus and plate. z
%is the meniscus height [m], r is the horizontal distance from the symmetry
%axis. In other words, the radius of the meniscus at height z. Angles are
%calculated in radians.
%   1-12-2016

%% Three cases possible, t2>90 degr, t2<90 degr and t2 = 90 degr.
% Fourth case? t2 = 0 degr
 if r(end-1,1)>r(end,1)          % Theta2 is larger than 90 degrees
     tobj_calc = pi-atan((z(end-1)-z(end))/(r(end-1,1)-(r(end,1))));

 elseif r(end-1,1)<r(end,1)
     tobj_calc = atan((z(end-1)-z(end))/(r(end,1)-(r(end-1,1))));

 elseif r(end-1,1) == r(end,1)
     tobj_calc = pi;

 elseif z(end-1,1) == z(end,1)
     tobj_calc = 0;
end
```

```
function Vcalc = f_calc_vol_coneplate(r, z, Px, Py)
%f_calc_vol_coneplate calculates the volume of the liquid bridge between a
%flattened conical tip and a flat surface, by revolving the mensiscus
%profile about its' center axis.

    global Rtip_ gap_

% Calculate revolved meniscus by summing volume of disks with height dz
Vrev = 0;                          % Introduce parameter: calculated volume

for m = 1:(length(z)-1)
   V_dz = pi*(r(m))^2*(z(m)-z(m+1));
   Vrev = Vrev + V_dz;
end

% Calculate cap volume
Vcap = pi*(Rtip_+0.5*(Px-Rtip_))^2 *(Py-gap_);

% Subtract cap from revolved meniscus volume
Vcalc = Vrev-Vcap;
```

```
function [Px, Py, y0] = f_calc_Pnew_coneplate(Px,Py,Vcalc,Verror,Step)
%f_calc_Pnew_sphereplate Calculates new starting point of meniscus on a
%conical gripper. If the calculated volume is smaller than the given
%volume, the meniscus starting point will lie further from the symmetry
%axis. If the calculated volume is larger than the given volume, the
%meniscus starting point on the gripper will move closer to the symmetry
%axis.
%   20-7-2017

global V_ Pxstart_ Rtip_ beta_ gap_ tgri_

```

```
if (Vcalc/V_) < (1−Verror)     % select point further from vert. axis.
   Px = Px + (1/2^Step)∗Pxstart_; % Hor. dist. of point P from symm. axis [m
   Py = gap_ + (Px − Rtip_)∗tan(beta_);
   % Calculate meniscus slope in P [rad]
   if tgri_+beta_ == pi/2
      drdz = 0;
   else
      drdz = −1/tan(tgri_+beta_);
   end
      y0 = [Px,drdz];
elseif (Vcalc/V_) > (1+Verror) % select point closer to vert. axis.
   Px = Px − (1/2^Step)∗Pxstart_;
   Py = gap_ + (Px − Rtip_)∗tan(beta_);
   % Calculate meniscus slope in P [rad]
   if tgri_+beta_ == pi/2
      drdz = 0;
   else
      drdz = −1/tan(tgri_+beta_);
   end
   y0 = [Px,drdz];
else
    % Calculate meniscus slope in P [rad]
    if tgri_+beta_ == pi/2
      drdz = 0;
   else
      drdz = −1/tan(tgri_+beta_);
   end
      y0 = [Px,drdz];
end
```

D

MATLAB SCRIPT FOR IMAGE PROCESSING

```
% Crop & Rotate
% This file collects the images associated with the distribution of the
% preload in the adhesion tests. The images are rotated and cropped for
% further processing and converted into Black/White images.

%% Load the filenames of the photo's from the directory raw data
dirname = uigetdir('');
cd(dirname);
[FileName,PathName] = uigetfile('*.jpg','Select all jpg files','MultiSelect','on' );

%% Read the image data (1 by one goes faster than the bulk)
for f = 1:length(FileName)
IM1 = imread(FileName{1,f});

%% Resize to the sample dimensions of 30x30mm
% Crop the image
imshow(IM1)
IM1Crop = imcrop(IM1);

pause(0.5)

% Pick 2 points at the top corners, starting at the left
imshow(IM1Crop)
[x, y] = getpts;

% Calculate the angle of rotation, and direction
if y(2) >= y(1)
    rot_rad = asin(((y(2)-y(1)))/(x(2)-x(1)));       %[rad]
    rot_degr = rot_rad*(180/pi);                    %[degr]
elseif y(2) <= y(1)
    rot_rad = -asin(abs(y(2)-y(1))/(x(2)-x(1)));     %[rad]
    rot_degr = rot_rad*(180/pi);                    %[degr]
elseif y(2) == y(1)
     rot_degr = 0;                                  %[degr]
end

% Rotate the image
IM1_rot = imrotate(IM1Crop,rot_degr);
imshow(IM1_rot)
```

```

% 'Crop the image again, along the edges'
IM1Crop2 = imcrop(IM1_rot);
% imshow(IM1Crop2);

%% Turn the image into Greyscale

IM1_gray = mat2gray(IM1Crop2);
% imshow(IM1_gray)
level = graythresh(IM1_gray);

%% And then into Black/white
BW = im2bw(IM1_gray,level);
% figure, imshow(BW)
title('B/W image')

BWimages(f,1) = struct('FileName', FileName(1,f),'BW',BW);
close all
end

savefile = 'BWimages.mat';
save(savefile,'BWimages');      % Is saved into current directory!
```

```
% This file requires a snapshot made with the webcam during the 29nov'17
% experiment on glass, of the contact between glass and the PDMS pillar
% structure. The image is cropped, converted into black & white and the
% preload is based on the mm2 area which is white. The force data of the
% 29nov'17 experiment is normalized by the area that made good contact.

% Jay van den Berg, 1-12-2017, TU Delft

% load('BWimages.mat')
load('BWimages_Adh6.mat')

%% Erode and dilate until preload regions are clear
% Chosen shapes for eroding and dilation
se1 = strel('cube',2);
se2 = strel('disk',4);
se3 = strel('disk',5);

for m = 1:length(BWimages)
    figure
    CurrentIM = BWimages(m).BW;

   for k = 1:2
       dilatedBW = imdilate(CurrentIM,se2);      % White regions grow
       CurrentIM = dilatedBW;
       erodedBW  = imerode(CurrentIM,se1);       % Black regions grow
       CurrentIM = erodedBW;
   end
   erodedBW  = imerode(CurrentIM,se3);
   CurrentIM = erodedBW;

   % Plot both original and processed image, for comparison
   subplot(1,2,1),imshow(BWimages(m).BW)
   title('B/W image')
```

```
    subplot(1,2,2),imshow(CurrentIM)
    title(strcat(['Eroded & Dilated: ',num2str(k),' cycles']));

%% Calculate the ratio white to the total pixels

    IM_Dimensions = size(CurrentIM);
    Totalpixels = IM_Dimensions(1)*IM_Dimensions(2);

    % Count the number of white pixels in the image.
    W_pixels = 0;
    for k = 1:IM_Dimensions(1)
        for j = 1:IM_Dimensions(2)
            if CurrentIM(k,j) == 1
                W_pixels = W_pixels + 1;
            end
        end
    end

    % Ratio of White pixels to total pixels
    PDMSConnectedArea = (W_pixels/Totalpixels)*30^2;    %[mm2]

    VisualPreload(m,1) = struct('FileName', BWimages(m).FileName,...
                    'BW',BWimages(m).BW,'ProcessedIM', CurrentIM,...
                        'PDMSConnectedArea', PDMSConnectedArea);
end

savefile = 'VisualPreload.mat';
save(savefile,'VisualPreload');     % Is saved into current directory!
```

E

GRAPHS: ADHESION FORCE VERSUS TIME

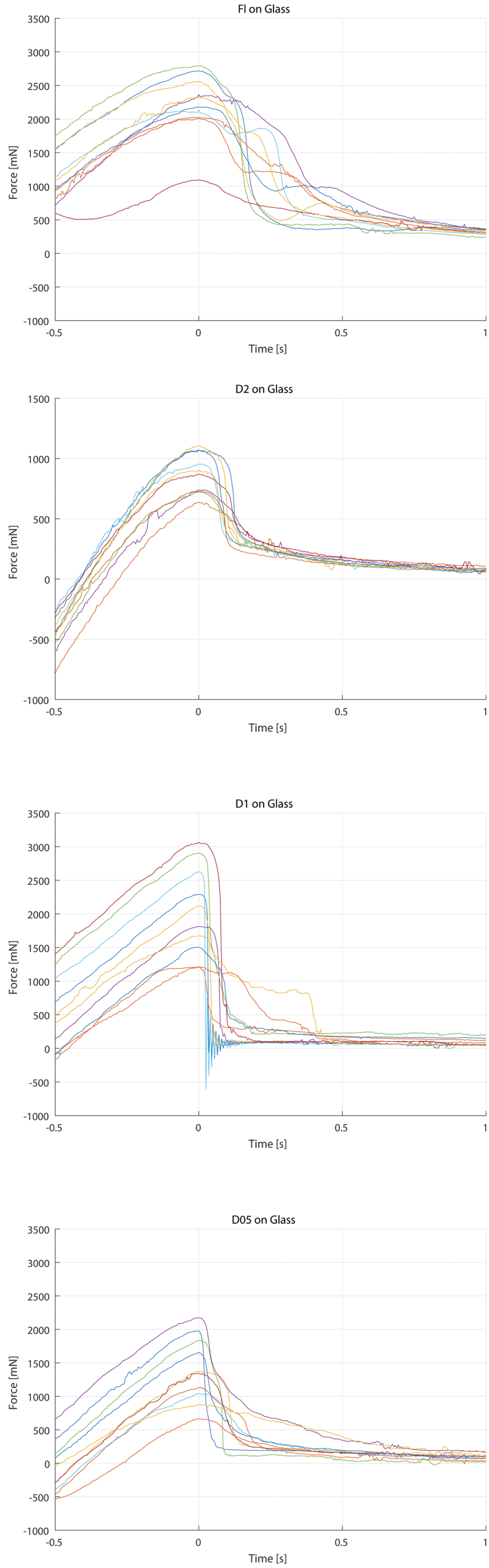

Figure E.1: Graphs of the adhesion force over time, for the glass substrate.

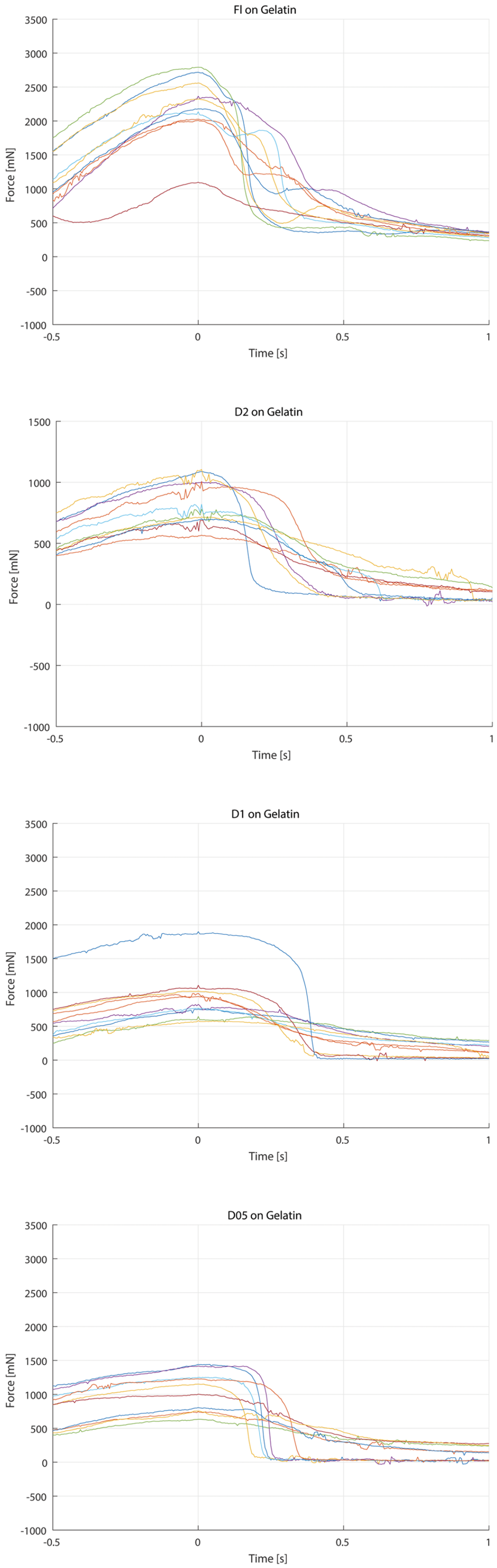

Figure E.2: Graphs of the adhesion force over time, for the gelatin substrate.

Bibliography

[1] P. Lambert, *Capillary forces in microassembly: modeling, simulation, experiments, and case study. microtechnology and mems,* (2007).

[2] J. Giltinan, E. Diller, C. Mayda, and M. Sitti, *Three-dimensional robotic manipulation and transport of micro-scale objects by a magnetically driven capillary micro-gripper,* in *Robotics and Automation (ICRA), 2014 IEEE International Conference on* (IEEE, 2014) pp. 2077–2082.

[3] J. Giltinan, E. Diller, and M. Sitti, *Programmable assembly of heterogeneous microparts by an untethered mobile capillary microgripper,* Lab on a Chip **16**, 4445 (2016).

[4] K. F. Bohringer, U. Srinivasan, and R. T. Howe, *Modeling of capillary forces and binding sites for fluidic self-assembly,* in *Micro Electro Mechanical Systems, 2001. MEMS 2001. The 14th IEEE International Conference on* (IEEE, 2001) pp. 369–374.

[5] N. Boufercha, J. Sägebarth, M. Burgard, N. Othman, D. Schlenker, W. Schäfer, and H. Sandmaier, *Fluidassem-a new method of fluidic-based assembly with surface tension,* in *International Precision Assembly Seminar* (Springer, 2008) pp. 149–159.

[6] C. Py, P. Reverdy, L. Doppler, J. Bico, B. Roman, and C. N. Baroud, *Capillary origami: spontaneous wrapping of a droplet with an elastic sheet,* Physical review letters **98**, 156103 (2007).

[7] L. Wang, M. Qiu, Q. Yang, Y. Li, G. Huang, M. Lin, T. J. Lu, and F. Xu, *Fabrication of microscale hydrogels with tailored microstructures based on liquid bridge phenomenon,* ACS applied materials & interfaces **7**, 11134 (2015).

[8] C. Bark, T. Binnenbose, G. Vogele, T. Weisener, and M. Widmann, *Gripping with low viscosity fluids,* in *Micro Electro Mechanical Systems, 1998. MEMS 98. Proceedings., The Eleventh Annual International Workshop on* (IEEE, 1998) pp. 301–305.

[9] G. Arutinov, M. Mastrangeli, G. van Heck, P. Lambert, J. M. den Toonder, A. Dietzel, and E. C. Smits, *Capillary gripping and self-alignment: A route toward autonomous heterogeneous assembly,* IEEE Transactions on Robotics **31**, 1033 (2015).

[10] H. de Visser, *Grasping Safely: Instruments for bowel manipulation investigated,* Ph.D. thesis, Delft University of Technology (2003).

[11] H.-J. Butt and M. Kappl, *Normal capillary forces,* Advances in colloid and interface science **146**, 48 (2009).

[12] K. Brakke, *Surface evolver home page,* (2013), [Online; accessed 17-February-2017].

[13] H. Grutzeck, *Investigations of the capillary effect for gripping silicon chips,* Microsystem technologies **11**, 194 (2005).

[14] D. Labonte and W. Federle, *Scaling and biomechanics of surface attachment in climbing animals,* Phil. Trans. R. Soc. B **370**, 20140027 (2015).

[15] E. De Souza, M. Brinkmann, C. Mohrdieck, and E. Arzt, *Enhancement of capillary forces by multiple liquid bridges,* Langmuir **24**, 8813 (2008).

[16] M. J. Vogel and P. H. Steen, *Capillarity-based switchable adhesion,* Proceedings of the National Academy of Sciences **107**, 3377 (2010).

[17] N. Bezdenejnykh, J. Meseguer, and J. Perales, *Experimental analysis of stability limits of capillary liquid bridges,* Physics of Fluids A: Fluid Dynamics **4**, 677 (1992).

[18] H. Princen, *Comments on "the effect of capillary liquid on the force of adhesion between spherical solid particles",* Journal of Colloid and interface Science **26**, 249 (1968).

[19] G. Lian and J. Seville, *The capillary bridge between two spheres: new closed-form equations in a two century old problem,* Advances in colloid and interface science **227**, 53 (2016).

[20] G. Lian, C. Thornton, and M. J. Adams, *A theoretical study of the liquid bridge forces between two rigid spherical bodies,* Journal of colloid and interface science **161**, 138 (1993).

[21] S. Cheng and M. O. Robbins, *Nanocapillary adhesion between parallel plates,* Langmuir **32**, 7788 (2016).

[22] E. Cheung, M. E. Karagozler, S. Park, B. Kim, and M. Sitti, *A new endoscopic microcapsule robot using beetle inspired microfibrillar adhesives,* in *Advanced Intelligent Mechatronics. Proceedings, 2005 IEEE/ASME International Conference on* (IEEE, 2005) pp. 551–557.

[23] T. Yasuda, T. Okuno, and H. Yasuda, *Contact angle of water on polymer surfaces,* Langmuir **10**, 2435 (1994).

[24] D. Vonck, R. Goossens, D. Van Eijk, I. De Hingh, and J. Jakimowicz, *Vacuum grasping as a manipulation technique for minimally invasive surgery,* Surgical endoscopy **24**, 2418 (2010).

[25] P. Lambert and A. Delchambre, *Parameters ruling capillary forces at the submillimetric scale,* Langmuir **21**, 9537 (2005).

[26] H. Grutzeck and L. Kiesewetter, *Downscaling of grippers for micro assembly,* Microsystem Technologies **8**, 27 (2002).

[27] A. Mata, A. J. Fleischman, and S. Roy, *Characterization of polydimethylsiloxane (pdms) properties for biomedical micro/nanosystems,* Biomedical microdevices **7**, 281 (2005).

[28] P. Kuang, J.-H. Lee, C.-H. Kim, K.-M. Ho, and K. Constant, *Improved surface wettability of polyurethane films by ultraviolet ozone treatment,* Journal of applied polymer science **118**, 3024 (2010).